



**Development of endovascular stent-grafts based on a nanocomposite
polymer**

**A Thesis Submitted in partial fulfilment of the requirements for degree of MD
(Res), University College London**

Mital Yogeshkumar Desai MB BS MS MRCSEd

July 2012

CONTENTS

<u>List of contents</u>	2
<u>Abstract</u>	9
<u>Publications, Presentations & Awards</u>	11
<u>Dedication</u>	16
<u>Acknowledgements</u>	17
<u>List of abbreviations</u>	19
<u>List of Figures</u>	21
<u>List of Tables</u>	25
<u>Chapter 1</u>	26
Polyhedral oligomeric silsesquioxane nanomaterials for cardiovascular applications	
1.1 Polyhedral oligomeric silsesquioxane (POSS)	27
1.2 Cardiovascular applications of POSS	28
1.3 Prospects	29
<u>Chapter 2</u>	30
Introductory review of scientific literature pertaining to Abdominal Aortic Aneurysm (AAA) stent-grafts with emphasis on past and present problems and future prospects	
2.1 Introduction	31
2.1.1 Epidemiology and Natural History of AAAs	31
2.1.2 Surgical management of Abdominal Aortic Aneurysms	33
2.1.3 Introduction to Endovascular aneurysm repair	33
2.1.4 Early Devices	35
2.1.5 Basic Design	35

2.1.6	Current Devices	36
2.1.7	EVAR ineligibility due to complex aortic anatomy	40
2.2	EVAR Failure Mechanisms	40
2.2.1	Profile of Delivery systems	40
2.2.2	Endoleaks and Graft Migration	42
2.2.2.1	Type I and Migration	43
2.2.2.2	Type II	45
2.2.2.3	Type III	45
2.2.2.4	Type IV	47
2.2.3	Endotension	47
2.2.4	Stent fatigue and fracture	49
2.2.5	Deployment Problems and Repositioning	50
2.2.6	Limb occlusion	50
2.2.7	Biocompatibility	51
2.2.8	Compliance Mismatch	52
2.2.9	Aortoduodenal fistulas	52
2.2.10	AAA Rupture	53
2.2.11	Secondary interventions and mortality	54
2.3	Outcomes based on anatomic and device-specific analysis	57
2.3.1	Cook Zenith	57
2.3.2	Gore Excluder	57
2.3.3	Medtronic AneuRx	58
2.3.4	Medtronic Talent	58
2.3.5	Endologix Powerlink	58
2.4	Further discussion	59
2.4.1	The EVAR Trial I	59
2.4.2	The EVAR Trial II	59
2.4.3	DREAM Trial	60
2.4.4	EUROSTAR Registry	61
2.5	Conclusions &Prospects for the future	64
2.6	Hypothesis, Aim & Objectives	66

Chapter 3

Design and analysis of aortic stent-grafts based on an engineered approach using surface modified Nitinol and a Nanocomposite polymer

3.1	Introduction	69
3.2	Development of an endovascular stent-graft for AAA using Origami folding technology	70
3.2.1	Origami pattern in polymer	71
3.2.2	Moulding	72
3.2.2.1	Model	72
3.2.2.2	Dip coating procedure	73
3.2.2.3	Results and discussion	74
3.2.3	Casting approach	74
3.2.3.1	Method	75
3.2.3.2	Results and discussion	75
3.2.4	Scaffold	77
3.2.5	Adhesion testing	79
3.2.5.1	Results and discussion	83
3.2.6	Scaffold manufacture	84
3.2.7	Graft manufacture	85
3.2.8	Assembled prototype	86
3.3	Mechanical testing of Nitinol alloy	87
3.3.1	Materials and methods	87
3.3.2	Results and discussion	89
3.4	Development of a curved thoracic endovascular stent-graft	90
3.5	Conclusion	94

Chapter 4 **95**

Development of an aortic model for the physiological assessment of an advanced stent-graft system and *in vitro* compliance measurement

4.1	Introduction	96
------------	---------------------	-----------

4.2	Methods and Materials	97
4.2.1	Acquisition of porcine abdominal aorta	97
4.2.2	Development of an aortic model using a novel nanocomposite polymer	98
4.2.3	Latex synthetic aortic model	98
4.2.4	Compliance methodology	98
4.2.4.1	Flow Circuit	98
4.2.4.2	Measurement of vessel wall movement	101
4.2.5	Data Analysis and Statistical Methods	102
4.3	Results	103
4.3.1	Flow Circuit hemodynamic values	103
4.3.2	Compliance and stiffness value averaged over entire mean pressure range for porcine aorta, and latex and polymer synthetic aortas	105
4.4	Discussion	109
4.4.1	Methodological considerations	110
4.4.2	Anisotropy and Isotropy	110
4.4.3	Comparison of compliance of porcine abdominal aorta and synthetic polymer and latex models	111
4.4.4	Utility of B stiffness index for in vitro measurements	112
4.4.5	Compliance match between model and graft material	112
4.4.6	Limitations	113
<u>Chapter 5</u>		114
	Fatigue Analysis and Accelerated Durability Testing of AAA stent graft based on Nitinol scaffold bonded to a Nanocomposite polymer	
5.1	Introduction	115
5.2	Methods and Materials	116
5.2.1	Fabrication of a sutureless non-modular aortic stent-graft	116
5.2.2	Fatigue-testing circuit	119
5.2.3	Surface topography	121
5.2.3.1	Scanning electron microscopy	121

5.2.3.2	Fourier transform infrared spectroscopy	121
5.2.4	Compliance analysis	122
5.2.5	Mechanical resistance and elasticity	122
5.2.5.1	Radial stress-strain studies	122
5.2.5.2	Linear elasticity	124
5.2.6	Thermo-mechanical resistance	124
5.2.6.1	Differential scanning calorimetry	124
5.2.6.2	Thermo-mechanical analysis	125
5.2.7	Acceptance Criteria	125
5.2.8	Statistical analysis	126
5.3	Results	126
5.3.1	Surface topography and migration	127
5.3.1.1	Visual inspection and scanning electron microscopy	127
5.3.1.2	Fourier transform infrared spectroscopy	131
5.3.2	Compliance analysis	132
5.3.3	Mechanical strength and elasticity	134
5.3.3.1	Radial stress-strain studies	134
5.3.3.2	Linear elasticity	136
5.3.4	Thermo-mechanical resistance	138
5.3.4.1	Differential scanning calorimetry	138
5.3.4.2	Thermo-mechanical analysis	139
5.4	Discussion	140
5.5	Conclusion	143
<u>Chapter 6</u>		144
A Nanocomposite Polymer Based Thoracic Endoprosthesis to Improve Aortic Compliance Mismatch Following Endovascular Repair		
6.1	Introduction	145
6.2	Methods	147
6.2.1	Material properties for the curved stent-graft	147
6.2.2	Design of a curved stent-graft for thoracic aorta and the aortic arch	149

6.2.3	Stent-graft control	149
6.2.4	Flow phantom	150
6.2.5	Measurement of vessel wall movement	152
6.2.6	Haemodynamic and arterial parameters	153
6.2.7	Statistical analysis	154
6.3	Results	155
6.3.1	Stent-graft design	155
6.3.2	Compliance measurement	156
6.3.3	Stiffness index	158
6.4	Discussion	159
6.5	Limitations	161
6.6	Conclusions	161
 <u>Chapter 7</u>		162
 Magnetic Resonance Signal Attenuation and Image Artefact Testing of a Nanocomposite Polymer Nitinol Thoracic Stent-graft		
7.1	Introduction	163
7.2	Methods	164
7.2.1	Magnetic resonance imaging (MRI) assessment	164
7.2.1.1	Static fluid MRI signal assessment	165
7.2.1.2	Flow encoded MRI signal assessment	166
7.2.2	Statistical analysis	168
7.3	Results	168
7.3.1	Stent-graft design	168
7.3.2	Subjective data analysis for image artefact testing	168
7.3.3	Objective data analysis for signal magnitude on image artefact testing	170
7.3.4	Analysis of flow measurement	173

7.4	Discussion	174
7.5	Conclusion	177
	<u>Chapter 8</u>	178
	Discussion, Conclusions & Future work	
8.1	Discussion	179
8.1.1	Endovascular stent-grafts	180
8.1.2	Contemporary graft materials	180
8.1.3	POSS-PCU nanocomposite polymer as graft material	181
8.1.4	Metallic stent designs in modern endografts and folding efficiency	182
8.1.5	Bonding versus suturing of graft material to metal skeleton	183
8.1.6	Physiological model for in vitro testing	183
8.1.7	Long-term fatigue and durability analysis	185
8.1.8	The curved design: the first step towards a new branched endograft	186
8.1.9	Improving compliance mismatch: POSS-PCU versus ePTFE	187
8.1.10	Magnetic Resonance Imaging conditioning: mandatory in new designs	188
8.2	Conclusion and Future work	188
	<u>References and Bibliography</u>	191

ABSTRACT

Objective:

To use a novel nanocomposite polymer based on polyhedral oligomeric silsesquioxane-poly(carbonate-urea)urethane with superior bio-mimetic properties in the development of endovascular stent-grafts.

Methods:

A self-expanding and sutureless aortic stent-graft was developed using nanocomposite polymer bonded to Nitinol. A new aortic model was designed for physiological assessment of stent-grafts and compliance and viscoelasticity were measured and compared with porcine aortas as control. The stent-grafts (n=4) were fatigue tested using *in vitro* accelerated model for 400-million cycles equivalent to 10-years in human body and compared with zero-cycled control. A curved and conformable stent-graft was developed for thoracic aorta and aortic arch. Compliance and stiffness index of the thoracic stent-graft were measured *in vitro* and compared to FDA-approved Gore TagTM stent-graft based on ePTFE (expanded polytetrafluoroethylene). MRI compatibility of the thoracic stent-graft was assessed by analysing signal attenuation and velocity measurements (flux) and compared to FDA-approved Medtronic ValiantTM.

Results:

The stent-graft had expanded diameter of 31.1 mm and was successfully collapsed to 6.5 mm to achieve delivery profile similar to current devices. The thoracic stent-graft had uniform graft thickness of $150.7 \pm 6.6 \mu\text{g}$ and conformed to the curvature of aortic arch. The new aortic model was significantly more compliant than porcine aortas with no significant difference in elastic stiffness. All the stent-grafts successfully completed accelerated pulsatile fatigue testing. Scanning electron microscopy images confirmed

uniform surface topography. There was no loss of tensile strength, or compliance and no evidence of thermo-mechanical degradation in the nanocomposite polymer. Compliance of the thoracic stent-graft was significantly better compared with ePTFE stent-graft (3.3 ± 0.61 vs. 2.3 ± 0.95 %/mm Hg $\times 10^{-2}$; $P=0.0003$). On MRI, there was no significant signal attenuation and no significant difference in flux between Valiant and nanocomposite polymer stent-grafts (102 ± 2.27 vs. 99.8 ± 2.4 ml/sec; $P=0.33$).

Conclusions:

A new endovascular stent-graft based on novel design and nanocomposite polymer with properties of compliance, viscoelasticity, anti-thrombogenicity and MRI compatibility has been developed. Sutureless technology with new biocompatible material bonded to Nitinol stents proved to be robust with no separation over accelerated 10-year cycle. These stent-grafts have the potential to address poor long-term durability, thrombogenicity, and compliance mismatch associated with present generation devices and reduce reintervention rate.

AWARDS

1. Charles Clarke Memorial Prize, University College London **22 Oct 2010**
2. Circulation Foundation Clinical Research Fellowship and grant of £20,000, Circulation Foundation, **14 Aug 2009**
3. Divisional Student Conference Fund (£250), University College London, **9 May 2010**
4. Nomination for BJS Prize 2008 for Best Scientific Paper: Presentation at the Vascular Society of Great Britain and Ireland Annual General Meeting, Bournemouth, **12 Nov 2008**

PUBLICATIONS

Peer-reviewed Manuscripts

1. **Desai M**, Bakhshi R, Zhou X, Odlyha M, You Z, Hamilton G, Seifalian AM. A sutureless endovascular aortic stent-graft based on nitinol scaffold bonded to nanocomposite polymer is durable for ten years in a simulated in vitro model. *J Endovasc Ther.* 2012 Jun; 19(3): 415-27.
2. **Desai M**, Ahmed M, Darbyshire A, You Z, Hamilton G, Seifalian AM. An aortic model for the physiological assessment of endovascular stent-grafts. *Ann Vasc Surg* 2011 May; 25(4): 530-7. PMID: 21439773.
3. **Desai M**, Eaton-Evans J, Hillery C, Bakhshi R, You Z, Lu J, Hamilton G, Seifalian AM. AAA Stent-Grafts; Past Problems and Future Prospects. *Ann Biomed Eng* 2010 Apr; 38(4): 1259-75. PMID: 20162359.

In Progress

1. **Desai M**, Ahmed M, Zhou X, You Z, Seifalian AM, Hamilton G. A Nanocomposite Polymer Based Thoracic Endoprosthesis to Improve Aortic Compliance Mismatch Following Endovascular Repair.

2. **Desai M**, Clough RE, Gaddum NR, Rhode K, Zhou X, You Z, Hamilton G, Seifalian AM. Design of a Nanocomposite Polymer Nitinol Thoracic Stent-graft and *in vitro* Evaluation of Signal Attenuation during Magnetic Resonance Imaging.

Abstracts

1. **Desai M**, Ahmed M, Zhou X, You Z, Seifalian AM, Hamilton G. A Nanocomposite Polymer Based Thoracic Endoprosthesis to Improve Aortic Compliance Mismatch Following Endovascular Repair. *Br J Surg* **2012**; 99(S4): 16.
2. **Desai M**, Clough RE, Gaddum NR, Rhode K, Zhou X, You Z, Seifalian AM, Hamilton G. Design of a Nanocomposite Polymer Nitinol Thoracic Stent-graft and *in vitro* Evaluation of Signal Attenuation during Magnetic Resonance Imaging. *Br J Surg* **2012**; 99(S4): 14-5.
3. **Desai M**, Bakhshi R, Darbyshire A, Ahmed M, Eaton-Evans J, Zhou X, You Z, Seifalian AM, Hamilton G. Thermo-Mechanical Resistance of a Nanocomposite Polymer Exposed to Simulated *in Vivo* Hydrodynamic Fatigue for Ten Years in Development of a Sutureless Endovascular Stent-graft. *J Vasc Surg* **2011**; 53(17S): 86S.
4. **Desai M**, Bakhshi R, Darbyshire A, Zhou X, You Z, Odlyha M, Seifalian AM, Hamilton G. Durability of a sutureless endovascular stent-graft based on nitinol scaffold bonded to a nanocomposite polymer. *Br J Surg* **2011**; 98(S2): 32-3.
5. **Desai M**, Bakhshi R, You Z, Seifalian A, Hamilton G. Thermo-mechanical resistance of a nanocomposite polymer exposed to simulated *in vivo* fatigue in the development of an endovascular stent-graft. *Br J Surg* **2011**; 98(S5): 52-3.
6. **Desai M**, Ahmed M, Darbyshire A, Seifalian AM, Hamilton G. An Aortic Model for Physiological Assessment of Aortic Stent-grafts and *In Vitro* Compliance Measurement. *J Vasc Surg* **2010**; 51(11S): 76S.

7. **Desai M**, Ahmed M, Darbyshire A, Seifalian AM, Hamilton G. An aortic model for physiological assessment of aortic stent-grafts and in vitro compliance measurement. *Br J Surg* **2010**; 97(S2): 194.

PRESENTATIONS

1. **A conformable and compliant nanocomposite polymer stent-graft for endovascular repair of aortic arch**
Oral presentation at Vascular Research Initiatives Conference (VRIC) and oral/poster presentation at Arteriosclerosis, Thrombosis & Vascular Biology 2012 Scientific Sessions, Chicago, USA, *18-20 Apr 2012*
2. **Stationary signal and flow velocity assessment by MRI of a new nitinol nanocomposite polymer stent-graft**
Poster presentation at Arteriosclerosis, Thrombosis & Vascular Biology 2012 Scientific Sessions, Chicago, USA, *18-20 Apr 2012*
3. **A nanocomposite polymer based thoracic endoprosthesis to improve aortic compliance mismatch following endovascular repair**
Oral presentation at Society of Academic and Research Surgery (SARS) Annual Meeting, Nottingham, UK, *4 Jan 2012*
4. **Magnetic resonance signal attenuation and image artefact testing of a nanocomposite polymer nitinol thoracic stent-graft**
Oral presentation at Society of Academic and Research Surgery (SARS) Annual Meeting, Nottingham, UK, *4 Jan 2012*
5. **Thermo-mechanical resistance of a nanocomposite polymer exposed to simulated in vivo fatigue in the development of an endovascular stent-graft**

- ❖ Oral presentation at ASGBI International Congress, Bournemouth, UK, *13 May 2011*
 - ❖ Poster and e-poster presentations at Arteriosclerosis, Thrombosis & Vascular Biology scientific sessions, Chicago, USA, *28-30 Apr 2011*
 - ❖ Poster & short oral presentation at SVS Vascular Annual Meeting, Chicago, USA, *16-18 Jun 2011*
- 4. Durability of a sutureless endovascular stent-graft based on Nitinol stents bonded to a Nanocomposite polymer (Winner of Charles-Clarke Memorial Prize)**
- ❖ Oral presentation at SARS Annual Meeting, Dublin, *6 Jan 2011*
 - ❖ Oral presentation at Pearce Gould Visiting Professor meeting, University College London Medical School, *22 Oct 2010*
- 5. An endovascular stent-graft for aortic aneurysms using a Nanocomposite polymer: Concepts and Analysis (Winner of Charles-Clarke Memorial Prize)**
- Oral presentation at Pearce Gould Visiting Professor meeting, University College London Medical School, *22 Oct 2010*
- 6. Development and analysis of new aortic stent-grafts based on a Nanocomposite polymer**
- Invited for poster presentation at 2010 Annual Meeting of Vascular Society of Great Britain and Ireland, Brighton, *24-26 Nov 2010*
- 7. Development Of An Innovative Endovascular Stent-graft For Aortic Aneurysms Using A Nanocomposite Polymer**

Interactive poster presentation at 12th Biennial Meeting of the International Society for Applied Cardiovascular Biology, Cambridge, USA, *22-25 Sep 2010*

8. An aortic model for the physiological assessment of aortic stent-grafts and *in vitro* compliance measurement

- ❖ Oral presentation at SVS Research Initiative in Vascular Disease, San Francisco, USA, *7 Apr 2010*
- ❖ Poster presentation at the ASGBI Surgical Congress, Liverpool, UK, *14-16 Apr 2010*
- ❖ Poster and short oral presentation at SVS Vascular Annual Meeting, Boston, USA, *11 Jun 2010*

9. Novel nanocomposite polymer for the development of a new aortic stent-graft (Nomination for BJS Prize for Best Scientific Paper)

Oral presentation at Vascular Society of Great Britain and Ireland Annual General Meeting, Bournemouth, UK, *12 Nov 2008*



DEDICATION

*To my parents, my beautiful wife Manasi
and to Vivaan, the loveliest kid in the world
who has enriched my life more than
I could have ever imagined*

ACKNOWLEDGEMENTS


This work is the result of an excellent collaboration between different researchers within the Division of Surgery and Interventional Science at University College London. Therefore I would like to express my sincere gratitude to those that were indispensable for my MD project.

I am forever grateful to Professor George Hamilton for believing in my abilities and inspiring me to achieve my full potential. Thank you for giving me the opportunity to carry out this project and providing immense supervision and support and also for involving me in several other prestigious projects within the department.

I wish to express my deepest gratitude to Professor Alexander M Seifalian, whose unending supervision, help and patience have been invaluable. Thank you very much for your unremitting support and confidence in finding my own path to get the work done, for your constructive criticism and for helping me stay focused.

There are so many others in the Department of Engineering at Oxford University and Department of Surgery at University College London who have given me constant support and encouragement. My sincerest thanks to Dr. James Eaton-Evans, Dr Xiang Zhou and Dr Zhong You at Oxford and Dr. Raheleh Bakhshi and Mr Maqsood Ahmed at UCL, and most particularly to Mr. Arnold Darbyshire. This work would have not been possible without all his help and advice. Thank you also for all the insightful conversations and valuable comments.

I am very grateful to all staff and my colleagues at Department of Vascular Surgery at Royal Free Hospital for their constant support and most of all for their friendship. In particular, I want to extend my sincere thanks to Miss Janice Tsui for her considerable help and for giving me motivation and encouragement.



I am obliged to Circulation Foundation for their generous grant of £20, 000. I would also like to thank EPSRC for their financial support.

And most importantly my thanks go to my dearest parents, my lovely wife Manasi and my beloved son Vivaan for their sacrifice, love and support in numerous ways on my personal development.

LIST OF ABBREVIATIONS

3D	Three Dimensional
AAA	Abdominal Aortic Aneurysm
ADF	Aorto-duodenal Fistula
ARM	Aneurysm-related Mortality
ASTM	American Society for Testing and Materials
ATR	Attenuated Total Reflectance
C	Compliance
CG	Cationised Gelatin
CI	Confidence Interval
CT	Computed Tomography
CTA	Computed Tomography Angiography
Diff.	Difference
DMAC	N-dimethylacetamide
Dd	Diastolic Diameter
Ds	Systolic Diameter
DSC	Differential Scanning Calorimetry
EHDA	Electrohydrodynamic Atomisation
EM	Electron Microscopy
Ep	Peterson's Elastic Modulus
ePTFE	Expanded Polytetrafluoroethylene
EUROSTAR	The European Collaborators on Stent-Graft Techniques for AAA and Thoracic Aortic Aneurysm and Dissection Repair
EVAR	Endovascular Aneurysm Repair
FDA	Food and Drug Administration
FFE	Fast Field Echo
FTIR	Fourier Transform Infrared Spectroscopy

Fr	French
ICU	Intensive Care Unit
LVH	Left Ventricular Hypertrophy
MDI	Methylene Di-isocyanate
MR	Magnetic Resonance
MRA	Magnetic Resonance Angiography
MRI	Magnetic Resonance Imaging
NiTi	Nitinol
NP	Nanocomposite Polymer
OVER	Open vs. Endovascular Repair
OSR	Open Surgical Repair
PCU	Poly (carbonate-urea) Urethane
Pd	Diastolic Pressure
POSS	Polyhedral Oligomeric Silsesquioxanes
Ps	Systolic Pressure
PTFE	Polytetrafluoroethylene
PU	Polyurethane
RCT	Randomised Clinical Trial
RF	Radiofrequency
ROI	Region of Interest
SAR	Specific Absorption Rate
SD	Standard Deviation
SEM	Scanning Electron Microscopy
TAA	Thoracic Aortic Aneurysm
TEVAR	Thoracic Endovascular Aneurysm Repair
T _g	Glass Transition Temperature
TiO ₂	Titanium Oxide
T _m	Melting Temperature
TMA	Thermo-mechanical Analysis

LIST OF FIGURES

Figure 2.1: Schematic diagrams showing (A) abdominal aortic aneurysm before endovascular intervention and (B) aneurysm post-intervention with a stent-graft *in situ*

Figure 3.1: Plaster of Paris used to cast models of Origami pattern. Plaster casting arrangement (A) and Plaster of Paris origami model (B)

Figure 3.2: NP defined with origami pattern using casting method with number of rows of rectangular elements (A), Folded version of A showing collapse efficiently to a minimum volume (B)

Figure 3.3: Thin walled cylinder folding pattern. Scaffold orientation in opposing fashion as indicated by dashed lines.

Figure 3.4: Shape setting of zigzag pattern with wire constrained in pins in a rig (A) and helical pattern with zigzag wire hoops placed around a collapsible mandrel (B)

Figure 3.5: Zigzag superelastic wire hoop (A) and wire hoop series (B)

Figure 3.6: Peel test arrangement. Polymer coating held at the top grip and nitinol wire at the bottom grip. Arrow shows the moving directions of the grips

Figure 3.7: Peel strength test for untreated and treated NiTi strip. Graph shows peel extension in mm in comparison to the load applied in N (◇) 100 μm electrospayed coating on treated NiTi; (◆) 50 μm electrospayed coating on treated NiTi; (■) Cast coating on treated NiTi; (●) Untreated NiTi.

Figure 3.8: Combined peel strength test for untreated and treated NiTi strip with peel extension in mm on X-axis and load (N) applied on Y-axis

Figure 3.9: (a) Stent-graft first prototype alongside paper model of desired folding pattern and (b) perspective view of stent-graft in expanded and folding configurations

Figure 3.10: Stent-graft modified prototype with removal of nitinol straight-wire segments (from first prototype) due to concern about graft material perforation

Figure 3.11: Custom-designed grips used for tensile testing of NiTi strip. Front view on the left and sectional view on the right.

Figure 3.12: Mechanical response of NiTi strip. The stress-strain curve showed in this graph following a non-linear loop characteristic of nitinol.

Figure 3.13: Schematic diagram showing step-wise development of a curved stent-graft. Aortic arch dimensions from patient's MRI used and 3D mandrel developed which is dip-coated with POSS-PCU polymer.

Figure 3.14: A curved stent-graft in fully expanded shape and matching curvature of aortic arch.

Figure 4.1: Diagrammatic representation of the flow model used for measurement of compliance and elastic stiffness index. ADC, analogue-to-digital data acquisition recording system; FWC, flow waveform conditioner; MHFO, maxima hollow fibre oxygenator (Medtronic, Anaheim, CA, USA); P₁ and P₂, Millar Mikro-tip pressure transducer; TMF, Transonic Medical flowmeter system; VSECP, variable-speed electromagnetic centrifugal pump; WTS, wall-tracking system

Figure 4.2: Distention-time curve generated by wall-tracking system to show change in vessel wall diameter with each cardiac cycle. Distention in μm on X-axis and time in seconds on Y-axis

Figure 4.3: Compliance-Mean Pressure curves for porcine aorta, polymer and latex models. Data presented as mean and error bars represent standard deviation

Figure 4.4: Stiffness Index-Mean Pressure curves for porcine aorta, polymer and latex models. Data presented as mean and error bars represent standard deviation

Figure 4.5: Latex model showing significant distension on increasing mean pressure from 90 mm Hg to 120 mm Hg

Figure 5.1: Three-dimensional structure of polyhedral oligomeric silsesquioxane molecule with hard and soft segments of polyurethane attached to POSS nanocage.

Figure 5.2: Final assembled stent-graft prototype deployed in a compliant polymer model, ready to be implanted in the fatigue-testing circuit.

Figure 5.3: Schematic of the pulsatile flow circuit used in the experiment. Sample-holder connected to the pumping system and monitor. A valve controlling pressure and motor connected to eccentric and linked to diaphragm by connecting rod.

Figure 5.4: Schematic for stress-strain studies. The polymer film clamped in the pneumatic machine grips.

Figure 5.5: Images of the stent-grafts post-fatigue testing. Visual inspection revealed intact polymer and nitinol with no signs of breakage.

Figure 5.6: Scanning electron microscopy images of stent-grafts (160X magnification). (a) Inner surface of zero-cycled control POSS-PCU (b) Outer surface of control POSS-PCU (c) Inner surface of fatigue-tested POSS-PCU (d) Outer surface of fatigue-tested POSS-PCU. No significant signs of degradation seen.

Figure 5.7: Fourier transform infrared spectroscopy curves for POSS-PCU (fatigue-tested and control). Wavelength on X-axis and %Transmittance on Y-axis.

Figure 5.8: Comparison of the intensity of main bonds of fatigue-tested and control POSS-PCU by FTIR (%Transmittance based on their wavelengths)

Figure 5.9: Compliance study results across mean pressure range 60-120 mm Hg. Columns represent mean values and error bars represent standard deviation. Fatigue-tested POSS-PCU in red and control POSS-PCU in blue.

Figure 5.10: Combined compliance results of fatigue-tested (F) and control (C) specimens. Data presented as mean and error bars represent standard deviation

Figure 5.11: Stress-strain curve of fatigue-tested (F) and control (C) POSS-PCU. Data presented as mean and error bars represent standard deviation.

Figure 5.12: Linear elasticity test. Data presented as mean. Length stretched in % on X-axis and distance in mm on Y-axis.

Figure 5.13: DSC thermal analysis curves of fatigue-tested and control POSS PCU specimens. Temperature in °C on X-axis and DSC in mW/mg on Y-axis.

Figure 5.14: Typical TMA thermo-graph curve of POSS PCU (fatigue-tested and control specimens). Temperature in °C on X-axis and TMA (%) on Y-axis.

Figure 6.1: Diagrammatic representation of the flow model used for measurement of compliance and elastic stiffness index. ADC, analogue-to-digital data acquisition recording system; FWC, flow waveform conditioner; MHFO, maxima hollow fibre oxygenator (Medtronic, Anaheim, CA, USA); P₁ and P₂, Millar Mikro-tip pressure transducer; TMF, Transonic Medical flowmeter system; VSECP, variable-speed electromagnetic centrifugal pump; WTS, wall-tracking system

Figure 6.2: Distension-time curve generated by wall-tracking system. The Y-axis is represented by Distention in μm on the graph above and Pressure in mm of Hg in the graph below. The time in seconds is on X-axis for both the graphs

Figure 6.3: A fully expanded curved stent-graft from POSS-PCU NP bonded to nitinol and having curvature similar to aortic arch

Figure 6.4: The smooth inner surface of the stent-graft with uniform thickness and curved design.

Figure 6.5: Compliance results. Data presented as mean values. Pressures in mm Hg on X-axis and Compliance in $\%/\text{mm Hg} \times 10^{-2}$ on Y-axis.

Figure 6.6: Elastic Stiffness Index Results. Data presented as mean values. Pressures in mm Hg on X-axis and Elastic stiffness index β on Y-axis

Figure 7.1: Phantom setup for NP stent-graft. Stent-grafts were scanned separately in a glass cylindrical container filled with water dosed with 10mL gadopentetate dimeglumine.

Figure 7.2: Schematic diagram illustrating the MRI flow phantom setup. Large elevated fluid reservoir connected to fluid tank on the floor using Tygon tubing. Stent-grafts positioned as shown with corresponding uncovered tubing for baseline comparison.

Figure 7.3: MR static images for Medtronic ValiantTM stent-graft. Minimal susceptibility artefacts were seen, however the image quality was good.

Figure 7.4: MR static images for NP stent-graft. No significant susceptibility artefacts affecting imaging quality were seen.

Figure 7.5: Axial slice from Medtronic ValiantTM stent-graft showing signal magnitude inside and outside used to calculate % signal attenuation.

Figure 7.6: Axial slice from NP stent-graft showing signal magnitude inside and outside used to calculate % signal attenuation.

Figure 7.7: Velocity flux comparison for Medtronic and NP stent-grafts. Columns represent mean values and error bars represent standard deviation

LIST OF TABLES

Table 2.1 General characteristics of the various grafts available on the US and EU markets.

Table 2.2 Patient numbers and endpoints from pivotal clinical trials for the various stent-grafts

Table 2.3 Categorisation of Endoleaks

Table 2.4 Possible etiologies of endotension

Table 2.5 Incidence rates of EVAR failure modes at different time-points

Table 4.1 Typical Flow Circuit haemodynamic values (mean \pm SD)

Table 4.2 Compliance (C) and Stiffness index (β) values across a range of pressures

Table 5.1: Test parameters from fatigue-testing circuit

Table 5.2: Test parameters for flow circuit to measure compliance

Table 5.3: Radial stress-strain results

Table 5.4: Linear elasticity test results

Table 6.1: Typical Flow Circuit haemodynamic values (mean \pm SD)

Table 6.2: Typical Mechanical Properties of POSS-PCU



Chapter 1

**Polyhedral oligomeric silsesquioxane nanomaterials for cardiovascular
applications**

Nanocomposites are materials whose components are mixed at a nanometer scale. Due to their quantum-scale sizes, they can serve as bridges between molecules in the polymer. This nature allows them to exhibit different properties from conventional microcomposites. Their behavior is governed by the method of nano-reinforcement, the nano-interface, the synthetic process utilised, its microstructural effects, and the interaction between the polymeric and reinforcing component.

Nanostructured composite materials are combinations of at least two constituent materials, a matrix (host) and a reinforcement component (guest, nanofiller)¹. It is known that the properties of the materials change considerably when the size is significantly small, i.e, within 1–100 nm size range. Since these materials have improved physical, chemical, and mechanical properties, they are significantly versatile for a wide range of applications. The method by which nanomaterials are synthesised is a crucial factor behind the behavior of nanocomposite materials.

1.1 Polyhedral Oligomeric Silsesquioxane (POSS)

The chemical structure of the silsesquioxane family is defined as $R_nSi_nO_{1.5n}$, which makes a structure consisting of an inner inorganic framework of silicon and oxygen atoms, externally covered by organic groups (R). Conventionally, cage-like silsesquioxanes appear as polyhedral oligosilsesquioxanes or polyhedral oligomeric silsesquioxanes (POSS). POSS is one of the molecules in the silsesquioxane family which has a regular three-dimensional (3D) shape (polyhedral = many-side, 3D) formed by a few units (oligomeric), each containing silsesquioxane. Incorporation of POSS can change the surface properties including hydrophobicity, surface energy, and surface topography. Physical and thermal properties improved by incorporation of POSS include, low dielectric constants, increased glass transition temperature, low coefficient of thermal expansion, thermal stability, and heat evolution². Improvement in the mechanical properties comprise tensile strength, viscosity, and enhanced viscoelastic

properties³. Further improvements have also been reported such as improved oxidation resistance, reduction of inflammability, oxygen permeability, and reduced inflammatory reactions, revealing the advantage of using these materials in various applications⁴. The unique characteristics of POSS nanoparticles offers diverse application potential in a wide range of areas, including the biomedical field, which is intensely under investigation.

1.2 Cardiovascular applications of POSS

Application of biomaterials in cardiovascular system and blood contacting devices necessitates specific characteristics such as blood compatibility and antithrombogenicity. To meet the essential requirements for these applications, we have developed a nanocomposite material by introducing POSS moieties into poly(carbonate-urea)urethane (POSS-PCU) as a pendant chain. Studies on its cytocompatibility, antithrombogenicity, and biostability have shown that this new nanocomposite polymer has unique characteristics for these applications.⁵ The enhanced characteristics of POSS-PCU make it an ideal material of choice for the development of advanced cardiovascular implants. This polymer is currently being used in the fabrication of many biomedical devices, including synthetic leaflet heart valves, percutaneous valve prostheses, small and large diameter bypass graft, and coated stents.

Development of new generation implants based on advanced novel materials can potentially overcome the main problems in current clinical practice. The candidate material for this particular application should offer enhanced hemocompatibility and biostability to ensure improved long-term performance of the implant. POSS-PCU, as a paradigm POSS material, is a pioneering prototype of advanced novel materials which possesses superior hemocompatibility, biostability, antithrombogenicity, and calcification resistance, owing to its enhanced physicochemical properties and nano-reinforced structure and surface nanotopography. Its superior properties compared with

conventional polymers are among the main advantages of using this material in the cardiovascular system. Early results of the development of small diameter bypass grafts and heart valve prototypes using this novel nanocomposite have been very promising.

1.3 Prospects

With a nanocomposite suitable for cardiovascular application, attempts are now focused on development of new generation cardiovascular devices with improved hemocompatibility and long-term performance. If successful in the long run, the clinical implications would be tremendous, as the superior properties of the new generation cardiovascular implants could overcome the complications and limitations of currently available devices. Projects on the development of percutaneous heart valves, and coated stents based on these POSS containing novel nanocomposites are currently active. In addition, small diameter POSS-PCU graft has recently shown exceptional results in an in vivo study and will undergo clinical trial in coronary artery bypass grafting and renal access soon. Besides the mentioned properties, resistance to calcification, enhanced mechanical and surface properties, capability of grafting bioactive peptides to enhance attachment, proliferation, and differentiation of circulatory stem cells into endothelial cells are among other advantages of using these materials in the development of cardiovascular devices. By the emergence of new generation cardiovascular devices based on POSS nanomaterials, it is likely to overcome some of the major problems of current implants, saving lives and improving the quality of life of a significant number of patients.

In this work, we present the use of POSS-PCU for development of endovascular stent-grafts for abdominal aortic aneurysms and thoracic aortic pathologies, based on engineering approaches to achieve optimum folding efficiency and superior durability.



Chapter 2

Introductory review of scientific literature pertaining to Abdominal Aortic Aneurysm (AAA) stent-grafts with emphasis on past and present problems and future prospects

Endovascular aneurysm repair (EVAR) has quickly gained popularity for infrarenal abdominal aortic aneurysm (AAA) repair during the last 2 decades. The improvement of available EVAR devices is critical for the advancement of patient care in vascular surgery. Problems are still associated with the grafts, many of which can necessitate the conversion of the patient to open repair, or even result in late rupture of the aneurysm. This review attempts to address these problems, by highlighting why they occur and what the failings of the currently available stent-grafts are, respectively. In addition, the review gives critical appraisal as to the novel methods required for dealing with these problems and identifies the new generation of stent-grafts that are being or need to be designed and constructed in order to overcome the issues that are associated with the existing first and second-generation devices.

2.1 INTRODUCTION

2.1.1 Epidemiology and natural history of AAA

AAA occurs when weakened areas of abdominal aortic wall result in ballooning of the blood vessel. An AAA is defined as an enlargement of the aorta of at least 1.5 times its normal diameter or greater than 3 cm diameter in total. AAAs are more commonly located in an infra-renal position. Attributed risk factors include increased age, smoking, atherosclerosis and hypertension⁶. AAAs are about 3 times more common in men than in women. They account for 1.81% of deaths in people over the age of 65 years in England and Wales, with an incidence of 3.5 new aneurysms occurring for every 1000 person years⁷.

Most AAAs are detected incidentally during clinical investigation (for example, ultrasound or X-ray) for other conditions. Because most AAAs are asymptomatic, it is difficult to estimate their prevalence, but screening studies in the UK have estimated a

prevalence of 1.3–12.7% depending on the age group studied⁸. The incidence of symptomatic AAA in men is approximately 25 per 100,000 at age 50, increasing to 78 per 100,000 in those older than 70 years⁸. The implementation of a national screening programme for AAA is under way and the first centres started screening in March 2009. The remaining centres will be managed in a phased roll-out over the next 5 years.

Symptoms that can occur as an aneurysm enlarges include a pulsating sensation in the abdomen, back pain and abdominal pain that may spread to the back. Patients with a symptomatic AAA need rapid medical attention. Among patients with a ruptured AAA the mortality rate is about 80% which increases up to 90% when in-hospital deaths are included⁹. Even when they undergo emergency surgery, only about half survive beyond 30 days. It has long been established that, for large aneurysms at least, prophylactic measures are required to prevent aneurysm rupture⁷ and one in three aneurysms will rupture if left untreated¹⁰. The risk of rupture increases with the size of the aneurysm, and those aneurysms larger than 6 cm in diameter have an annual risk of rupture of 25%.

Several studies indicate that without surgery the 5-year survival rate for patients with aneurysms larger than 5 cm is about 20%⁸. In current UK clinical practice, elective surgery is generally recommended for patients with aneurysms larger than 5.5 cm in diameter and with aneurysms larger than 4.5 cm in diameter that have increased by more than 0.5 cm in the past 6 months. Current guidelines from the Vascular Society and the National Screening Committee recommend that patients with asymptomatic aneurysms of less than 4.5 cm in diameter should be followed up with ultrasonography every 6 months, and aneurysms of 4.5–5.5 cm in diameter should be followed up every 3 or 6 months.

2.1.2 Surgical Management of Abdominal Aortic Aneurysms

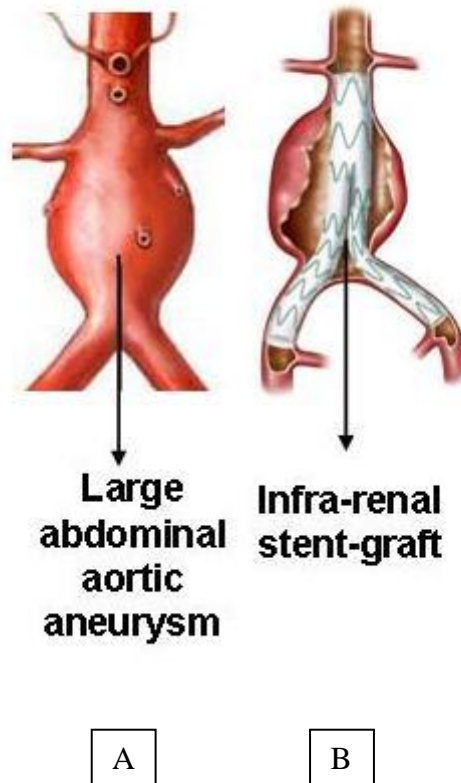
Patients can be treated by conventional open surgical repair (OSR) which involves laparotomy and insertion of a prosthetic graft to replace the aneurysmal aorta. OSR can also be performed laparoscopically, either by hand-assisted laparoscopic surgery or totally laparoscopic surgery. However, AAAs can also be treated by a minimally invasive approach which involves placement of an endoluminal stent-graft through the transfemoral approach. This procedure called as Endovascular Aneurysm Repair (EVAR) has revolutionised the treatment of AAAs in the last 2 decades.

For over half a century, OSR has been used as the standard treatment modality for AAA with a high degree of success, mortality rates having been reduced from 20% to ~5% in the past 30 years¹¹. However, there are still several complications associated with OSR: it is a highly invasive procedure (an incision is made from the sternum to the pubic bone or across the waist) that is most often performed on the elderly. In addition, although mortality rates are reasonably low in uncomplicated cases (5%), higher rates are often associated in those with co-morbid diseases such as coronary artery disease and renal failure¹². OSR may also result in significant harm to the patient, with myocardial infarction, respiratory and renal failure and changes in functional status possibly occurring^{13;14}. Finally, recovery rates are in the region of several months, resulting in a reduction in quality of life for the patients for up to 3 months post-operatively¹⁵.

2.1.3 Introduction to Endovascular aneurysm repair

Because of these problems, and due to the high number of patients for whom OSR was contraindicated, in 1991, Volodos et al¹⁶ reported his clinical experience of using self-fixing synthetic remote endoprosthetics for aorta reconstruction. In the same year, Parodi et al. reported repair of AAA in five subjects using an endovascular approach with a modified stent and graft material¹⁷. The concept of inserting the graft with the metallic stents at either end has been considered before, and at least four

Figure 2.1 Schematic diagrams showing (A) abdominal aortic aneurysm before endovascular intervention and (B) aneurysm post-intervention with a stent-graft *in situ*¹⁸



patents exist for this process¹⁹⁻²². The stent-graft system reported by Parodi was initially developed and patented by Lazarus in 1987²². Lazarus^{22;23} subsequently developed a device specific for endovascular treatment of AAA at the same time as Parodi. In Parodi's report, the device used had just one short stent allowing adequate proximal anchorage only; in most cases reflux at the distal end of the graft was found, and reintervention was required. Nonetheless, a comparative improvement in aneurysm size was found in all patients post-operatively, suggesting that EVAR of AAA was at least technically feasible.

2.1.4 Early devices

Following this initial clinical study, further trials ensued²³⁻²⁵, coupled with rapid commercialisation and the development of the first tube graft, created by Endovascular Technologies (later to be taken over by Guidant, Menlo Park, CA) which was first implanted in 1993. This graft was then further developed into the Ancure device, which has now been withdrawn from the market following a \$92.4 million lawsuit⁹ for failing to report device malfunction and adverse events to the FDA. Since 1993, around 15 other types of stent-grafts have been developed, come to the market and into clinical usage²⁶, with each claiming an advantage over the others. Some, however, have followed the Ancure endograft and have been withdrawn from the market. These include the Vanguard (Boston Scientific, Natick, MA), the Parodi and the Chuter all of which had design flaws, and caused an increased risk to the patient as compared with OSR. In addition, high development costs have seen the withdrawal of the Lifepath by Edwards Lifescience (part of Baxter Healthcare Corp. Irvine, CA), even though the Lifepath recently had positive results from its clinical trial²⁷.

2.1.5 Basic Design

The basic design of all endografts is somewhat similar; the aortic aneurysm is ‘crossed’ by a tubular graft that has a wide diameter (~20-36 mm) and is supported by stents along its length (see Figure 2.1). The tube either bifurcates into two smaller diameter stent-grafts that sit into the iliac arteries, or it simply decreases in size so that it sits in one iliac artery and a femoro-femoral bypass is carried out (this is called an aortouniiliac device). Aortouniiliac and bifurcated stent-grafts are usually modular in design i.e. the main body and a short length of the iliac stent-grafts are initially implanted, and extenders are added to make the device itself longer. In this manner, the stent-graft can be altered to fit the anatomy of the patient easily.

2.1.6 Current devices

Tables 2.1 and 2.2 show some of the main stent-grafts available on the worldwide market, their different characteristics, and some primary and secondary outcomes from their pivotal clinical trials. It should be noted, however, that these trials have been sponsored by the device company and may, therefore, be subject to some conflicts of interest.

Only five, the Aneurx and Talent (Medtronic Inc. Minneapolis, MN), the Excluder (WL Gore and Associates, Flagstaff, AZ), the Zenith (Cook Inc., Bloomington, IN) and the Powerlink (Endologix, Irvine, CA), currently have FDA approval and are available commercially, and therefore clinically in the US. All the other devices shown have investigational device exemption and are undergoing trials in the US and many of them have been approved in the EU.

Table 2.1 General characteristics of the various grafts available on the US and EU markets.

Keys: SE, self-expanding; BE, balloon-expanding, F, French; P, proximal (i.e. the stent-graft body); D, distal extenders; PTFE, polytetrafluoroethylene *a Co-based alloy with high Cr content

<i>Device and approval</i>	<i>Profile; SE/BE</i>	<i>Design type</i>	<i>Metal</i>	<i>Graft</i>	<i>Neck</i>	<i>Proximal fixation method</i>	<i>Diameter of the artery</i>	<i>Graft attachment</i>
Aorfix (CE)	22 F (P); SE	Bifurcated with contralateral limb and extenders	Nitinol	Polyester	>20 mm	Oversizing and hooks	24-31	Embroidered
Aneurx (FDA)	21 F (P); 16 F (D) SE	Bifurcated with contralateral limb and extenders	Nitinol	Woven polyester	>10 mm	Oversizing	18-26	Sutures; graft inside stent
Excluder (FDA)	18 F (P); 12 F (D) SE	Bifurcated with contralateral limb extenders	Nitinol	PTFE	≥15 mm	Anchors 2 mm long	19-26 aorta 8-13.5 iliac	Chemically bonded; graft inside stent
Zenith (FDA/CE)	18/20 F (P); 14 F (D) SE	Bifurcated main body and two iliac legs	Stainless steel	Polyester	>15 mm	Suprarenal barbs	22-32 aorta; 8-24 iliac	Sutures; graft outside stent

Powerlink (CE)	21 F (P) SE	Unibody with extenders if required	Co-Cr alloy	Woven polyester	≥15 mm	Oversizing	26	Sutures; graft outside stent
Anaconda (CE)	18/20 F (P); 16 F (D) SE	Fully modular, main body and two legs	Nitinol	PTFE	≥15 mm	‘Saddle’ of oversized nitinol ring	16-31.5	Sutured at proximal and distal ends; graft outside stent
Lifepath (CE)	25 F (P); 19 F (D) BE for main body, SE for legs	Bifurcated main body and two iliac legs	Elgiloy *	Woven polyester	≥15 mm	Oversizing	27	Sutures; graft outside stent
Talent (FDA)	22–24 F (P); 18 F (D)	Bifurcated with contralateral limb and extenders	Nitinol	Polyester	15 mm	Oversizing	16-36 aorta 8-22 iliac	Sutures; graft outside stent

Table 2.2 Patient numbers and endpoints from pivotal clinical trials for the various stent-grafts.

Keys: Mortality, mortality to AAA related; No, number; OR, open repair

Author	No	Mortality	Endoleak	Aneurysm size post-op	Conversion to OR
Aorfix	24	0% at 30 day	8% at 30 days	No data available yet	4% in 60 days
Aneurx ²⁸	1193	2.5% at 4 y	14% at 30 days 14% at 12 mths 14% at 4 years	Increase >5mm, 11.5% at 4 years	4.4% in 4 years
Excluder ²⁹	235	0% at 2 y	22% at 30 days 17% at 12 months 20% at 24 months	No data available	1.3% in 2 years
Zenith ³⁰	200	0.5% at 12 m	17% at 30 days 7.4% at 12 months 5.4% at 24 months	Decrease > 5mm, >75% at 24 months	1.5% in 12 months
Powerlink ³¹	192	0.5% at 24 m	6.76 at 24 months	Decrease >5 mm 64% at 24 months	1.5% in 12 months
Anaconda ^{32;33}	54	3.9% at >30 days	9.8% at >30 days 12.3% at 21 months	Decrease >7 mm at 6 months	2% at 21 months
Lifepath ²⁷	224	0.4% at >30 d	6.8% at 12 months	Decrease >5 mm 58% at 12 months	2.2% in 12 months
Talent ³⁴	240	0% at >30 d	10% at 12 months	Decrease >5 mm, 59% at 12 months	2.5% in 23 months

2.1.7 EVAR ineligibility due to complex aortic anatomy

The feasibility of EVAR depends mainly on anatomic factors that represent the important predictors of success. Anatomic selection criteria for EVAR are based principally on characteristics of the proximal infrarenal neck, aneurysm sac, and iliac arteries. An unfavourable neck anatomy, based on its diameter, length, angulation, morphology, and presence of calcification and mural thrombus, is the most frequent cause of exclusion from EVAR^{35:36}. In a study by Arko et al³⁵, 55% patients were considered suitable for EVAR and 45% patients deemed ineligible. The primary anatomical reason for ineligibility was a short infrarenal neck (44%), a large proximal neck diameter (25%), iliac aneurysms (10%), extremely tortuous or calcified neck (7%), iliac occlusion (6%) and small distal aortic bifurcation and accessory renal arteries (5%). In addition 4% were rejected due to poor quality imaging.

Similarly, Carpenter et al³⁷ reported short aneurysm neck (54%), inadequate access from small iliac arteries (47%), wide aneurysm neck (40%), bilateral common iliac artery aneurysms (21%), excessive neck angulation (14%), excessive mural thrombus in aneurysm neck (10%), and accessory renal arteries (6%) with many patients having a combination of factors.

The guidelines of EVAR are constantly being redefined, mostly as a result of increasing operator experience and improvement in stent-graft technology that is constantly providing new and versatile devices. Although, with new technology the number of patients eligible for EVAR will increase, complex aortic anatomy will be a significant limitation, at least in the foreseeable future.

2.2. EVAR FAILURE MECHANISMS

2.2.1 Profile of Delivery Systems

In terms of profiles, the problems that exist with the currently available stent-grafts are that the femoral and iliac arteries are often too small or tortuous for easy

passage of the delivery system. In order for the stent-graft to be placed across the aneurysm, it must first be inserted into the femoral artery using a cut-down process. Therefore, both of the femoral and iliac arteries must be patent, must have as little tortuosity as possible, and one of them must allow a catheter, up to 24 French (Fr) (8 mm) in diameter, to be introduced to the aorta. In most bifurcated devices, the other femoral artery must allow a ~16 Fr catheter access so that the contralateral iliac artery is stented. In many patients, especially women, the arteries are too small to allow access^{37,38}. In addition, subjects with AAA often have concomitant vascular disease, so the femoral and iliac arteries can be atherosclerotic or tortuous and access is therefore not possible³⁹. Calcification also compromises passage of the delivery sheath for the stent.

This has been overcome by one commercially available device to date. The Powerlink (Endologix, Irvine, CA) is the only commercially available bifurcated, unibody device. This device requires one artery to be patent to allow a 21 Fr catheter to pass, and the contralateral to allow a 9 Fr catheter to pass³¹. Another stent-graft, currently in Phase I clinical trials, is the Trivascular Enovus graft (Santa Rosa, CA) which was initially acquired by Boston Scientific, Natick, MA⁴⁰. They performed a phase II clinical trial in United States in 2006, but the study was terminated as they found it too expensive to pursue. The Enovus is now being tested by TriVascular2, a company in which the original inventors are involved. In order to deploy this stent-graft, the graft alone is inserted into the aorta and is placed in its correct position. The graft material has many channels where the struts of a normal stent-graft would be. Once the graft is in place, a biopolymer (currently patent protected) is injected into these channels, expanding the graft material to its correct diameter. This biopolymer hardens in the body and becomes the ‘metal struts’ of a normal stent, thus providing the strength a stent-graft needs. Using this method, the diameters of the catheters required to deliver this unibody device are as low as 14 Fr for both arteries.

2.2.2 Endoleaks and Graft Migration

Endoleak is recognized as the main problem associated with stent-grafts, and is used as an endpoint in clinical trials^{27;34;41}. Post-procedural leakage can cause aneurysm rupture and is therefore the chief cause of aneurysm-related mortality and the need to convert to OSR⁹. Four different types of endoleak exist; the definitions of each are given in Table 2.3.

Table 2.3 Categorisation of Endoleaks

Categorisation of endoleaks	Definition
Type I	Inadequate seal at graft ends, resulting in leaks at the proximal or distal anchorage sites
Type II	Residual blood flow into aneurysm sac from patent arteries, e.g. lumbar and mesenteric
Type III	Integrity of graft compromised; leak from modular components
Type IV	Porous graft material

2.2.2.1 Type I and Migration. This type of endoleak was the primary cause for stent-graft failure in the initial trial performed by Parodi. Even today, the existing tubular stent-grafts are often difficult to use as the distal neck of the aorta is often too short and calcified to allow secure tubular stent attachment³⁰. Since Parodi's work, most aneurysms are treated using a bifurcated device, and oversizing at the distal end usually provides satisfactory anchorage⁴².

With respect to proximal endoleaks, the main cause is that of stent-graft migration. A variety of methods are used to prevent stent-graft migration, such as oversizing the stent by ~15%, the use of suprarenal uncovered stents to provide extra frictional attachment, and the use of hooks, barbs, radial force, and longitudinal columnar support. The use of barbs is somewhat controversial, as these require full penetration of the wall of the aorta, and may lead to rupture of adjacent structures⁴³. They may also lead to damage of the endothelial cell layer, possibly causing uncontrolled proliferation of smooth muscle cells, thus potentially leading to intimal hyperplasia and possible stent-graft failure.

Regardless of fixation, migration has been noted with all current endovascular devices. The migration rate is ~2% at 1 year using each of the FDA-approved devices^{29;44;45}. Graft migration has been shown to occur with infrarenal fixation and is thought to relate to aneurysm neck length, aneurysm neck and device apposition zone length, and distal device support within the iliac system⁴⁵⁻⁴⁹. Fogarty et al⁵⁰ reported an incidence of 8% at 5 years, suggesting low deployment of the device below renal arteries as the most important predictor of subsequent migration. For each millimetre increase in the distance between renal arteries and the top of the stent-graft on post deployment CT scans, the risk of migration increased by 6%⁵¹.

A total of 1119 patients, who received treatment in the Aneurx clinical trial and had a minimum of two years follow up, were examined by Zarins et al⁴⁵ for stent migration. The authors found that migration was more likely to occur in patients whose

fixation length (i.e. the length of neck covered by the stent-graft) was less than 10 mm of the aneurysm neck (19% versus 9% in patients with a fixation length greater than 15 mm). The authors suggested that the predictors of migration were fixation length and renal artery to stent-graft distance. Factors that were not predictive include: age, pre-implantation aneurysm size, neck length, neck diameter, degree of device oversizing and use of extender cuffs at implantation. They concluded that type I endoleak is primarily caused by poor imaging of the renal arteries during deployment (inferior image quality, lack of magnification, movement or parallax) and substandard patient selection.

Stent-graft migration is now considered to be preventable by positioning the device just below the renal arteries and extending the device to the level of hypogastric arteries bilaterally.

Type I endoleak can also be caused by suture fracture, as occurred with the Vanguard device^{52;53}. This device comprised rows of stents each attached to the other via sutures. Fracture of these sutures leads to row separation at the anchorage sites leading to Type I endoleak.

Type I endoleaks can be often identified on completion angiogram on table following EVAR. They require proximal adjunctive procedures to obtain a primary seal. This can be in the form of balloon dilatation; further intervention will also depend on whether there is associated graft malposition. For type I proximal endoleaks without graft malposition during stent deployment, a giant Palmaz stent is used to encourage stent apposition to the proximal neck. However, if an endoleak appears to be due to graft migration during deployment, they may then require proximal aortic cuff, generally oversized to prevent further endoleaks⁵⁴. Type I endoleak is associated with a significant risk of rupture if untreated, so if endovascular procedures are unsuccessful, conversion to open repair may be required⁵⁵.

2.2.2.2 Type II. During OSR, occlusion of patent vessels can be carried out to prevent blood from entering the aneurysm sac. Such a procedure cannot be performed during EVAR, and blood flow into the aneurysm sac from the lumbar and mesenteric arteries can lead to Type II endoleak. It has been suggested^{56;57}, that the best method for dealing with those who have this type of endoleak is to increase their surveillance compared with those who do not have it. There is some controversy regarding the best method for dealing with Type II endoleak. Initially, it was suggested by the EUROSTAR registry that there is no increased risk of aneurysm rupture⁵⁸, although this has now been revised and the authors have suggested that this type of endoleak may increase the size of the aneurysm and the incidence of reintervention but they still do not suggest that it is a direct cause for rupture⁵⁷. Others, however, have found a direct link to aneurysm rupture caused by Type II leak⁵⁶. Many of these endoleaks were treated by radiological or surgical intervention because of the fear of rupture. Several techniques exist for the treatment of Type 2 endoleaks, including embolisation via a transarterial or translumbar route, laparoscopic ligation of aortic sac side branches and vessels and thrombin injection⁵⁹. Reintervention usually repairs the problem without difficulty⁶⁰, however it has been reported that there is a high risk of treatment failure and overall outcome may not be altered⁵⁹.

The management of Type 2 endoleaks has evolved with time. Recently, a more conservative approach has been adopted because many of them seem to be relatively benign.

2.2.2.3 Type III. The graft material is sutured to the stent in all devices, with the exception of the Excluder graft which is heat bonded. With suture fracture, graft erosion may occur, particularly in areas of severe angulation. Stent fracture can also cause Type III endoleak, with the stent strut pushing through the graft material, causing a large hole, although it is claimed that this is not a frequent occurrence⁶¹.

An additional issue with Type III leak is that most stent-grafts available are modular. Although this modular design is, in concept, a valuable addition that allows changes in the shape of the stent-graft according to the patient's needs, it does increase the possibility of leakages occurring around the connecting areas and allows bowing and kinking to occur. In most devices, the connections are simply held together by friction, i.e. no active gating mechanisms are used and leaks can therefore occur between each of these connections.

Type III endoleaks require treatment due to their association with enlargement and considerable risk of aneurysm rupture^{55;62;63}. If a modular separation is the cause of the endoleak, the aim is to restore continuity of the graft elements by inserting an appropriately sized cuff. Fabric defects may be treated by relining the device with another stent-graft, either bifurcated or uniiliac.

In order to overcome these problems, ongoing research into using polymeric materials, other than expanded polytetrafluoroethylene (ePTFE) and polyethylene terephthalate (Dacron/polyester), as suitable grafts is being carried out⁶⁴. A possible solution to overcoming some of the problems with Type III endoleaks would be to develop both a new polymeric material that can be chemically bonded to the stent and a new stent design in which the graft and stent are merged into one deployable structure, rather than the graft simply lying outside the stent as a separate entity only attached via stitching or chemical bonds. By integrating the stent with the graft, this will reduce the chance of graft failure and so endoleak itself. To a certain degree, this has been achieved by the Endofit prosthesis (Endomed Inc., Phoenix, AZ), where the graft material encapsulates the stent, resulting in a stent-free lumen and a smooth channel through which the blood can flow, but the polymer is still based on ePTFE and the design does not integrate the graft with the stent. Additionally, superior methods of connecting the extender cuffs to the main body should be investigated. For instance, a gating mechanism that locks the cuffs to the main body would potentially aid in

mitigating against Type III leaks.

2.2.2.4 Type IV. Currently, the ePTFEs and woven polyesters used are very thin so that the profile of the device can be kept to a minimum. The Anaconda uses a particularly thin Dacron (0.15 mm vs. ~0.35 mm), and the porosity of all existing grafts are approximately the same, at ~65%⁶⁵, with the incidence of Type IV endoleak being fairly high peri-operatively (this is known as ‘contrast blushing’).

Post-operatively, as general thrombosis of the graft usually occurs quickly, treatment is rarely required for Type IV endoleak after endograft deployment. However, the Endofit, mentioned above, uses laminated ePTFE which provides an impermeable barrier, preventing any Type IV endoleak from occurring. In this manner, Type IV endoleak can be reduced or prevented.

2.2.3 Endotension

Endotension is the continued pressurisation of the sac with subsequent sac enlargement in the absence of apparent endoleak; it is often caused by pressure transmission through a sealed or thrombosed endoleak⁶⁶. Although the pathophysiology of endoleak is beginning to be elucidated and its management is being established, controversy exists about the etiology and clinical consequences of endotension. Gilling-Smith⁶⁷ classified endotension into subcategories according to the pressure characteristics: grade I (high pressure and high flow); grade II (high pressure and low flow); and grade III (high pressure and no flow), which is true endotension or sealed endoleak. Table 2.4 includes the possible etiologies of endotension.

An increase in aneurysm size can occur with endotension, but if there is no demonstrable endoleak or the aneurysm is shrinking in size, additional intervention is usually not required⁶⁷. Several procedures are possible: open replacement of the graft, wrapping the endograft by a new graft through laparotomy, and endovascular relining of the stent-graft. Conversion to OSR usually treats endotension satisfactorily⁶⁸.

Table 2.4 Possible aetiologies of endotension

Pressure transmission to the AAA sac around the ends of graft

Layer of thrombus between the graft and aortic wall
Graft displacement exposing thrombus layer at aortic neck
Endoleak channel sealed by thrombus
Undetected endoleak
Intermittent endoleak channel
Very low-flow endoleak channel

Pressure transmission through graft wall

High graft porosity
Microleak through graft interstices
Transudation/exudation of fluid through graft fabric
Graft pulsatility/wall movements

Pressure transmission from branch vessels

Thrombus over orifice of internal mesenteric or lumbar arteries

Pressure build-up from fluid accumulation in situ

Graft infection
Thrombus fibrinolysis/hygroma
Genetic modulation
Enzymatic activity
Hyper-osmolarity
Others

2.2.4 Stent fatigue and fracture

A study carried out by Jacobs and co-workers⁵², which examined fracture of stent-grafts over a 10-year period in their centre, found that of 404 devices examined 43 had metallic stent fracture, i.e. over 10% of all stent-grafts used had fractured within 4 years (the follow-up period for each patient). In addition, a further 17 had other problems with the graft (e.g. suture fracture, graft holes). Although this study included stent-grafts that are no longer commercially available and stent-grafts used for the treatment of thoracic aortic aneurysm, the results are, nonetheless, still of value in understanding the role of metal fatigue.

Unfortunately, Jacobs et al. did not describe the follow-up treatment given to the 43 subjects (observation, reintervention endovascular treatment, or conversion to OSR). However, as mentioned above, fracture of a stent strut may lead to a Type III endoleak, or if the attachment barbs and hooks fracture, the stent-graft may migrate leading to Type I endoleak.

Nevertheless, strut fracture can be obviated by superior in vitro life testing at higher pressures and better design. Although endografts are subjected to accelerated life-testing, for an equivalence of 10 years, before approval can be obtained from the FDA, it is thought that the mock silicone arteries that are used to perform these tests undergo a “frequency dependent change [potentially leading to] a lower than expected loading and an attendant reduction in [the actual] severity of testing”⁶⁹. Thus, it may be the case that the in vitro conditions in these bench tests do not mimic exactly in vivo conditions, and therefore evaluation of the fatigue properties of the stent-graft is not properly performed. It should also be noted that the aorta is subject to the highest pressures in the body, and, as mentioned previously, many of these patients will have concomitant high blood pressure. Therefore, testing of the stent-grafts should be carried out at blood pressures higher than normal (e.g. systolic, 160 mmHg; diastolic, 100 mmHg).

2.2.5 Deployment problems and repositioning

Except for the Lifepath stent-graft, all stent-grafts are self-expanding (although the Talent stent-graft is made from Nitinol, it also possesses a balloon for inflation to ensure total expansion of the stent, and to allow easy positioning⁷⁰). Many stents, such as the Zenith, have initial partial deployment which allows partial repositioning; no repositioning can be performed when the graft is fully deployed. Most stents cannot be repositioned after deployment, and in some, such as the Excluder stent-graft, the deployment system is designed to allow rapid expansion of the stent. Inaccurate deployment will also lead to the increased use of extenders, thus increasing the probability of Type III endoleak⁴⁵.

Although many of the stent-grafts do allow some manoeuvrability post-implantation, this is mostly in the form of moving the stent down the aorta, and if barbs/anchors have been deployed, too much movement may itself cause dissection of the artery. The Anaconda (Sulzer Vascutek, Austin, TX), however, appears to be unique in overcoming the problem of manoeuvrability by anchoring the stent-graft using an unusual 'saddle'-like ring-stent that provides a compliant seal against the vessel wall. It is possible to move this stent-graft around post-deployment without causing tears to the aortic wall.

2.2.6 Limb Occlusion

Kinking, caused by fracture of the stent or insufficient support given to the graft, can result in obstruction of a bifurcated limb³⁴. This often leads to endovascular reintervention being required, although this is usually successful. Limb occlusion was a serious problem with the Stentor/Vanguard, and with the Ancure devices, but is found less frequently now with more modern designs which are generally stiffer, thus preventing kinking. The Aorfix (Lombard Medical, Oxford, UK), for example, has been specifically designed to be a flexible stent-graft, making it resistant to kinking and twisting⁷¹. Additionally, this device can be used in aneurysm necks with angles up to

65°. Krämer et al⁷² studied the geometric changes in bifurcated aortic endografts and identified changes in the iliac limbs in response to physical forces, yet not fully understood, which may result in kinking of the prosthesis thereby compromising its haemodynamic properties and causing thrombosis and limb occlusion. It is therefore conceivable that these changes may have profound effects on durability of currently available devices and limit the long-term success of EVAR⁷².

2.2.7 Biocompatibility

Due to the large size of the aorta, problems such as intimal hyperplasia and restenosis are not usually an issue with EVAR. Consequently, the research currently being carried out on drug-eluting stents, aimed at preventing restenosis in small vessels, is not very relevant to AAA, and no incidence of AAA being treated with such a stent could be found in the literature. Additionally, most endografts are made from Nitinol, which has been shown to be selectively biocompatible⁷³, though there are reports that the nickel, which is toxic, does leach out slowly. This leaching may result in nickel corrosion, and might therefore be one of the causative factors for strut degradation (a failure mechanism of the device)⁷⁴. However, although this corrosion was identified in some first-generation nitinol stent-grafts^{74:75}, improved nitinol processing (i.e. reduced nickel content) has meant that so far there have been no reports of fracture due to corrosion in second generation devices⁵³. This could, of course, simply be due to the short follow up period carried out to date in these studies.

The issue of stent-graft incorporation into the aortic wall, however, remains a problem. In animal models, endothelialisation of the stent-graft seems to occur quickly (within 3 months) and along the whole length of the graft^{65:76}. Although there are occasional reports of this occurring in humans⁷⁷, it is thought that endothelialisation does not commonly take place⁷⁸. Therefore, further work on developing methods to encourage endothelialisation should be performed, so that the stent-graft becomes

integrated with the body. Work in our group is currently underway on the development of a polymer where ‘stem-cell switching’ occurs, thus encouraging endothelialisation in situ, from the circulating blood, onto the graft itself.

2.2.8 Compliance Mismatch

The movement of a stent within the aneurysm depends on the compliance of the stent, the compliance of the graft (which varies widely, depending on the state of expansion) and cyclical changes in the pressure. The natural history of AAA involves diameter enlargement, which may lead to rupture. Stent-graft design alters aortic wall dispensability (which is a surrogate marker for aortic compliance) at the aneurysm neck, the site of endograft sealing, which may have serious consequences for endograft efficacy and durability⁷⁹. Compliance mismatch is more relevant in the proximal aorta, which is the major contributor to total arterial compliance and is an important determinant of cardiac afterload. Reduction in compliance leads to an increase in systolic and pulse pressure while peripheral resistance remains unaltered. After reconstruction of the proximal aorta with noncompliant grafts, there is a significant increase in systolic and pulse pressure as well as left ventricular hypertrophy (LVH)⁸⁰. It has been shown that stiff vascular prosthesis increase pulsatile load (characteristic impedance), which results in LVH. The development of more compliant prostheses, which match the host artery compliance, is expected to reduce the haemodynamic changes induced after their implantation.

2.2.9 Aortoduodenal Fistulas

Aortoduodenal fistula (ADF) is an abnormal communication between the aorta and usually the fourth part of the duodenum. ADF constitutes a rare but life-threatening complication of aneurysm repair. Until recently, they were primarily associated with OSR, occurring at a rate of 0.4% to 2.4%⁸¹⁻⁸⁶. However EVAR patients are not immune to the development of ADF and a small number of cases have been reported in the literature^{47;81-83;85-92}. The exact cause for the development of ADF following EVAR

remains unclear. A strong hypothesis is that local infection, which could be secondary to the grafting procedure or pre-existent (EVAR done for mycotic aneurysms) could result in intestinal necrosis and the formation of a fistula between the aneurysm and the intestinal wall. EVAR of inflammatory AAAs has been directly associated with ADF in previous reports; cultures taken at laparotomy grew micro-organisms of colonic origin⁹⁰.

Endotension may also lead to the formation of ADF resulting from pressure necrosis of the aneurysm against the intestinal wall⁸¹. Bertges et al⁸³ also suggested that extensive sac embolisation after EVAR may eventually lead to an ADF; therefore it may be wise to limit the embolisation sessions and the number of coils inserted into the sac to treat an endoleak.

The surgical treatment of ADF following EVAR is similar to infections after OSR, consisting of graft removal and revascularisation coupled with repair of adjacent area of bowel and placement of omentum between the intestinal and aortic repairs⁹³. Endograft explantation may vary with different device designs. In the case of stent-grafts without suprarenal fixation, the excision of the graft is not a complex procedure; stent-grafts with suprarenal barbs frequently necessitate supraceliac control⁹⁴. These procedures carry significant perioperative morbidity and mortality. A high index of suspicion and emergency treatment is essential for aortic graft infections.

2.2.10 AAA Rupture

Sac regression, a reassuring sign of aneurysm exclusion and depressurisation of aneurysm sac, are the primary goals of EVAR⁹⁵. Sac enlargement after EVAR, however, is associated with continued or intermittent pressurisation of the sac, secondary to endoleak or endotension, and has been associated with late aneurysm rupture^{96;97}. Determination of AAA rupture following EVAR may be difficult to verify; however Brewster et al¹⁸ reported an incidence of 1.5% occurring at a mean interval of 30 months following stent-graft placement. Abbruzzese et al⁹⁸ reported a similar incidence of 1.1%. The causes of rupture included late-onset type I proximal attachment

leak, persistent type II endoleaks with sac expansion, device structural failure with late-onset type III endoleak, modular endograft component separation and fabric defect resulting from friction and erosion of the graft wall from an adjacent stent strut. Female gender, adverse anatomy with short, wide and angulated infrarenal necks responsible for causing stent migration and late endoleaks are predictors of late rupture post-EVAR¹⁸. Mortality following treatment for late-rupture is variable in different reported series from 43%⁹⁸ to 83%⁹⁹.

Regular life-long follow up is essential following EVAR to detect endoleaks and sac expansion and with appropriate treatment, the incidence of late rupture and subsequent mortality can be hopefully reduced.

2.2.11 Secondary interventions and Mortality

As discussed above, the common indications for reintervention following EVAR are persistent primary endoleaks, significant graft migration, late-onset endoleaks, and graft limb stenosis or thrombosis, and endotension causing sac enlargement^{18;98}. In some instances, changes in AAA sac and iliac artery morphology can cause graft-related problems although sac shrinkage has occurred as a result of effective aneurysm exclusion, a phenomenon termed as “paradox of success”⁹⁹. The procedures required commonly include placement of proximal and distal extension limbs, coil embolisation of branch vessels, angioplasty and stenting of graft limb kinks and open procedures like conversion to OSR, graft limb thrombectomy, repair of common femoral artery pseudoaneurysms and extra-anatomic bypass for limb occlusion. Hobo et al¹⁰⁰ studied the influence of endograft extensions during the primary EVAR procedure on the postoperative complications, mortality and secondary interventions. Based on the data of the EUROSTAR (The European Collaborators on Stent-Graft Techniques for AAA and Thoracic Aortic Aneurysm and Dissection Repair) registry, they reported a substantial increase in late device kinking and secondary transfemoral interventions in patients with an iliac device limb extension. This indicates that single devices are potentially less vulnerable to late failure. In a separate study¹⁰¹, they also reported that

though the overall incidence of secondary interventions after EVAR had decreased significantly as compared to earlier experience, trans-abdominal and extra-anatomic reinterventions had decreased less and are associated with an increased mortality risk. This finding suggests continuing need for surveillance for device-related complications.

Several studies have demonstrated that EVAR reduces the rate of complications and mortality compared with open repair even though EVAR patients as a group are older with multiple co-morbidities¹⁰²⁻¹⁰⁴. In randomised controlled studies, perioperative mortality was 4.6% after open repair and 1.2% to 1.6% after EVAR^{102;104}. Compiled data from published series on surgical conversion report an average mortality rate of 22%¹⁰⁵.

A recent series has shown that after the introduction of EVAR, elective repairs have increased, ruptured AAAs have decreased, and procedure-related mortality has decreased for both intact and ruptured AAA¹⁰⁶. This has led to decrease in overall AAA-related deaths despite an unchanged mortality rate of elective open AAA repair. The need for any reintervention, large preoperative AAA size, family history of aneurysmal disease, and renal insufficiency have been identified as the most important predictors of aneurysm-related mortality (ARM)¹⁸. Overall mortality from late conversion is markedly higher than elective primary OSR and is influenced by rupture and infection.

Incidence rates of EVAR failures at different time points are outlined in table 2.5.

Table 2.5 Incidence rates of EVAR failure modes at different time-points^{58;107}

<i>No.</i>	<i>Mode of failure</i>	<i>Incidence (%)</i>	
		<i>30 days</i>	<i>12 months and beyond</i>
1.	Endoleak Type I Type II Type III Type IV	3.5 14.0	6.8 10.3 4.2 10 (earlier reports: now significantly reduced)
2.	Endotension	1.5-5 (overall)	
3.	Stent fatigue and fracture	3.1 (overall)	
4.	Iatrogenic injury to access artery	4.8 (immediate)	
5.	Graft limb thrombosis		2.5 (12 months), 3.9 (beyond 12 months)
6.	Graft stenosis	0.3	1.5
7.	Aortoduodenal fistula	0.4-2.4% (overall)	
8.	Stent migration		1.4 (12 months) 4.0 (beyond 12 months)
9.	AAA rupture	0.3	0.6
10.	Conversion to open repair	1.7	2.0
11.	Secondary interventions	16.2 (overall)	
12.	Mortality	2	2.6

2.3. OUTCOMES BASED ON ANATOMIC AND DEVICE-SPECIFIC ANALYSIS

2.3.1 Cook Zenith. Unlike most other commercially available stent-grafts, the Zenith device has undergone remarkably few changes since its introduction in 1997¹⁰⁸. The initial report of the Zenith Multicenter Trial provided evidence that endovascular repair of AAA with the Zenith stent-graft was superior to open surgery for both associated morbidities and aneurysm-related death³⁰. The conclusions were tempered by the expectation that endovascular repair would require more detailed follow-up than open repair and might not provide as durable a result. However middle and long term data suggest positive results with a very low incidence of previously reported adverse endovascular outcomes like limb thrombosis, stent fracture, and component separation¹⁰⁸. The occurrence of late endoleaks and persistent sac enlargement was noted in a subset of patients which will require further investigation and long-term follow up. Overall, the application of Zenith endovascular graft to infrarenal aneurysms with appropriate anatomy is associated with a very low risk of failure and provides a promising platform for future developments¹⁰⁸.

2.3.2 Gore Excluder. EVAR with the original-permeability Excluder (W.L. Gore & Associates, Flagstaff, Ariz) has been associated with postoperative sac expansion in the absence of endoleak. The graft material was modified to reduce its permeability and released for commercial use in mid-2004. In early follow-up, the low-permeability Excluder device is associated with a significantly greater aneurysm shrinkage rate than the original version¹⁰⁹. Clinically important enlargement also appears significantly different within 1 year of implantation. Despite these promising results, longer follow-up is needed to determine whether these differences will persist. When evaluated in a retrospective review, the Excluder had similar clinical outcomes at 5 years compared to other commercially available devices⁹⁸. There were no differences in postoperative mortality, aneurysm rupture, ARM, conversion to open repair, or reintervention rates.

2.3.3 Medtronic AneuRx. In a retrospective review by Abbruzzese et al⁹⁸, AneuRx was the most commonly used stent-graft at their institute (49%) over a period of 6 years (1999 to 2005). The clinically relevant outcomes were similar when compared with Zenith and Excluder stent-grafts. The ARM was low (3.6%) with 95% freedom from reintervention at 5 years. The graft related adverse events were low as well. Smith et al¹¹⁰ reported similar results suggesting that endovascular treatment with modular AneuRx is safe and effective, producing acceptable results of disease-free survival and mid-term clinical outcome. A word of caution for the AneuRx device is an earlier report of significant risk of endograft migration¹¹¹, the incidence of which increased with time. This is associated with adverse neck anatomy but since its first use, at least two major graft and delivery system upgrades have been made which have reduced this risk¹¹².

2.3.4 Medtronic Talent. The Talent device is a modular endograft system that uses a self-expanding skeleton of serpentine Nitinol stent springs inlaid in a woven polyester fabric. While the Talent device allows for treating more adverse neck anatomy, it does require a slightly larger delivery sheath¹¹². In a report by Brown et al comparing the Cook Zenith and the Medtronic Talent endograft within the EVAR trials within the United Kingdom, no statistically significant differences were found in regard to secondary interventions, aneurysm-related death, or all-cause mortality¹¹³. However, the Talent device is associated with worse clinical outcome in patients with aneurysms > 6 cm in combination with proximal neck > 2.6 cm, so this group of patients should have more intensified surveillance during follow-up for endoleak and migration¹¹⁴.

2.3.5 Endologix Powerlink. The Powerlink device is a unibody bifurcated endovascular graft utilised for the repair of AAAs. It is thus different from other commercially available devices. Its delivery is achieved through one surgically exposed femoral artery as opposed to two. The Powerlink device appeared to be durable and effective in excluding aneurysm flow and prevention of sac enlargement over a period of long-term follow up¹¹⁵. The graft and the stent materials have been free from failure and fatigue.

The requirement for only one surgically exposed femoral artery facilitates graft placement in patients with limited access routes and reduces the morbidity of an additional groin wound. However the overall survival at 72 months was no different as compared to open repair, indicating that the Powerlink system is just as durable in protecting patients from aneurysm-related death as open repair¹¹⁵.

2.4. FURTHER DISCUSSION

Although EVAR has evolved considerably since 1991, it is clear from the literature and clinical trials carried out to date that there is a long way to go before it will overtake OSR and become the modality of choice for treatment of AAA.

Results from Clinical Trials and Current state of EVAR

2.4.1 The EVAR Trial 1: EVAR trial-1 showed that although aneurysm-related death from EVAR is 3% less likely to occur when compared with OSR, overall survival in the two groups were similar. The results suggest that EVAR offers no advantage with all-cause mortality and Quality of Life, is more expensive and leads to a greater number of complications and re-interventions.

Apart from being not representative of current practice, important limitations of the EVAR trial-1 include the entry criteria with possible over-representation of more expert centres and relatively shorter follow up (4 years).

2.4.2 The EVAR Trial 2: The EVAR Trial 2 compared patients unfit for OSR and who received EVAR, with patients unfit for OSR who received no treatment¹¹⁶. All were followed-up for a minimum of 12 months. The investigators noted that 30-day mortality was “considerable” at 9% in the EVAR group. Additionally, after 4 years 30% of all patients had died from aneurysm-related causes and a total of 64% had died from all causes with no difference found in the two groups (62% in no-treatment group and 66% in EVAR group). Costs for the EVAR group were, however, considerably higher when

compared with the no intervention group (mean difference, £8649) with no difference found in health-related quality of life scores. This analysis is very interesting as the original aim in using EVAR was to treat patients such as those in this trial.

There are several limitations of the EVAR Trial 2. The reported 30-day mortality rate of 9% for EVAR and the 4-year mortality of 64% are both much higher than previously reported in high-risk patient cohorts. Patients assigned to EVAR who died while awaiting treatment (8% of the total, 14 deaths) were counted as receiving EVAR. In marked contrast to the treated group's mortality of 9%, the mortality rate in the 47 patients (27% of the no treatment group) who crossed over to receive an AAA repair was only 2%. Although level 1 evidence, the effect of treatment delays before receiving EVAR and the high rate of crossover to receive EVAR has undermined confidence in the conclusions drawn from its intent-to-treat results.

2.4.3 DREAM Trial: Four-year results of the DREAM Trial from the date of discharge suggest a higher mortality after EVAR as compared to open repair however the 3% perioperative benefit of the EVAR group was excluded in this analysis. Potentially there is a 10% to 15% benefit for open repair at four years from discharge likely to swamp the 3% benefit from perioperative period known to occur in the EVAR group. The Trialists believe that open repair could win in the long term in DREAM; however no such trends have been found in other trials comparing EVAR with OSR.

Although the DREAM trial patients were considered to be suitable for both open and endovascular repair, this decision was not based on standardized risk-stratification systems. Consequently, it is conceivable that patients were included in the DREAM trial who actually had an elevated risk of dying in the first 2 years after surgery. This would make the indication for AAA repair questionable in these patients. Furthermore, the trial has also been criticised for being underpowered. The sample size calculation was based

on primary endpoint of short-term mortality and complications and the trial's power to detect differences in follow up outcomes is unclear.

2.4.4 EUROSTAR Registry: The EUROSTAR registry evaluated the quality-adjusted life expectancy post-operatively for both EVAR and OSR and found that EVAR was likely to prolong a healthy 70-year old male's life by only 3 weeks. This was increased to 2 months in 70-year old men in poor health. They showed that in younger patients OSR is superior, but older patients still do better with EVAR. The age where both treatments are equivalent is 64 years. EVAR of infrarenal AAAs with the first- and second-generation devices that predominated in this study was associated with a risk of late failure, according to an analysis of observed hard end points of 3% per year. It is unclear from the report whether patients died from aneurysm-related or other causes. Early action against significant risk factors like proximal type I endoleak, mid-graft type III endoleak, graft migration and postoperative kinking of the graft has been recommended to improve long-term results.

Because participation in the EUROSTAR project is entirely voluntary, data collection is neither comprehensive nor complete. The best we can hope for is that the data submitted are reasonably representative of practice in European Hospitals as a whole. For effective benchmarking this is not good enough. To maintain a standard of data submission in terms of both quality and timing, all those patients from centres that consistently fail to deliver the data were excluded from the database. This resulted in near complete submission of follow-up information. When evaluating Eurostar results it is important to take account of the fact that, inevitably, the outcome of treatment with the earlier generations of endovascular devices will influence the overall results. Some of the devices are no longer commercially available and the newer generation stent-grafts may perform differently.

Results from other earlier studies comparing outcomes in patients treated with EVAR versus those treated with OSR are inconclusive. Both the EVAR trial-1¹⁰² and the EUROSTAR registry¹¹⁷ showed that there was little difference in outcomes in patients treated with EVAR compared with those treated with OSR. In contrast, Hua et al.¹¹⁸ found that there was a significant increase in both 30-day mortality ($P < 0.05$) and 30-day morbidity ($P < 0.0001$) in patients treated with OSR when compared with the EVAR group. It is often the case that 30-day mortality is found to be reduced for EVAR compared with OSR^{102;103}. Ultimately, all investigators conclude that longer-term follow-up is required before any firm conclusions can be made regarding the superiority of one treatment over the other.

One of the major problems with EVAR, compared with OSR, is the risk of endoleak. For instance, patients lost to follow-up after EVAR can be at risk of aneurysm rupture and possible death as a consequence of endoleak. In addition, reintervention is often required at a rate that is higher than that of OSR¹¹⁷. In fact, Becquemin et al.¹¹⁹ found that 27% of patients who underwent EVAR required a secondary procedure (mean follow-up was 28 months). Another issue is that hospital and physician time is required post-operatively to ensure the integrity of the stent-graft. Becquemin's group, for example, performed clinical examination, abdominal plain radiography, duplex scanning, and computed tomography at 1, 6, 12, and 18 months, and yearly thereafter on each of their EVAR patients. In contrast, Biancari et al.¹²⁰, who performed OSR on 284 patients, performed a mean of 2.2 ultrasound scanning examinations on 77 patients, a mean of 1.3 arteriography scans on 28 patients and a mean of 1.5 computed tomography scans on 11 patients. Clearly, physician and hospital times are less, post-operatively, for OSR patients compared with EVAR patients.

There is a subject of cost differences between OSR and EVAR. Given the clinical equipoise of the two treatment options, clearly cost will be the deciding factor in which option is used. If the cost of the grafts and stent-grafts used in OSR and EVAR, respectively, were equal, EVAR would be much the cheaper option. Hospital costs, such as length of stay in hospital¹²¹ and length of operation¹⁰² have been shown to be significantly less for EVAR compared with OSR. In a study by Dryjski et al¹²², the cost of graft in OSR was on an average \$750 which was much lower than the average cost of EVAR stent-graft (\$12,974) making the overall cost of EVAR higher than OSR in spite of lower ICU use and overall hospital stay. Moore and colleagues¹²¹ also found that the length of stay in the Intensive Care Unit (ICU) of the hospital was significantly shorter for the EVAR group compared with the OSR group ($p < 0.05$); however now most patients do not need any ICU stay following EVAR, especially in high volume institutions. In a review by Drury et al¹⁰⁷, it was suggested that when undertaking surgical repair in a high-risk patient, it can be difficult to organize the required critical care services, and consequently EVAR with its reduced requirements may have some advantages.

Thus, even given the follow-up costs (tests mentioned above in Becquemin's study) that are associated with EVAR, the endovascular approach would be the more cost-effective treatment, if the device cost was low. However, endografts can cost upwards of \$11,000, a cost that significantly adds to the overall costs. In Moore and co-workers' analysis, they found that the device accounts for 58% of total costs for EVAR patients. The authors suggest that this cost is prohibitively high to allow EVAR to become the treatment of choice, and that it is unlikely that the devices will become cheaper with time, as vast sums of money are required to develop them¹²¹. They go on to suggest that EVAR will only be used where the patient is unable to undergo OSR or by patient and physician preference, rather than financial considerations.

In the question of EVAR vs. OSR, as we have seen, the randomized controlled trial (RCT) evidence is limited. The enrolment period of the DREAM¹²³ trial was November 2000 to December 2003 and EVAR 1¹⁰² was September 1999 to December 2003. This RCT evidence may be dated. Further evidence may come from the ongoing large multi-centre trial, The Open vs. Endovascular Repair (OVER) trial for AAAs, which had an enrolment period beginning in 2001 and ending in 2010. The recruitment period will be more up-to-date and thus, based on the results from this analysis, we should expect lower perioperative mortality rates in both EVAR and OSR groups, but similar mortality differences, as well as lower rates of endoleaks and ischaemia¹²⁴.

EVAR has been increasingly used for the treatment of ruptured abdominal aortic aneurysms and it has a clear benefit as laparotomy, aortic cross-clamping and retroperitoneal dissection is avoided thereby reducing haemodynamic shifts as well as the likelihood of inflammatory response¹²⁵. Significantly decreased mortality of endovascularly repaired ruptured AAA at 30 days vs. OSR has been demonstrated in three prospective trials¹²⁵⁻¹²⁷. However, institutional and surgeon experience is essential to fully benefit from the use of this procedure for the treatment of ruptured AAAs. In a recent survey, a significant survival benefit was independently associated with increased institutional volume⁷⁸.

2.5 Conclusions & Prospects for the Future

This past decade has witnessed a remarkable evolution and transformation in our approach to the treatment of aortic aneurysms. Even with the learning curve and early clinical trial results included, recent studies have suggested that the long-term outcomes of endovascular infrarenal AAA repair are excellent.

The endograft market is one in constant flux. Lessons learnt from the past 14 years of EVAR have meant that stent-grafts themselves are constantly evolving (e.g. Cordis have produced the Quantum, followed by the Fortran and are now developing a third-generation stent-graft). With this in mind it is difficult to evaluate where EVAR will be in the next decade. It is likely that, with further developments and new generation devices arriving on the market, the problems mentioned above will be overcome, and that EVAR could become the treatment of choice for AAA. In the next decade, we can expect continuing improvements in endovascular device design to include the treatment of suprarenal and thoracoabdominal aneurysms. The role of OSR will diminish but not disappear. As more experience and skill in EVAR is gained, surgeons will be challenged to maintain their skills in open repair.

EVAR is associated with a life time risk of rupture because most patients will live for several years after the procedure¹¹⁷. Purpose of future research should be improving the efficiency of the follow-up schedule after EVAR and evaluation of new stent-graft designs to prevent graft failure. Graft materials and construction are constantly undergoing testing to provide better configurations. Hopefully, new generations of devices with improved material and stent design will minimise EVAR complications while providing increased indications for its use and durability.

Our group have developed the POSS-PCU polymer with several superior properties as discussed earlier. In this work, we have used this polymer to develop novel aortic stent-grafts with unique sutureless design. We have used a new aortic model for their physiological assessment *in vitro* and analysed its long-term durability and compliance. We have also evaluated compatibility with magnetic resonance imaging, which is a crucial factor for their development. The hypothesis, aim and objectives are outlined below.

2.6 Hypothesis, Aim & Objectives

2.6.1 Hypothesis

As discussed here, there is an unmet clinical need to develop new devices to improve long-term durability of endovascular stent-grafts and reduce the risk of complications and reinterventions. The use of a novel nanocomposite polymer which has superior properties of compliance, biocompatibility, and increased mechanical strength, sutureless technology with polymer bonding to nitinol and engineered approach can lead to the development of state-of-the-art stent-grafts which will have long-term durability. These devices can help in reducing the risk of complications, and improve the patient outcomes following endovascular aneurysm repair.

2.6.2 Aim

To develop aortic stent-grafts using a novel nanocomposite polymer based on polyhedral oligomeric silsesquioxane – poly (carbonate-urea) urethane (POSS-PCU)

2.6.2 Objectives

The main objectives of this work are:

1. To utilise POSS-PCU bonded to surface-modified Nitinol to develop a sutureless aortic stent-graft for abdominal aortic aneurysms
2. To develop a prototype using engineered approach and modified origami technology and assess folding efficiency in comparison to current device (Medtronic Talent™)
3. To use the same principles and develop an innovative curved device conforming to the anatomy of thoracic aorta and aortic arch, which will potentially allow manoeuvring and tracking for varying patient anatomies
4. To test a new physiologic aortic model based on POSS-PCU and analyse its compliance and elastic stiffness in comparison to presently used latex model

5. To confirm durability of the sutureless design by extensive in vitro analysis in a simulated pulsatile flow model (for 400 million cycles equivalent to 10 years in human body) based on recommendations by Food and Drug Administration (FDA)
6. To test structural, mechanical, elastic and thermal properties of the fatigue-tested POSS-PCU and compare them to zero-cycled control
7. To analyse compliance, viscoelasticity and elastic stiffness of the curved device in comparison to presently used thoracic stent-graft (Gore TagTM)
8. To compare magnetic resonance properties (image artefacts, signal attenuation and flow velocity) of the curved POSS-PCU nitinol stent-graft with a device in current clinical use (Medtronic ValiantTM)



Chapter 3

Design and analysis of aortic stent-grafts based on an engineered approach using surface modified Nitinol and a Nanocomposite polymer

3.1 INTRODUCTION

Improvement of device durability is a major challenge facing stent-grafts for aortic aneurysms. The stent-graft device is essentially a combination of a traditional textile vascular graft and an intravascular stent. This design is potentially linked to many of the device's difficulties, including incompatibility failures between the device scaffold and cover material, protein absorption and thrombogenic effects, cover material degradation, large device insertion profile and poor device trackability.

We present an innovative design for a self-expanding stent-graft that incorporates a Nitinol (NiTi) alloy scaffold with a polyhedral oligomeric silsesquioxane-poly (carbonate-urea) urethane nanocomposite polymer, chosen for its excellent biocompatibility and superior vascular properties. The polymer is a new type of biomaterial that is hydrophobic and non-thrombogenic, and has been shown to favour endothelialisation^{5;128}. The proposed device combines deployable structure technology to improve the folding efficiency and performance of the device *in vivo*. The scaffold geometry is designed similar to the aortic vessel. This design is further analysed using numerical methods to simulate the nonlinear response of a NiTi alloy scaffold. The fatigue resistance is confirmed by comparing predicted strain amplitude values to published data. These principles are used to develop a stent-graft for infrarenal abdominal aortic aneurysms (AAA).

In addition, we also aim to address the problems associated with the present generation of thoracic aortic endovascular devices by developing a novel stent-graft using the above principles. The new technology allows pre-forming of the angulation of the host aortic arch into the device and due to the bonding of the graft around the metal skeleton, reduces the risk of mechanical stress-related disruption, kinking, migration, and endoleak. Because of the folding technology a more flexible and potentially narrower gauge delivery system can be employed but most importantly the device can

be constructed so that once deployed it will be inherently stronger, more stable and have the degree of angulation tailored to the individual patient. There is also scope to include branch grafts in the folded metal structure to incorporate the major vessels. Such a device has the potential to treat many more patients with this increasingly common condition in our ageing population. It will reduce the need to occlude or reconstruct the great vessels thus significantly reducing complications and risk of operative death associated with hybrid procedures.

3.2 DEVELOPMENT OF AN ENDOVASCULAR STENT-GRAFT FOR AAA USING ORIGAMI FOLDING TECHNOLOGY

This paper proposes to improve the performance of the device using a new approach to stent-graft design that utilises deployable technologies. Specialised folding patterns derived from the art of origami³, were adapted for folding of a stent-graft system to produce a device that packs efficiently and which is small enough to be inserted percutaneously. In addition, it is proposed to improve the *in vivo* performance of the device by using a nanocomposite polymer for the device graft material. The polymer is a type of polyurethane that has been developed specifically for vascular applications. Polyurethanes are composed of hard and soft segments, incompatibility between which, results in microphase separation. This behaviour infers tough, viscoelastic response, that is ideal for vascular applications^{5;128}. Biostability is achieved by incorporation of a biologically stable soft segment group made up of polycarbonate molecules to form a poly (carbonate urea-urethane) (PCU). The material's surface properties are defined by Polyhedral Oligomeric Silsesquioxane (POSS) groups that are covalently bonded to the polymer backbone. These nanoparticle pendant groups modify the material's surface morphology making it resistant to thrombus formation and they are also suitable for chemical modification to promote endothelialisation or for drug delivery.

This paper describes the prototyping and analysis of a stent-graft design which incorporates deployable structures technology with a nanocomposite PCU graft and a Nitinol self-expanding scaffold. It aims to document a new stent-graft design concept and provide a methodology for device scaffold optimisation.

An efficient folding pattern for a thin tube has been developed that is based on origami paper folding theory³. It is proposed to incorporate this pattern in the device to optimise folding and to thereby minimise the device insertion profile. The main objectives of this study are:

1. To define the origami pattern in the nanocomposite polymer (NP) and develop a methodology for folding the tubular structure
2. To optimise bonding between Nitinol and NP
3. To design a device scaffold that facilitates deployment, is compatible with the origami folding pattern, is flexible and provides the necessary radial strength when implanted
4. Embed the wire scaffold in PCU material

3.2.1 Origami Pattern in Polymer

It has been demonstrated that origami derived folding patterns can be used to minimise the diameter of a folded tubular structure and it is proposed to use this technology to achieve a minimal insertion profile for the stent-graft device. However, there are a number of challenges in adoption of this pattern in the NP. These include:

- Developing a methodology for defining the pattern hinge lines in the NP material. (The high flexibility of the polymer material increases the difficulty of this task.)
- Incorporating a scaffold that infers suitable radial strength, is compatible with the origami folding pattern and which folds efficiently to minimise the device insertion profile.

- Ensuring that the stent has a smooth inner surface to minimise turbulence in the blood flow.

3.2.2 Moulding

3.2.2.1 Model

Plaster of Paris was used to cast models of the origami pattern. The casting mould was made using plastic sheet, which was folded into the desired origami pattern and formed into a cylindrical shape. The mould was then positioned vertically in a container of sand as shown in figure 3.1. A tube was fitted over the outside of the plastic mould to maintain its cylindrical shape and a wooden dowel was aligned with the central axis mould to add reinforcement to the casting. Plaster was cast into the mould in 10 mm thick layers, the first of which sealed the base of the plastic model. This approach reduced the risk of leakage at joins in the plastic mould. This method was used to produce a 55 mm diameter model (shown in figure 3.1) of the partially deployed origami pattern and if dip coated, would allow a NP moulding of the pattern to be produced.

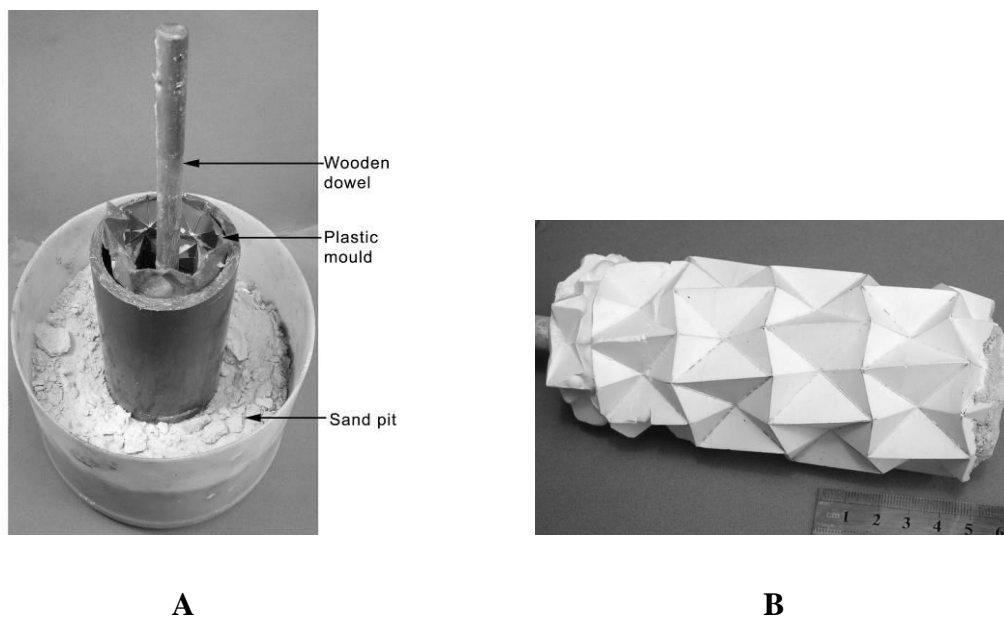


Figure 3.1: Plaster of Paris used to cast models of Origami pattern. Plaster casting arrangement (A) and Plaster of Paris origami model (B)

3.2.2.2 Dip Coating Procedure

A low viscosity or *thin* polymer formulation was chosen for dip coating to promote a homogenous coating. This formulation was developed by adding additional N, N-dimethylacetamide (DMAC) to a 20 wt% polymer solution and resting it overnight to ensure that the DMAC was fully dissolved. The plaster of Paris model was manually dipped in the polymer solution and allowed to dry at room temperature for 30 minutes. While drying, the mould was rotated to minimise dripping and to promote an even coating along the pattern hinges and valleys lines. After this period the model was placed in an oven for 4 hours at 60 °C to evaporate residual solvent, before the procedure was repeated three times. When the target thickness of approximately 100 µm was achieved, the coated model was maintained at 60 °C overnight to ensure all solvent

was removed and the polymer was suitable for removal from the model.

3.2.2.3 Results and Discussion

NP cylinder was moulded with an origami pattern using the dip coating procedure. The moulding was approximately 55 mm in diameter and 115 mm in length. Although this approach was successful in defining the origami pattern, a number of limitations were identified. Firstly, unless the moulding was tensioned both in the hoop and longitudinal directions the material exhibited a non-uniform surface topography that corresponded to that of the plaster of Paris model. This effect is undesirable as it could interfere with the blood flow through the device and result in negative biological effects. In addition, close examination shows that mould was thicker at the valley hinge lines, showing evidence of voids and other defects at these areas. This may be related to shrinkage effects as the N, N-dimethylacetamide (DMAC) solvent was evaporated from the polymer, or possibly due to absorption of the polymer material into the plaster model. Although qualitative testing showed that the moulding tended to fold at the designated hinge lines, close examination showed that this was related to a localised thickness gradient, where the thickest section lay at along the hinge line. Hence, folding was actually occurring to either side of this line and not exactly along the line itself. Accurate location of hinge lines is essential for efficient operation of the pattern and therefore, this effect was seen as a significant limitation. Embedding the scaffold during, or after the dip coating process represented a further challenge. It was concluded therefore, an alternative approach should be investigated and this is described below.

3.2.3 Casting Approach

The origami pattern functions by means of preferential fold lines, or hinge lines. Hinge lines can be created by introducing area of locally thin section. This approach was investigated using flat cast sheets of the NP material, with the aim of developing a methodology that addressed the limitations of moulding approach.

3.2.3.1 Method

1. A 100 μm thick, flat sheet of polymer was cast into a stainless steel tray
2. The origami pattern was printed on paper and taped to the PU sheet so it could be viewed through the sheet
3. A second polymer sheet was cast (200 μm) and cut into panels that corresponded to the origami pattern used in (2), however, which had been reduced in size by 10%
4. The cut panels were glued to the surface of the cast polymer sheet, using the printed pattern as a location guide. The polymer was used as glue.

3.2.3.2 Results and Discussion

A NP sheet was manufactured using the procedure described and the result is shown in figure 3.2. The pattern hinge lines are located between the panels, i.e. where the material is locally thinner. The structure could easily be manually folded (see figure.3.2(B)) indicating that this approach showed promise for fabrication patterns with significantly smaller elements. Although the outer surface of the sheet had a non-uniform surface topography, the inner surface was smooth, making it ideal for inner surface for the graft. No significant defects were identified in the fabrication and qualitative testing indicated that it demonstrated good mechanical strength and toughness. It is proposed to wrap this sheet into a cylindrical form and glue it in place.

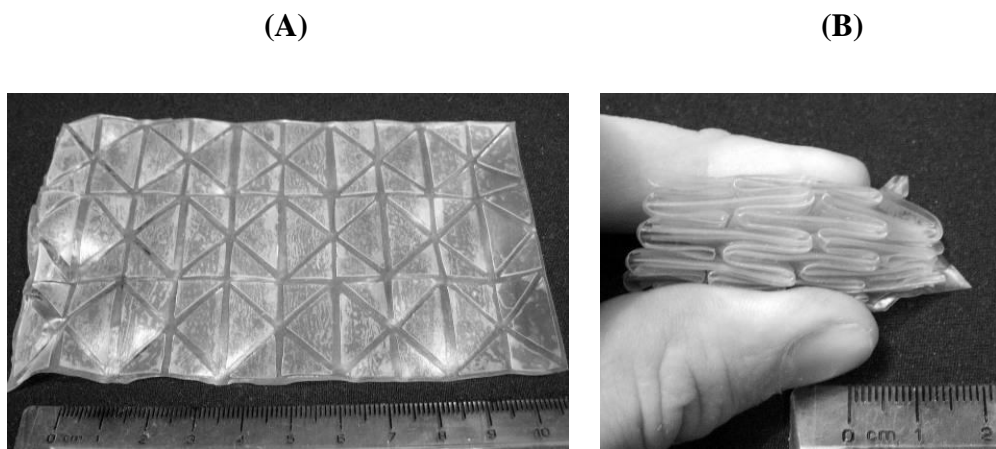


Figure 3.2 NP defined with origami pattern using casting method with number of rows of rectangular elements (A), Folded version of A showing collapse efficiently to a minimum volume (B)

Compact packaging of a tubular structure, such as a stent-graft, can be achieved by introducing carefully designed creases that behave as line hinges. The cylinder shown schematically in figure 3.3(a) shows a folding pattern composed of a number of rows of rectangular elements. Each repeated element is comprised of fold lines that allow it to collapse efficiently to a minimal volume. This folding system can be incorporated into a stent-graft design by orientating the scaffold in an opposing fashion as indicated by the dashed lines shown on figure 3.3(b).

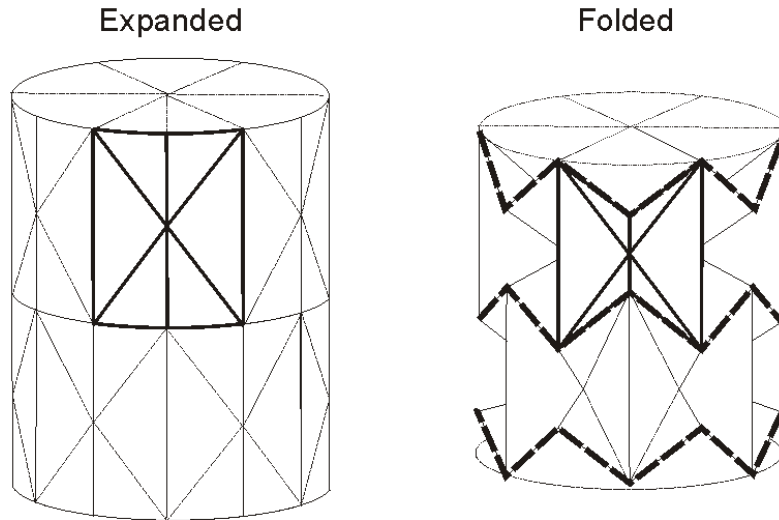


Figure 3.3: Thin walled cylinder folding pattern. Scaffold orientation in opposing fashion as indicated by dashed lines.

3.2.4 Scaffold

The polymer cover material is highly flexible. To overcome this and to facilitate the deployment of the device, a metallic scaffold was embedded in the NP cover. The scaffold has a number of requirements

- drive deployment
- radial strength when fully deployed
- flexibility when folded for delivery
- minimal insertion profile
- compatible with origami folding pattern

A NiTi alloy commonly known as *Nitinol* was used to construct the device scaffold. Nitinol is classed as a *superelastic* material as it can elastically recover strains in excess of 8% via a stress induced (reversible) transformation. The stress-strain curve follows a non-linear path with significant thermal variations occurring as the material undergoes the phase change. The phase change can also be thermally activated at certain critical temperatures. This provides the facility to *freeze* large deformations into the material that can be elastically recovered upon heating above a critical temperature; hence the term *shape memory alloy*. These unusual properties can be used to facilitate the elastic deployment of the device from the catheter tip.

This section describes the procedure used to fashion NiTi wire into support scaffolds for the stent-graft device. NiTi wire of 0.6 mm diameter was shape set into a zigzag pattern using the rig shown in figure 3.4 (A). The following procedure was used:

1. Wire was constrained between pins in rig.
2. The constrained wire was heated in an oven at 550 °C for 15 minutes.
3. The constrained wire was removed from oven and air cooled until it could be safely handled and removed from the rig.

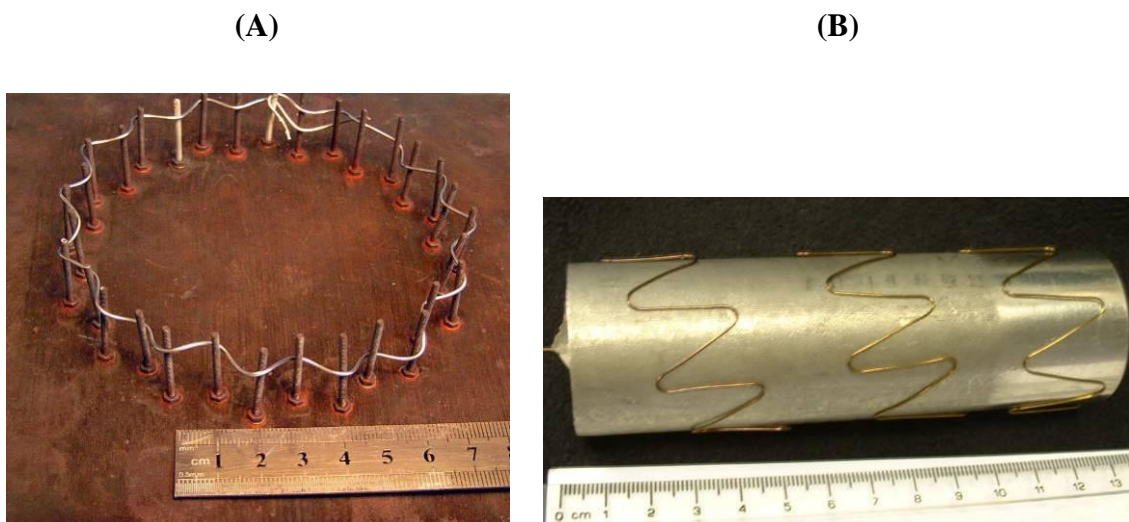


Figure 3.4: Shape setting of zigzag pattern with wire constrained in pins in a rig (A) and helical pattern with zigzag wire hoops placed around a collapsible mandrel (B)

The shape setting procedure was then repeated, however this time to form the wire into a hoop:

4. The zigzag wire was wrapped around a cylindrical tube and bound in place using stainless steel wire figure 3.4 (B).
5. The arrangement was again heated in an oven at 550 °C for 15 minutes and air cooled.
6. The wire was cut to a suitable length and joined using copper sleeves to form a hoop (figure 3.5).



Figure 3.5: Zigzag superelastic wire hoop (A) and wire hoop series (B)

Preliminary testing was conducted to investigate the capabilities of the shape setting procedure and its application for design of the stent-graft. Figure 3.5 shows examples of NiTi alloy hoops (approximately 50 mm in diameter) shape set for use in mould stent-graft cover described earlier. The hoops were joined by overlapping a short section of the wire ends and clamping them with a brass sleeve.

3.2.5 Adhesion Testing

Surface modification of nitinol to promote its bonding with POSS-PCU nanocomposite polymer has been performed by Dr Raheleh Bakhshi, under supervision of Professor Alexander M. Seifalian and these results have been recently published. However, this

work has been referenced here as this concept is critically important and has been integrated in the development of endovascular stent-grafts, as described in this chapter.

Prolonged implantation of NiTi in the human body can result in corrosion of the material and the release of deleterious ions, leading to harmful biological consequences. Coating the NiTi surface with a nonbiodegradable polymer, such as the PCU, can enhance surface resistance to the biological environment, improving its biocompatibility⁴. Furthermore, a surface coating can be used to infer desirable characteristics; for example drug elution and cell attachment. However, polymer coatings can be difficult to apply and it can be difficult to maintain an effective bond for extended periods *in vivo*¹²⁹⁻¹³². In the case of coated vascular stents, it must be demonstrated that any coating can withstand the high strains associated with device deployment without delamination and also maintain its integrity for an extended period post-implantation.

The risk of delamination can be reduced by modifying the substrate surface to promote adhesion. The integrity of the thin film and the adhesion properties between a coating and a metallic substrate surface depend on the surface chemical composition and its physical properties, including, morphology and roughness of the metallic substrate prior to the film deposition¹³³.

We have previously developed and optimised an electrohydrodynamic atomisation (EHDA) deposition process for stent coating¹³⁴. To complete the process of coating, the NiTi strip has to be sprayed for 3 hours.

An Instron 5565 tensometer equipped with a 500 N load cell was used to measure the peel strength of the POSS-PCU coated NiTi strips. The coated specimens were loaded in the test machine as shown in figure 3.6. The peeling process was initiated manually. The lower machine grip was used to clamp the NiTi strip and the upper grip held the polymer film, with an initial distance of 10 mm between the grips. The test was conducted with a crosshead displacement rate of 5 mm/min to a final extension of 40 mm. The thickness of the POSS-PCU coating on the samples tested was determined using SEM.

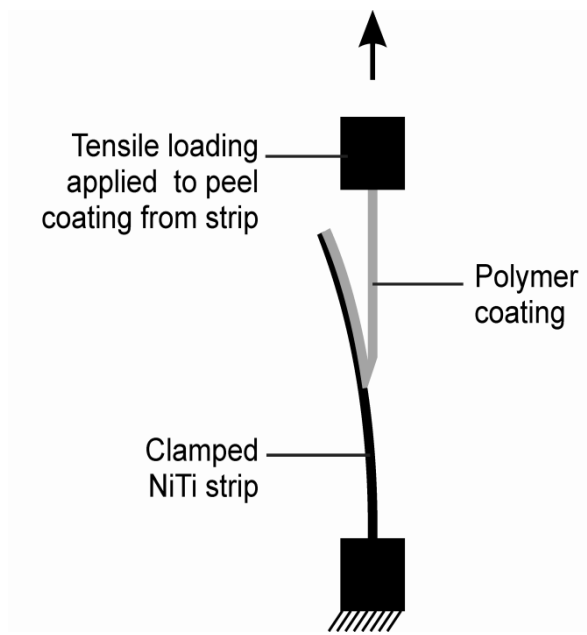


Figure 3.6: Peel test arrangement. Polymer coating held at the top grip and nitinol wire at the bottom grip. Arrow shows the moving directions of the grips

The susceptibility of POSS-PCU coated-NiTi to disintegration has been assessed *in vitro* by incubating the coated strips in biological/chemical solutions. For each type of coating as well as control, five nitinol strips were used for peel strength assessment. For each sample, the test was repeated three times. Peel strength data (figure 3.7) confirms that a significant improvement in adhesion can be achieved by using the modification procedures. Analysis of the data shows that above an extension of 25 mm the load

required to remove the polymer from the modified strip for all the samples is on average 3 times greater than that for the control.

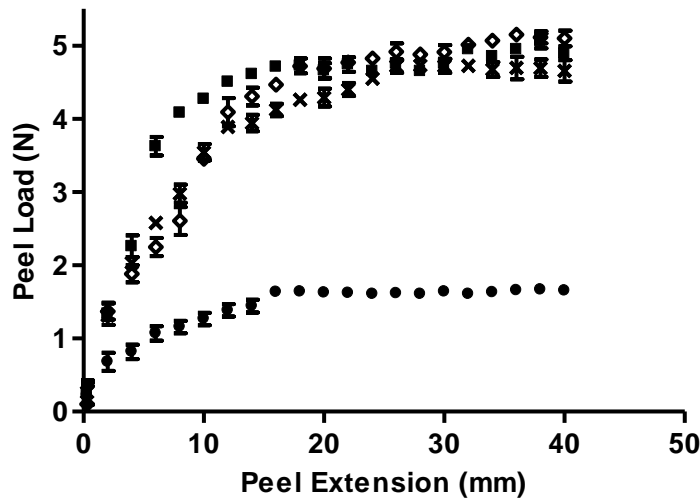


Figure 3.7: Peel strength test for untreated and treated NiTi strip. Graph shows peel extension in mm in comparison to the load applied in N (◇) 100 μm electro sprayed coating on treated NiTi; (◆) 50 μm electro sprayed coating on treated NiTi; (■) Cast coating on treated NiTi; (●) Untreated NiTi

Comparative *in vitro* degradation of the coating on modified and non modified NiTi demonstrates the ability of the coating to remain integral with the stent upon long time exposure to biological environments. The coating has potential to protect the materials surface, mitigate corrosion and increase the longevity of the device *in vivo*.

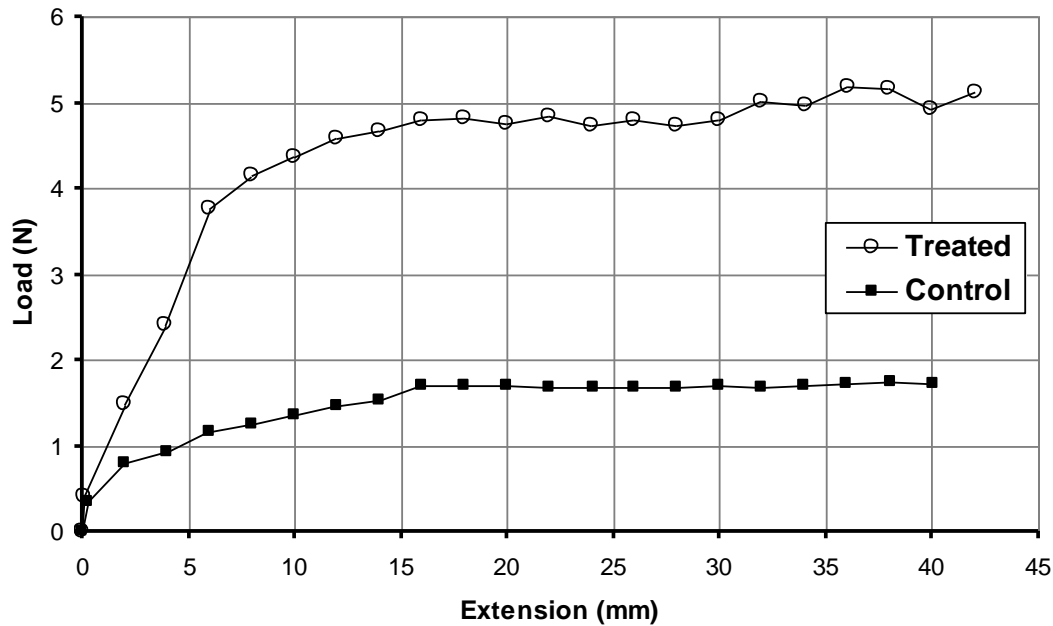


Figure 3.8: Combined peel strength test for untreated and treated NiTi strip with peel extension in mm on X-axis and load (N) applied on Y-axis

3.2.5.1 Results and Discussion

The results of the peel strength tests are shown in figure 3.8. The data confirms that a significant improvement in adhesion can be achieved using the surface treatment procedure. Analysis of figure 3.8 shows that above an extension of 25 mm the load required to remove the polymer from the treated strip is on average 3 times greater than that for the control. It should be noted that below an extension of 10 mm both curves show a positive slope. In this range the applied load is not great enough to break the bond between the polymer and the strip; however, the applied extension causes the exposed polymer (i.e. the polymer that was manually peeled from the strip) to strain.

This initial region of the curve should be ignored and is not significant to the overall peel strength measured.

The peel strength test results are important and necessary to be included here as these set the scene for subsequent studies. Comparative in vitro degradation testing on modified and non-modified nitinol demonstrates the ability of the coating to remain integral with the stent upon long time (70 days) exposure to biological environments under static condition. The results of peel strength have shown that an increase in the bond strength of the POSS–PCU to the metal alloy can be readily achieved upon surface modification. In addition, nickel release profiles showed the dramatic effect that POSS–PCU had on the corrosion resistance of nitinol samples.

Work is currently on going to confirm the repeatability of the values shown in figure 3.9 and to investigate if the treatment process can be optimised further. However, the results of preliminary testing have shown that significant improvement to the bond strength can be readily achieved.

3.2.6 Scaffold Manufacture

A prototype was made to investigate if the folding system could be implemented in physical device. A device scaffold was constructed from Nitinol wire. The wire was constrained in the desired shape and annealed at 550 °C for five minutes followed by air cooling⁵. This shape-setting process was applied twice: firstly to define the zigzag

shape, and secondly to apply the cylindrical curvature. The wire ends were joined using a stainless steel microtube sleeve that was crimped to secure it in place. Flared versions of the hoops, designed for device fixation system, were constructed using a similar process. Straight wire segments, which would act as spacers between the hoops, were cut from virgin material. The scaffold sub-components were subjected to a surface

modification process to enhance the bond between the NiTi wire and the PCU polymer. This process is described elsewhere.

3.2.7 Graft Manufacture

The device was moulded from a PCU polymer blend made from methylene diisocyanate, polycarbonate diol and ethylene diamine in DMAC. The DMAC acted as a solvent, which was removed by raising the temperature to 60 °C. A low viscosity (20 wt %), polymer formulation was selected to assist with achieving a uniform coating. The PCU polymer graft was manufactured by coating a stainless steel tubular mould that could be collapsed to permit removal of the graft. A single coat was applied to the mould and dried before the scaffold segments were positioned over the mould. A second coating was applied to embed the scaffold in the polymer. In parallel with this step, a 250 µm thick polymer sheet was cast in a glass dish. The straight wire segments were embedded in the sheet during the casting process and were subsequently cut from the sheet allowing a 0.5 mm border (approx.) to help prevent the sharp wire ends from piercing through device cover. The straight segments were then glued in place using the polymer and a further two more thin coats were applied to develop a graft wall thickness of approximately 200 µm.

3.2.8 Assembled Prototype

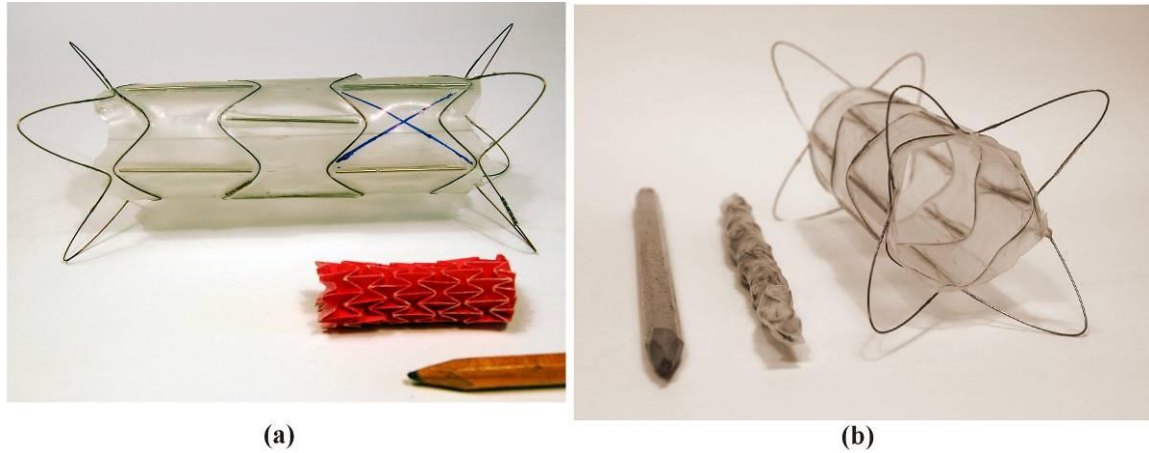


Figure 3.9: (a) Stent-graft first prototype alongside paper model of desired folding pattern and (b) perspective view of stent-graft in expanded and folding configurations

Figure 3.9 (a) shows the completed prototype together with a paper model of the folding pattern described earlier. The scaffold configuration corresponds to the folding pattern used in the paper model. Wire spacers were located between the scaffold hoops to improve the torsional stiffness, whilst also ensuring good definition of the folding pattern and therefore, efficient packing of the graft material between the hoops. Figure 3.9(b) shows a perspective view of the expanding device alongside a folded device. The device was folded by feeding it through a reducing funnel and into sheath that was heat shrunk to constrain the device in its folded condition. A collapsed diameter of 6.5 mm was achieved from an expanded diameter of 31.1 mm. The prototype's folding ratio compares favourably with commercially available systems. For example, the Medtronic Talent stent-graft system, which was initiated in the United States in 1998¹³⁵, has delivery profiles between 7.3 and 8.3 mm for expanded diameters between 22 and 46 mm. Moreover, improvements to the packing and sheathing systems used should make it possible to reduce the packaged diameter to less than 4mm, thereby making it suitable for percutaneous insertion.

Straight-wire segments were used in the first version, but later removed due to the fear that they may pierce and damage the polymer. In the second version, the distance between the hoops was reduced as well (figure 3.10).

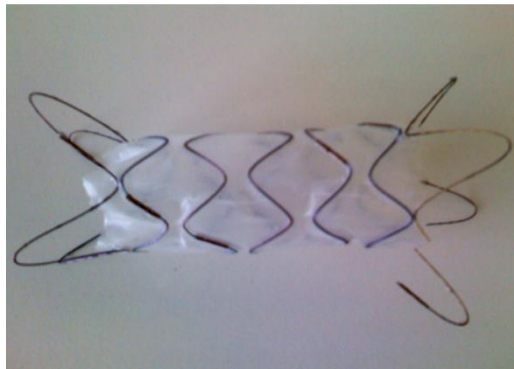


Figure 3.10: Stent-graft modified prototype with removal of nitinol straight-wire segments (from first prototype) due to concern about graft material perforation

3.3 MECHANICAL TESTING OF NITINOL ALLOY

The mechanical properties of superelastic NiTi alloys are highly dependent of material composition, heat treatment history and mechanical processing. Tensile tests were therefore conducted to characterise the mechanical behaviour of the grade of material in use. The first phase of testing was conducted on NiTi strip used during the adhesion testing described earlier. Further test will also be conducted on the wire used in the scaffold prototyping; however, this will be included in future work.

3.3.1 *Materials and Methods*

Mechanical tests were conducted on a strip of NiTi alloy that was 5.715 mm in width and had a thickness 0.254 mm. The material was bought from a supplier in strip form, but had been rolled and subsequently annealed to restore its superelastic properties. The

specimen was held in custom designed grips, shown schematically in figure 3.11, with a gauge length of 143 mm. An Instron static test machine, equipped with a ± 20 kN load cell, was used to apply a tensile load to the specimen with a constant strain rate of 20×10^{-3} /s. A preload of 100 N was applied to remove any slack from the system. The test was conducted in two steps: 1) the specimen was loaded and unloaded to characterise the superelastic behaviour. 2) The same specimen was then loaded to failure to determine the tensile strength and the failure characteristics of the material.

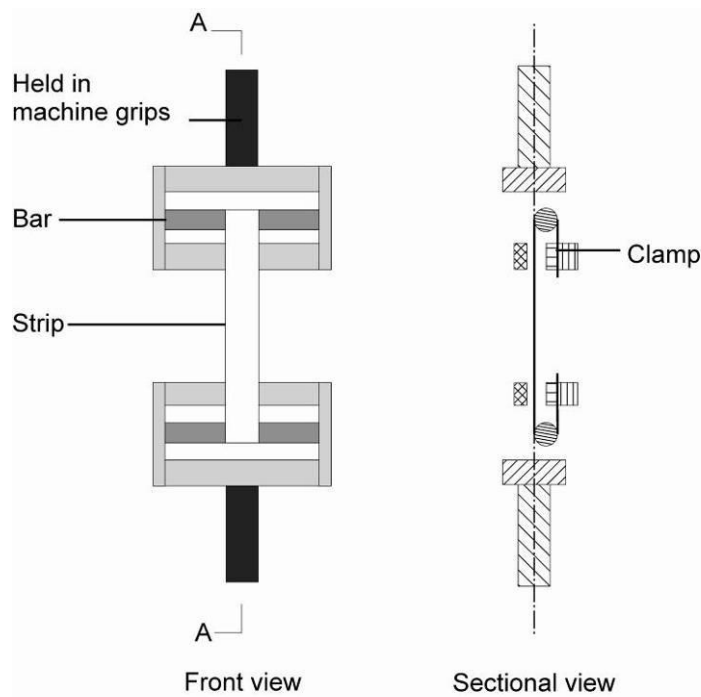


Figure 3.11: Custom-designed grips used for tensile testing of NiTi strip. Front view on the left and sectional view on the right

3.3.2 Results and Discussion

Figure 3.12 shows the stress versus strain curve obtained. In the first loading cycle, the specimen is tensioned to a stress of approximately 650 MPa before being unloaded. This stress was high enough to induce a full transformation to martensite, with the stress-strain curve following a non-linear loop that is characteristic of the superelastic response of Nitinol. This behaviour confirms that the material is operating above its A_f temperature and fully superelastic at room temperature.

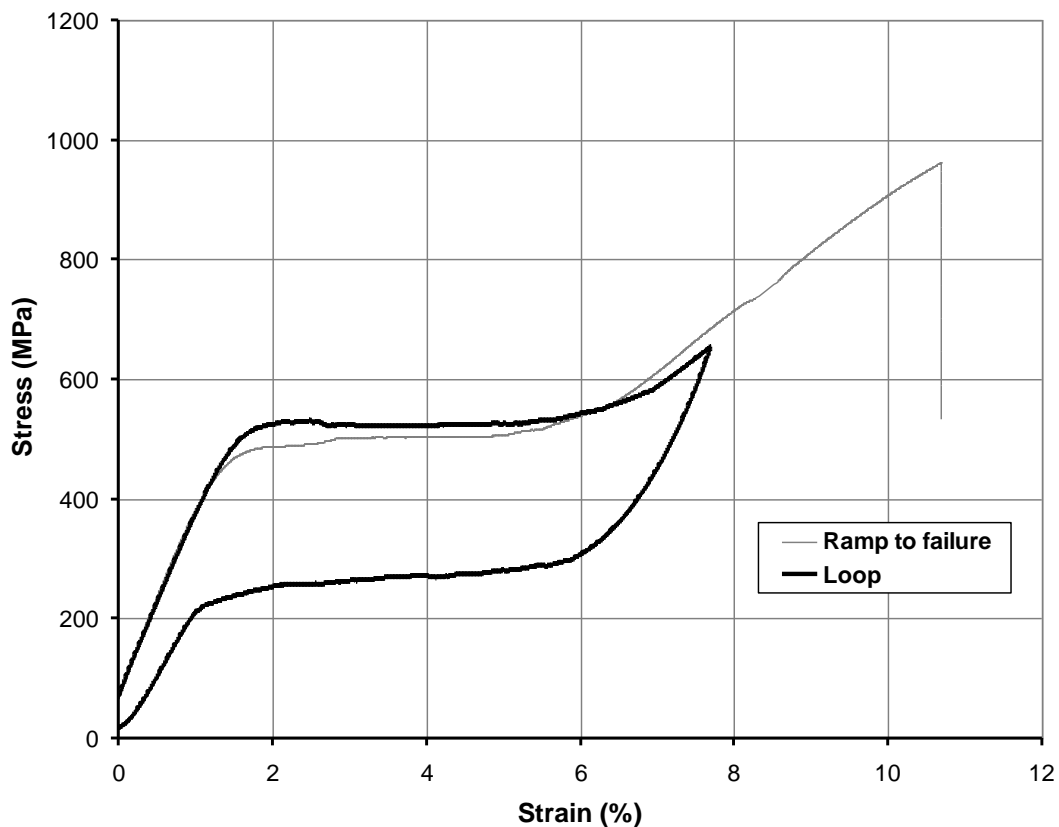


Figure 3.12: Mechanical response of NiTi strip. The stress-strain curve showed in this graph following a non-linear loop characteristic of nitinol

Qualitative analysis of the stress-strain curve profile shows that the Young's modulus of the material varies greatly across its superelastic strain range. In the austenite phase the material has a Young's modulus of 29.4 GPa, which was 3 times greater than that for the martensite phase (9.7 GPa). Moreover, the Young's modulus increases by 61.5% to 25.2 GPa, when the material is unloaded from the martensite phase.

The same specimen was then loaded to failure and the stress-strain curve obtained is also plotted in figure 3.12. Transformation to martensite occurs at a stress of approximately 470 MPa, which is 18.7% lower than that for the first loading cycle. This is likely to be related to residual martensite content from the first loading, which is known to reduce the stress required for initiation of the phase transformation. After the transformation plateau, the material becomes fully martensite and regains its strength.

The specimen failed in a brittle manner with an ultimate tensile stress of 962.2 MPa. This value is slightly lower than typical values quoted in the literature and the material did not exhibit a plastic region, as expected. The brittle properties may be related to the significant amount of cold work seen by the material to flatten it from a circular cross-section to from a strip; however, further testing should be conducted on more specimens to confirm this effect.

3.4 DEVELOPMENT A CURVED THORACIC ENDOVASCULAR STENT-GRAFT

Currently, EVAR stent-grafts, as an alternative to more dangerous open surgery repair, are used to treat AAA/TAA diseases. These stent-grafts consist of a combination of the traditional expandable stent made of metallic mesh wires and a flexible cover. The packaging is achieved by folding the metallic mesh structure.

The cover, which is stitched or bonded to the structure, is considered to be flexible enough to fold neatly between the metallic mesh wires as the mesh is compressed. However, there can be physical and mechanical incompatibilities between the metallic structure and the cover that lead to incomplete deployment of the device, uneven distribution of stresses, or even rupture / tearing of the cover during the expansion of the stent-graft. Furthermore, there is no such device existing on the market which has a natural curved shape to fit the shape of thoracic aorta. This report describes a novel curved stent-graft which is designed specifically for the treatment of TAA and aortic arch pathologies.

This stent-graft consists of zigzag nitinol rings and a graft made of polymer. The nitinol rings can be formed from nitinol wires or from laser cutting on nitinol tubes. At each end of the stent-graft, an additional nitinol ring, which has a conical shape, is attached to provide anchorage of stent-graft inside the aorta.

Upon folding, the stent-graft is first straightened in a way that some polymer partly climbs onto the nearest nitinol ring. Then, the stent-graft can be easily folded as a traditional straight stent-graft because the nitinol rings are positioned in a way that the peaks of a nitinol ring point the valleys of the adjacent nitinol ring.

The folded stent-graft is kept in a delivery catheter and can be delivered to the lesion site just as the tradition stent-graft does. Once the stent-graft is correctly positioned, the catheter is retrieved slightly by first releasing the distal end of stent-graft. Because the end of the stent-graft has a conical shape, it will help to anchor the stent-graft in position. Then, the catheter is further pulled back to gradually release the rest of the stent-graft.

To manufacture such a curved stent needs to follow the steps described in figure 3.13.

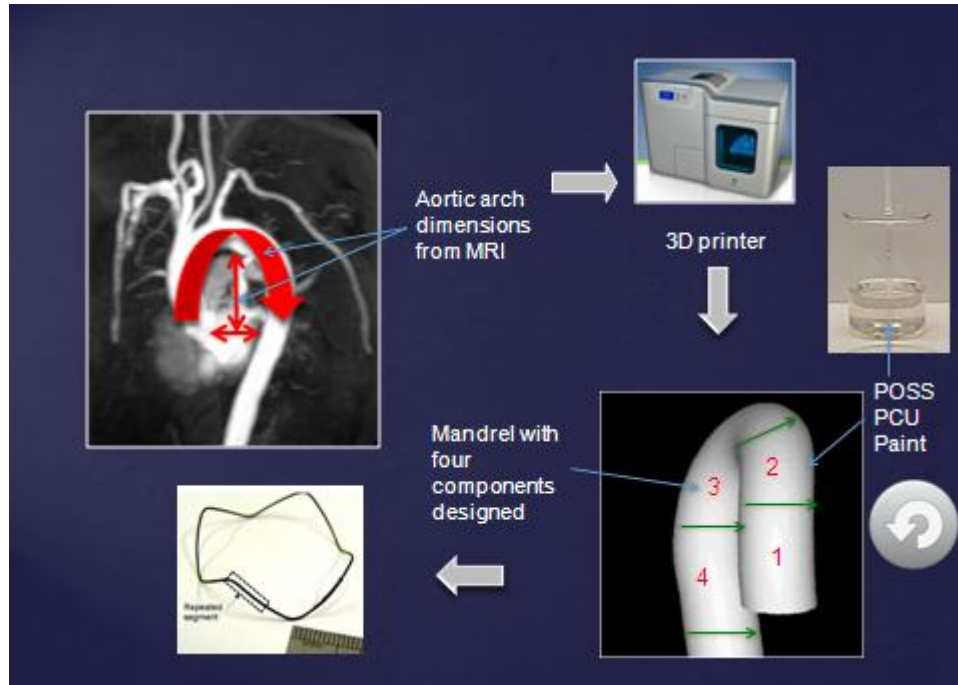


Figure 3.13: Schematic diagram showing step-wise development of a curved stent-graft. Aortic arch dimensions from patient’s MRI used and 3D mandrel developed which is dip-coated with POSS-PCU polymer

First, a curved plastic mandrel, the geometry of which can be carefully defined to match the shape of TAA, is made on a 3D printer.

Second, this mandrel is placed in a box into which silicone mould compound (for example, SE2005 from ACC Silicone Ltd) is poured; wait the silicone compound to dry and take the plastic mandrel out of the silicone mould.

Third, melt Alloy 117 at an elevated temperature and pour the Alloy 117 into the silicone mould; lower the temperature below Alloy 117’s melting point; take the Alloy 117 mandrel, which has exactly the same shape as that of the previous plastic mandrel, out of the silicone mould.

Fourth, paint one thin layer of polymer on the Alloy 117 mandrel; wait until the polymer to dry.

Fifth, place the nitinol rings over the polymer layer on the Alloy 117 mandrel.

Sixth, paint another thin layer of polymer over the entire mandrel; wait until the polymer to dry so that the nitinol rings are embedded in the polymer.

Finally, bring the whole assembly to an elevated temperature which is higher than the melting point of Alloy 117 to let the Alloy 117 mandrel melt and run out of the stent-graft.

The final assembled prototype in fully expanded shape is shown in figure 3.14.



Figure 3.14: A curved stent-graft in fully expanded shape and matching curvature of aortic arch

3.5 CONCLUSION

Combining deployable structures technology with advanced biomaterials provides exciting possibilities for improving stent-graft design. In this study, a prototype has been presented that demonstrates the feasibility of combining these technologies to create a sutureless device with an efficient folding system. The prototype represents the first step in a development process; work is underway to enhance the design by exploiting its capability to be moulded to fit a particular arterial anatomy.

The next stage of this work will be development of a model for physiological assessment of this stent-graft, measure compliance and analyse long-term durability of the sutureless design.

ACKNOWLEDGEMENT

The engineering approach based on Origami pattern was conceptualised and developed by Dr James Eaton-Evans and Dr Zhong You at Oxford. Nitinol surface modification and adhesion testing was performed by Dr Raheleh Bakhshi.



Chapter 4

Development of an aortic model for the physiological assessment of an advanced stent-graft system and *in vitro* compliance measurement

4.1 INTRODUCTION

Polyurethanes have been extensively investigated for biomedical applications, because of their excellent biocompatibility, chemical versatility, and superior mechanical properties¹³⁶. As described earlier, we have developed and patented a non-biodegradable nanocomposite polymer based on polyhedral oligomeric silsesquioxanes (POSS) and poly (carbonate-urea) urethane (PCU), where the POSS nanocages are pendant groups covalently attached to the polymer backbone (POSS-PCU). This polymer is viscoelastic, durable, and has been shown to be biologically stable¹³⁷. In addition, the POSS nanocages alter the surface morphology of the material they are attached to, resulting in a surface that is non-thrombogenic¹³⁸. In the earlier chapter, we have described development of an innovative self-expanding, suture-less stent-graft for endovascular aortic aneurysm repair (EVAR) use that incorporates a Nitinol alloy scaffold bonded with this nanocomposite polymer. Because of novel physicochemical and biological properties, this new polymer has superior properties to Dacron and PTFE and favours spontaneous endothelialisation¹³⁹. The next stage of our work is to accurately test the fatigue life of the stent-graft under physiological conditions simulating the nature of the pumping heart.

We identified the need to develop an aortic model in which these stent-grafts could be deployed during their assessment under simulated physiological conditions as they need to be analysed for 400-million cycles of pulsatile mechanical fatigue (equivalent to 10 years in human body) according to Food and Drug Administration (FDA) guidelines. Current models of aortic aneurysms for stent-graft assessment and development are anatomically correct but do not match physiological properties of living aortic tissue. A need exists for a circulation model that behaves in a physiological manner for testing vascular devices in normal and pathological states. Our main goal was to develop a synthetic tube using a material which exhibits properties of compliance, anti-thrombogenicity and spontaneous endothelialisation. So we made a preliminary assessment of elastic properties of porcine abdominal aorta. We developed

an aortic model using nanocomposite polymer due to its superior properties as described above. We also used latex synthetic aortic model which has been used before for *in vitro* testing in cardiovascular research^{140;141}.

The compliance is a function of the diameter and a vessel is defined as distensible or compliant when a small change in pressure translates into large volume change^{142;143}. The mechanical properties of the arterial wall have a significant effect on blood flow characteristics and should therefore be mimicked in any model of the circulation. To perform compliance studies, we fabricated a flow circuit specifically designed accurately to reproduce the haemodynamic characteristics of pulsatile arterial blood flow.

4.2 MATERIALS AND METHODS

4.2.1 Acquisition of porcine abdominal aorta

Porcine abdominal aortas were obtained from the animal research centre at Northwick Park Hospital, London. All abdominal aortas were excised from the same portion and stored in an ice box before the experiment. The vessel diameter varied from 18-mm to 22-mm. The aortas were removed and stored with surrounding tissues. Before the study, bench surgery was performed to dissect and skeletonise the aortas. Six pieces were used from six different animals. The main branches of the aorta were controlled taking sutures with Silk 3-0. The tissues were stored in Ringer Lactate's solution at 4°C and studied within 24 hours of harvest. The tissues were obtained in accordance with the local ethics committee standing orders regarding experimental use of animal tissues and the care of animals was in accordance with the institution guidelines and National Research Council's guide. They were stored in Ringer Lactate's solution at 4°C and studied within 24 hours of harvest.

4.2.2 Development of an aortic model using novel nanocomposite polymer

The nanocomposite polymer POSS-PCU developed by our group was used. A cylindrical rod of 25-mm diameter was immersed in the polymer and allowed to dry for 15 min. A small portion of the polymer dripped down. It was then re-immersed for two more times in a similar fashion. The rod coated with triple-layered polymer was then placed in an oven overnight at 60°C. After 12 hours, the polymer had completely dried and formed a uniform layer. It was then peeled off the cylindrical tube thus forming a synthetic tube adjusted to a length of 20-cm.

4.2.3 Latex synthetic aortic model

For comparison, a latex tube of similar diameter (25-mm) was used. It has been used before in models for analysis of vascular stents and grafts.

4.2.4 Compliance Methodology

4.2.4.1 Flow Circuit

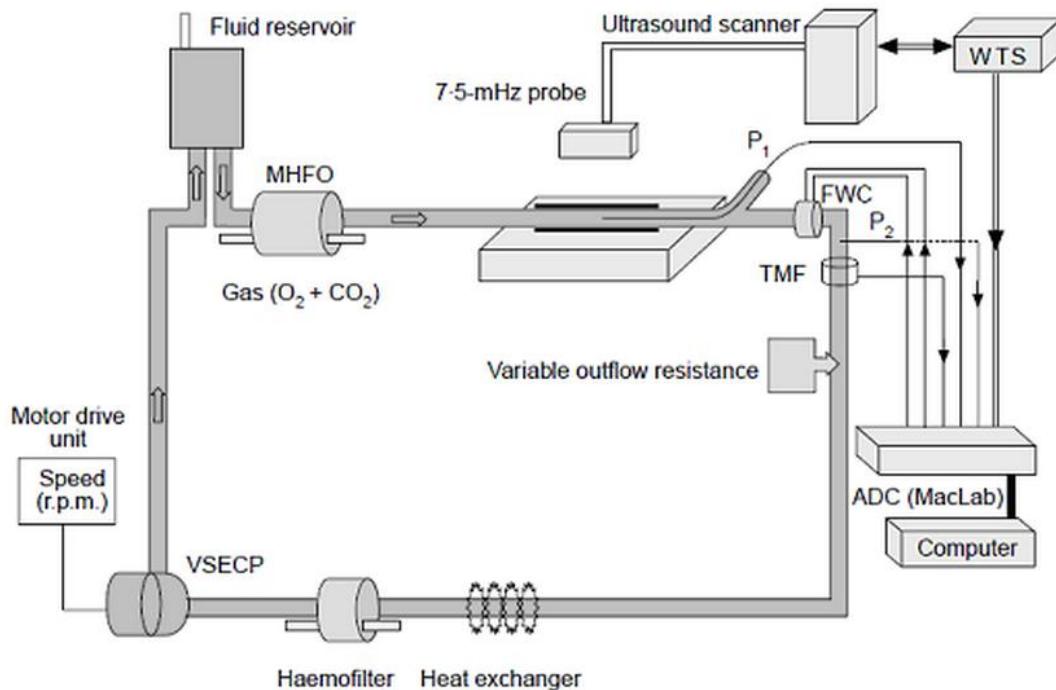
We have developed an ideal flow circuit for assessing the dynamic behaviour of grafts. The flow model comprised of a variable-speed electromagnetic centrifugal pump (Bio Medicus, Minnetonka, MN, USA), flexible plastic tubing and a fluid reservoir (Figure 4.1). A previously developed governable flow waveform conditioner was sited in series with the circuit and used to generate arterial flow waveforms. Instantaneous flow rate was measured using a 6-mm tubular flow probe connected to a Transonic Medical flowmeter system (HT207; Transonic Medical System, Ithaca, NY, USA). Serial intraluminal pressure measurements were made at discrete sites along the porcine and synthetic aortas using a Millar Mikro-tip catheter transducer (Millar Instruments, Houston, Texas, USA) introduced via a Y-connection port. For aortas, no difference was noted at different sites like juxta renal aorta, aortic bifurcation or opposite branches. The solution used for perfusion of porcine aortas was anticoagulated blood from the

Royal Free Hospital Blood Bank, to simulate the *in vivo* situation. For synthetic aortas, the perfusion solution was made using 8% low molecular weight Dextran (molecular weight 77000-Da; Sigma-Aldrich, Poole, UK) added to a solution of M199 (minimum essential medium), 20% fetal bovine serum, 7.5% sodium bicarbonate (Sigma-Aldrich), 200-mmol L-glutamine (Gibco BRL; Life Technologies, Paisley, UK), penicillin 10000-units/ml and streptomycin 10-mg/ml, buffered at pH 7.20 ± 0.01 . The viscosity of this medium has previously been determined to approach that of whole human blood using a cone plate viscometer (Low-Shear 30; Contraves, Zurich, Switzerland)¹⁴⁴. Studies using blood were feasible in our prosthetic models. However, we preferred to use a synthetic solution as this was the solution to be used for long-term fatigue-testing and we felt it would be appropriate to determine the compliance of this model keeping the physiological parameters constant. Blood was unsuitable for fatigue-testing due to the need for long-term usage (more than one year), limited availability and potential for pump-related cell damage in the fatigue-testing experiment. This perfusion fluid has practically Newtonian properties with linear relationship between shear rate and shear stress. It differs slightly from blood, which has higher viscosity at low shear rates, but this discrepancy is of importance only in capillaries and for the purpose of this study can therefore be ignored. A gas mixture of 95% oxygen and 5% carbon dioxide was bubbled through the fluid reservoir and the perfusate was maintained at 37°C via a heat exchanger (Portex, Hythe, UK). Pressure was varied by increasing the level of fluid reservoir above the graft segment and by varying the diameter of outflow resistance sited distally to the grafts.

The porcine abdominal aorta, 25-mm triple coated polymer tube and 25-mm latex tube were all studied. To ensure minimal leakage transmurally and through the branches, the aortic segments were subjected to a pre-clotting procedure. This was carried out by forcing 10-ml freshly obtained whole human blood through graft interstices; once the blood had clotted, a further 10-ml fresh blood was perfused through the graft and the

process repeated, if necessary until no further leakage of blood was observed. The aortas and the synthetic tubes were mounted in series with the flow circuit, exposed to flow and placed in a bath containing normal saline maintained at 37°C. All outputs were fed into a commercial analogue-to-digital data acquisition recording system (ADC/MacLab; AD Instruments, Hastings, UK).

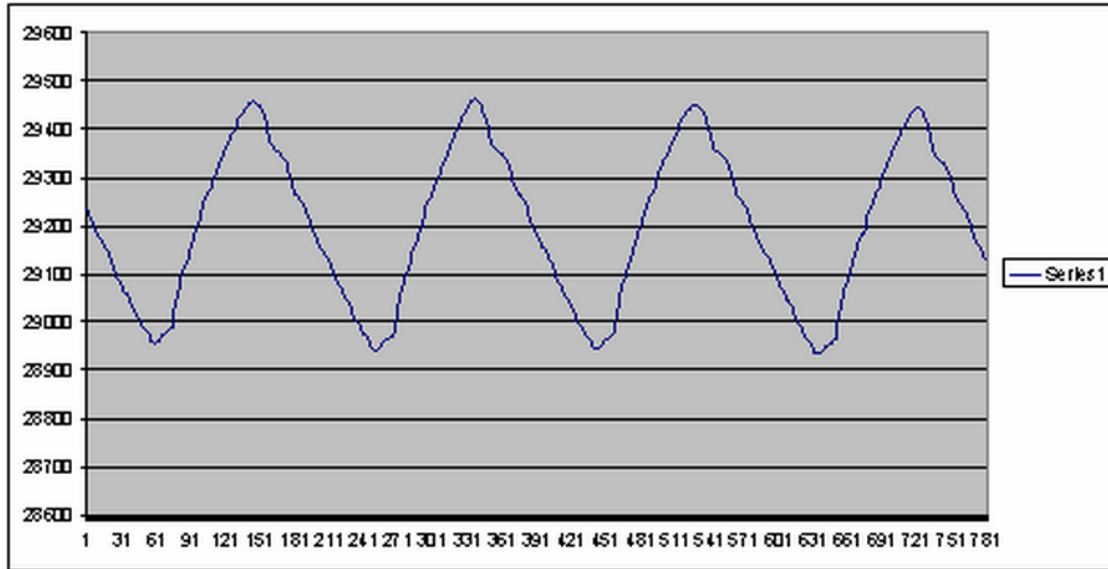
Figure 4.1: Diagrammatic representation of the flow model used for measurement of compliance and elastic stiffness index. ADC, analogue-to-digital data acquisition recording system; FWC, flow waveform conditioner; MHFO, maxima hollow fibre oxygenator (Medtronic, Anaheim, CA, USA); P1 and P2, Millar Mikro-tip pressure transducer; TMF, Transonic Medical flowmeter system; VSECP, variable-speed electromagnetic centrifugal pump; WTS, wall-tracking system



4.2.4.2 Measurement of vessel wall movement

The change in vessel wall diameter with respect to each cardiac cycle was measured at discrete sites along the graft, with measurements taken in the sagittal plane at 90° to the long axis of the tube. The segments of the aorta and the synthetic tubes were scanned with a specially adapted, duplex colour-flow ultrasonography system (Wall Track; Pie Medical Systems). This system allowed the measurement of vessel wall movement over time by automatically tracking assigned points of the induced radiofrequency signal deemed to be representative of the anterior and posterior arterial walls. A detailed description of the system has been published elsewhere^{145;146}. Briefly, a 7.5-MHz linear array probe was immersed in the bath and positioned directly over the segment under investigation. The M-mode cursor was positioned at the midpoint of each test segment and perpendicular to the direction of flow; the change in induced radiofrequency signal received from the vessel walls was then sampled over time. These data were then transferred to a personal computer for real-time display of the displacement waveforms of the anterior and posterior artery walls. In this way, end-diastolic and end-systolic intra-luminal diameters were determined automatically over the pulsatile cycle (Figure 4.2). Measurements were made using a near-constant pulse pressure over a range of mean pressures (Table 4.1). For each mean pressure and test segment, three measurements of wall movement were made, and the experiment was repeated six times.

Figure 4.2: Distention-time curve generated by wall-tracking system to show change in vessel wall diameter with each cardiac cycle. Distention in μm on X-axis and time in seconds on Y-axis



4.2.5 Data Analysis and Statistical Methods

Diametrical compliance (C) defined as the inverse of Petersen’s elastic modulus $E_p^{147;148}$, and expressed as per cent per millimetre of mercury $\times 10^{-2}$, was determined for each test segment at each mean pressure as follows:

$$C = (D_s - D_d / D_d) \times 10^4 / (P_s - P_d)$$

where D_s and D_d are systolic and diastolic diameter, and P_s and P_d are systolic and diastolic pressure, respectively.

Arterial wall stiffness index, β as formulated by Kawasaki *et al*¹⁴⁹, was calculated using

$$\beta = [\log_e (P_s / P_d)] \times D_d / (D_s - D_d)$$

For each mean pressure, the compliance and stiffness values of porcine aorta, polymer tube and latex tube were compared with one-way analysis of variance and Bonferroni test¹⁵⁰.

4.3 RESULTS

When the aortas and tubes were inserted in the model, triphasic flow was seen in all of them with little difference in flow waveforms. The analysis was done on six aortas and four polymer models. For latex, two tubes were initially used but as the model failed, it was not carried any further.

4.3.1 Flow Circuit haemodynamic values

These values are shown in Table 4.1. For each model the frequency of pulsatile cycle was 1-Hz. The mean pressure range for the latex model is lower than the porcine aorta and polymer model; this is because the latex aorta was unable to withstand a mean pressure of 120 mm of Hg. The pulse pressure and flow rate were comparable for all three models. The perfusate temperature was constant at 37°C. The viscosity for the fluid used in the polymer and latex models was 0.035-poise.

Table 4.1 Typical Flow Circuit haemodynamic values (mean \pm SD)

Physical Parameter	Porcine aorta	Polymer aortic model	Latex aortic model
Mean Pressure (mm Hg)	30-120	30-120	30-90
Pulse Pressure (mm Hg)	54 \pm 8.8	54 \pm 8.8	50 \pm 4.6
Flow rate ml/min	138 \pm 35	140 \pm 25	132 \pm 24
Perfusate temperature (°C)	37	37	37
Perfusate viscosity (poise)	Blood	0.035	0.035

4.3.2 Compliance and stiffness index averaged over entire mean pressure range for porcine aorta, polymer and latex aortic models

A summary of the compliance and stiffness index values for porcine aorta and polymer and latex aortic models is provided in Table 4.2. The compliance values and stiffness index decreased with progressive increase in pressure for both porcine aorta and polymer model, but remained nearly constant for the latex model. Figures 4.3 and 4.4 depict the variation of compliance and stiffness index with respect to incrementally increased mean pressures from 30 mm Hg to 120 mm Hg. Curves of anisotropic vessels (aorta, polymer model) were generated using non-linear regression (single phase exponential decay model); however curve for isotropic latex model was generated using linear regression (Figure 4.3). The stiffness index-mean pressure curves were also generated in a similar way (Figure 4.4).

Arterial compliance was observed to behave in a non-linear fashion in response to elevation in mean perfusion pressure. Figure V shows how latex model failed by significant distension when the mean pressure was increased from 90 mm Hg to 120 mm Hg (figure 4.5).

Figure 4.3: Compliance-Mean Pressure curves for porcine aorta, polymer and latex models. Data presented as mean and error bars represent standard deviation

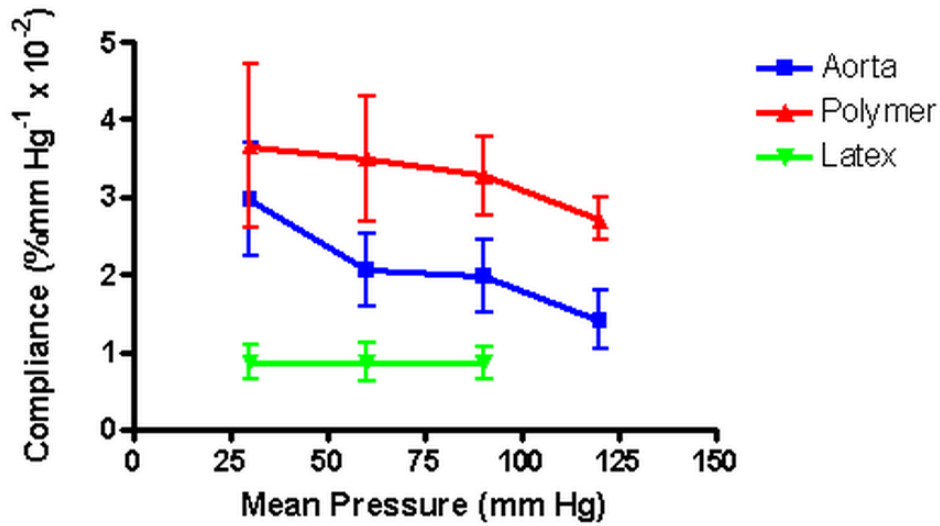


Figure 4.4: Stiffness Index-Mean Pressure curves for porcine aorta, polymer and latex models. Data presented as mean and error bars represent standard deviation

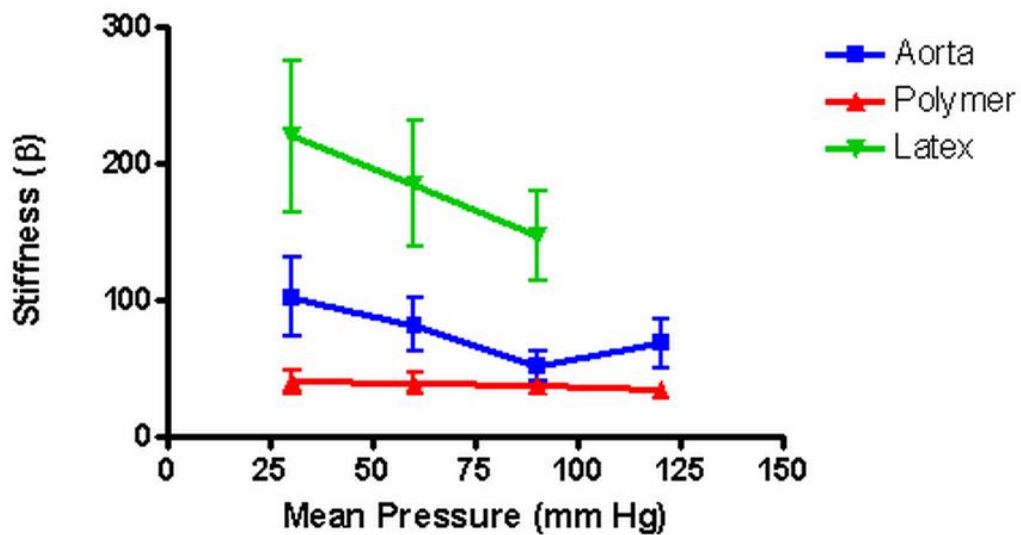


Table 4.2 Compliance (C) and Stiffness index (β) values across a range of pressures*Porcine Aorta*

Pressures (mm Hg)			Compliance	Stiffness Index
Mean	Systolic	Diastolic	C (mean \pm s.d)	β (mean \pm s.d)
30	66	12	2.97 \pm 0.72	101.6 \pm 28.9
60	94	43	2.07 \pm 0.47	81.7 \pm 20
90	120	75	1.98 \pm 0.47	51.3 \pm 10.7
120	164	98	1.42 \pm 0.37	68.2 \pm 17.5

Polymer aortic model

Pressures			Compliance	Stiffness
Mean	Systolic	Diastolic	C (mean \pm s.d)	β (mean \pm s.d)
30	66	12	3.66 \pm 1.05	39.8 \pm 8.5
60	94	43	3.50 \pm 0.81	39.2 \pm 7.5
90	120	75	3.28 \pm 0.51	37.0 \pm 5.5
120	164	98	2.72 \pm 0.28	34.2 \pm 3.8

Latex aortic model

Pressures (mm Hg)			Compliance	Stiffness
Mean	Systolic	Diastolic	C (mean±s.d)	β (mean±s.d)
30	66	12	0.87 ± 0.22	220.1 ± 55.6
60	94	43	0.87 ± 0.24	184.8 ± 45.7
90	120	75	0.86 ± 0.20	146.7 ± 33.1
Latex tube became distended at this point				

Figure 4.5: Latex model showing significant distension on increasing mean pressure from 90 mm Hg to 120 mm Hg



Compliance of aorta ranged from 2.97 ± 0.72 (mean \pm s.d.) to 1.42 ± 0.37 percent per mm of Hg $\times 10^{-2}$. By one-way analysis of variance, the polymer aortic model was significantly more compliant (range 3.66 ± 1.05 to 2.72 ± 0.28 ; $P < .05$) as compared to porcine aorta with no significant difference in elastic stiffness but similar anisotropic behaviour. This was further confirmed by Bonferroni's Multiple Comparison Test (Aorta vs. Polymer, Mean Diff.: -1.180, 95% CI: -2.175 to -0.184, $P < .05$). However the stiffness index, although lower than the aorta, did not reach statistical significance (Mean Diff.: 38.15; 95% CI: -9.967 to 86.27, $P > .05$) and as shown in Figure 4.4, it exhibited similar anisotropic behaviour on serial increment in mean pressure.

Latex tubes exhibited compliance lower than the aorta. This was significantly low on Bonferroni's testing (Aorta vs. Latex, Mean Diff.: 1.243, 95% CI: 0.169 to 2.318, $P < .05$) and it was significantly more stiff than the aortic tissue (Mean Diff.: -108.2, 95% CI: -160.1 to -56.2, $P < .001$). It also exhibited an isotropic behaviour unlike aorta.

4.4 DISCUSSION

Arteries are not merely passive conduits, conducting blood from one part of the circulation to another. Their elastic structure allows the energy-efficient transmission of pulsatile blood flow together with simultaneous damping of excessive pressure fluctuations and the matching of the impedance characteristics of the proximal arterial tree to distal branches¹⁵¹⁻¹⁵³. The aim of this study is to develop a new aortic model with physiological properties for the assessment of aortic stent-grafts under simulated conditions. The model should have compatible compliance and viscoelasticity for long-term fatigue analysis of vascular stents and grafts.

4.4.1 Methodological considerations

The elastic behaviour of a vessel can be determined statically by measuring incremental change in vessel diameter during step-wise inflation of an intraluminal balloon, but this approach does not allow for the contribution that vessel or graft wall viscosity (i.e. inertia) makes upon the *in vivo* elastic response¹⁵⁴. The amount of radial movement (strain) that a vessel wall exhibits in response to a change in intra-luminal pressure (stress) is not only dependent upon the magnitude of the pressure change but also the rate at which the pressure is applied *i.e.* wall behaviour is viscoelastic¹⁵³. Thus, in order to fully characterise likely *in vivo* graft or vessel viscoelastic behaviour, a dynamic approach was required. So, a pulsatile flow circuit, capable of supporting biological tissues, was designed to allow cyclical application of wall stress and the reproduction and manipulation of physiological flow parameters. This *in vitro* approach allowed rigorous control of the physical forces that the grafts or vessels were exposed to in order to allow valid comparison of different vessels and graft types.

An ultrasound echo-locked wall tracking system was used to record change in graft or vessel diameter over each pulsatile cycle. The perfusion rig allowed uniform stretch of the vessels. Both the anterior and posterior walls of the aorta or the synthetic tube being tested must be imaged by ultrasound wall tracking to be successful. The aim to use porcine aorta was to establish values of compliance for natural vascular tissue.

4.4.2 Anisotropy and Isotropy

It was decided to measure the elastic behaviour of the aortas and synthetic models over a range of mean pressures. This is because arterial tissue is heterogeneous; non-hookean (i.e. does not exhibit a linear pressure-distension curve) material whose compliance behaviour is strongly pressure-dependent^{151;155}. In patients with significant cardiovascular disease, central arterial stiffness becomes significantly nonlinear¹⁵⁶. At low pressures the load is predominantly borne by highly distensible elastic fibres but at high pressures it is transferred to the poorly elastic collagen fibres^{157;158}.

The stretch behaviour of arteries is anisotropic i.e. the extent of distension is dependent upon the degree of pre-stretch (the operating mean blood pressure) prior to the application of the stress (the pulse-pressure). Generally, non-biological prosthetic grafts do not exhibit this behaviour and there is little or no change in degree of circumferential stretch (compliance) as mean pressure changes, at least over the physiological range¹⁵⁹.

Our aim was to analyse a model that could be used for assessment of fatigue and pulsatile durability of an aortic stent-graft. We wanted to perform this testing using the ASTM standards (ASTM F2477 - 07 Standard Test Methods for in vitro Pulsatile Durability Testing of Vascular Stents). This test method requires that model used for durability testing is assessed for compliance at physiological pressures. So we decided to measure at this range achieving diastolic blood pressure up to 100 mm Hg. Our study did have a high mean pressure of 120 mm Hg and high systolic pressure of 164 mm Hg for accurate assessment over a wide pressure range. In this study, POSS-PCU did not fail at these pressures. We have not calculated burst pressures as it was not our aim but it has been analysed in a different series of experiments done in our department.

4.4.3 Comparison of compliance of porcine abdominal aorta and the synthetic polymer and latex aortic models

The new model appears “over-compliant” compared to aorta in this pressure range, principally because of the homogenous, uni-elastic quality of the honeycombed urethane. However, it can be argued from a theoretical viewpoint that this pattern of compliance might be advantageous. Following implantation, all prosthetic grafts become invaded by connective tissue elements that can fix the graft wall thereby diminishing the compliance that initially existed¹⁶⁰. Thus it may be necessary to engineer a degree of “over-compliance” into the prosthetic models in order to buffer subsequent tissue-induced stiffening. In addition, in humans a significant decrease in AAA compliance is immediately observed after endovascular stenting which reflects complex interactions between all components of stented aneurysms¹⁶¹.

Latex model was less compliant and significantly stiffer than aorta and on increase in pressure from mean of 90 mm Hg, it failed by significant distention. In addition, due to the isotropic and linear elastic response of the latex-wall and Laplace principle, it is not possible to simulate the non-elastic response effect, as found *in vivo*, in the latex model¹⁶².

4.4.4 Utility of stiffness index (β) for in vitro measurements

Stiffness index β was originally formulated in order to allow valid comparison of distensibility between vessels exposed to different mean blood pressure^{163;164} as comparison of compliance is only allowed when mean pressures are equivalent. Thus its maximum utility lies in the *in vivo* arena where comparison between subjects is desired. In this study, measurement of graft or vessel distensibility were undertaken for the same mean pressure over a pressure range of 30-120 mm Hg and therefore comparison of compliance values is valid. However the similarity in the stiffness index between the polymer and aortic tissue further confirms that this model exhibits similar physiological properties. The latex model is significantly stiffer.

4.4.5 Compliance match between model and graft material

We will be testing a stent-graft made from the same nanocomposite polymer as in the aortic model. It is fair to conclude that there is no compliance mismatch between this model and stent material. When the stent-graft is deployed in this model, it will result in increase in the thickness of the polymer exposed to pulsatile flow. In a previous study¹⁶⁵, compliance was assessed for different thicknesses of POSS-PCU (approximately 0.35 mm for thin grafts vs. 0.50 mm for thick grafts) and it was noted that with the increase in thickness, the compliance becomes more constant. So we think that this model is appropriate. This model has now been successfully used for fatigue-testing over a period of 12 months for 400 million cycles equivalent to 10 years in human body without any signs of failure or change in compliance.

4.4.6 Limitations

The criticism of using the *in vitro* approach is the limited applicability to the *in vivo* situation. *In vitro* studies may overestimate *in vivo* arterial elasticity as the latter is influenced by the degree to which adjacent connective tissues tether arterial wall excursion¹⁵¹. Furthermore, *in vivo* vessels experience a variable amount of smooth muscle tone secondary to sympathetic and humoral influences¹⁶⁶. Although artificial circulation testing systems cannot replace *in vivo* models, they can be used for mechanical fatigue testing and in addition, to develop experimental protocols, testing device feedback control algorithms, and investigating flow profiles.

4.5 CONCLUSIONS

Our work demonstrated that the new aortic model based on a novel nanocomposite polymer (POSS-PCU) provides a greater degree of compliance and stiffness match than the current available model. It has shown great promise for use in models of the arterial system. It is physiologically relevant exhibiting compatible anatomy, compliance and viscoelasticity which could be used for long-term fatigue analysis of vascular stents and grafts. The use of these compliant artificial vessels will allow the construction of more physiologically accurate flow systems with the possibility of making comparative measurements between a vascular model, normal subjects and patient group with aortic disease. The commercially available latex mock aortas can fail at physiological pressures. We have utilised this model for long-term fatigue and durability assessment of our stent-graft as described in the next chapter.



Chapter 5

Fatigue Analysis and Accelerated Durability Testing of AAA stent-graft based on Nitinol scaffold bonded to a Nanocomposite polymer

5.1 INTRODUCTION

As discussed in the introductory chapter, endovascular aneurysm repair (EVAR) has evolved but graft-related complications and reinterventions remain substantial and are associated with significant aneurysm-related mortality¹⁶⁷. Newer devices need to be developed in the quest to improve long-term durability of EVAR stent-grafts.

As mentioned, our stent-graft is based on polyhedral oligomeric silsesquioxanes (POSS) and poly (carbonate-urea) urethane (PCU) and its structure is shown in figure 5.1).

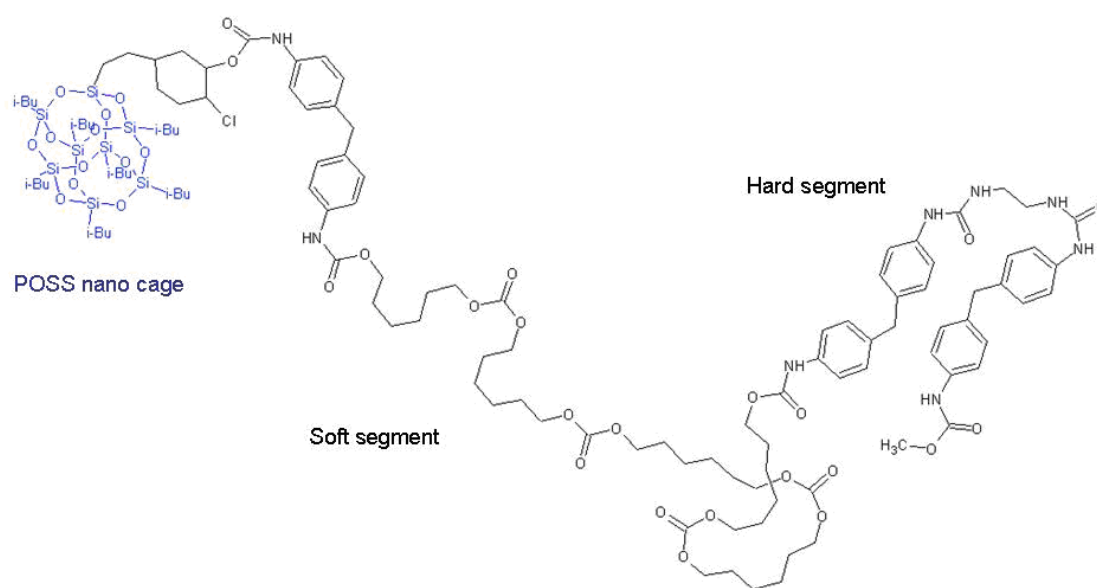


Figure 5.1: Three-dimensional structure of polyhedral oligomeric silsesquioxane molecule with hard and soft segments of polyurethane attached to POSS nanocage

Nanocomposite components interact at a nanoscale level conferring greater mechanical strength and anti-fracture properties to these polymers¹⁶⁸. As already mentioned, the POSS-PCU polymer is viscoelastic and durable, and has been shown to be biologically stable¹⁶⁹. In addition, it has a nonthrombogenic surface and shows potential for spontaneous endothelialisation¹⁷⁰⁻¹⁷². In our design, the graft material is bonded to the metal skeleton rather than being sutured. The scaffold design uses principles of maximised folding efficiency to provide effective long-term fatigue resistance. A surface treatment protocol for nitinol that uses anodisation and chemical surface modification increases its bond strength with the polymer.

The US Food and Drug Administration (FDA) recommends durability testing to the equivalent of 10-15 years of pulsatile loading (400- to 600- million cycles at 72 heartbeats per minute) for cardiovascular implant devices¹⁷³. Implant fatigue performance is of prime importance as stent-grafts are subjected to complex loading conditions *in vivo*. At the end of the testing phase, devices need to be examined for fractures thus resulting in a “pass/fail” acceptance criterion.

The main aim of this study was to assess durability of our aortic stent-graft under simulated physiological conditions for 10-years according to FDA guidelines analysing changes in surface, mechanical and thermal properties in comparison to control stent-graft of the same type with zero-cycles.

5.2 METHODS

5.2.1. Fabrication of the sutureless non-modular aortic stent-graft

The fabrication of non-modular stent-graft is revisited here with emphasis on coating strength and durability as it is a paramount factor.

The stent-graft was made using a 30-mm collapsible stainless steel scaffold dip coated with polymer. Its synthesis has been described previously¹⁷⁴. A low viscosity or thin polymer formulation was chosen to promote a homogenous coating. This formulation was developed by adding additional dimethylacetamide (DMAC) to a 20 wt% polymer solution rested overnight to ensure that DMAC was fully dissolved. Nitinol wire with shape-memory properties was constrained between pins in a rig to make Z stents. These were wrapped around a cylinder tube, heated in an oven at 550°C for 15 minutes and air cooled to allow cut to a suitable length and joined using copper sleeves to form a hoop. The collapsible mandrel was dipped in polymer solution and air-dried for one hour before being placed in an oven at 60°C for two hours. A second coat was similarly applied. In parallel, a 250 µm thick polymer sheet was cast in a glass dish. The wire segments were embedded in the sheet during the casting process and subsequently cut allowing a 0.5 mm border to protect sharp edges. The straight segments were then glued in place using the polymer and a further two more thin coats were applied to develop a graft wall thickness of approximately 100 µm.

The sutureless stent-graft design is based on the principles of our previous work on polymer coating of surface modified nitinol stent¹⁷⁵. The results of this work confirm that a three-fold increase in bond strength between nitinol and POSS-PCU polymer can be achieved by surface modification of metal alloy and comparative in vitro degradation studies demonstrate the ability of the coating to remain integral with the stent upon long time (70 days) on exposure to biological environment in static conditions. The coating stability has also been confirmed by exposing to plasma fractions and hydrolysis. The coating maintained its integrity and strong adhesion to the strut during the entire degradation process without any signs of instability or delamination.

The final assembled prototype deployed in a similarly made 25-mm cylindrical tube cutting from POSS-PSU with thickness of approximately 200 μm used as a mock artery is shown in figure 5.2. The deployment was similar to endovascular aneurysm repair without any external constraints. We have previously assessed the folding efficiency of this stent-graft and we achieved a collapsed diameter of 6.5 mm from expanded diameter of 31.1 mm and this corresponded to a reduction ratio of 4.8. This compared favourably to currently used device. For example, the Medtronic Talent has delivery profiles between 7.3 mm and 8.3 mm with expanded diameters between 22 and 46 mm¹⁷⁶. However as a part of this work, we did not focus on deployment using packing and sheathing systems and it was achieved manually. The choice of the inside diameter of the artificially simulated vessels is critically important to the effectiveness of the durability test. We selected a model with the diameter of 25-mm to match the size of the normal aorta. The stent-grafts deployed were 30-mm in diameter as a degree of oversizing is desirable.

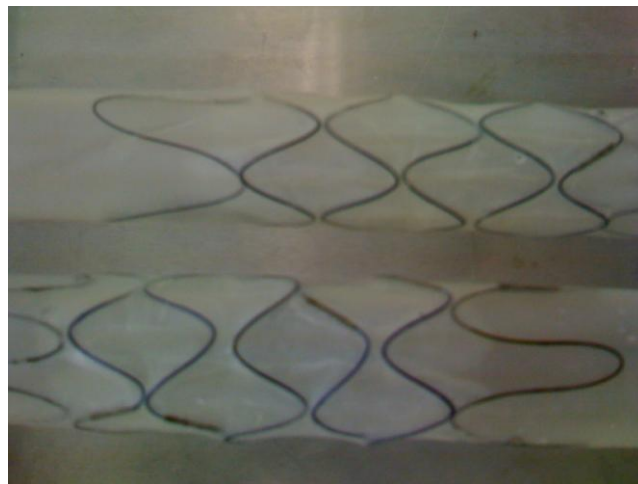


Figure 5.2: Final assembled stent-graft prototype deployed in a compliant polymer model, ready to be implanted in the fatigue-testing circuit

5.2.2. Fatigue-testing circuit

The designed apparatus used in this experiment is shown in figure 5.3.

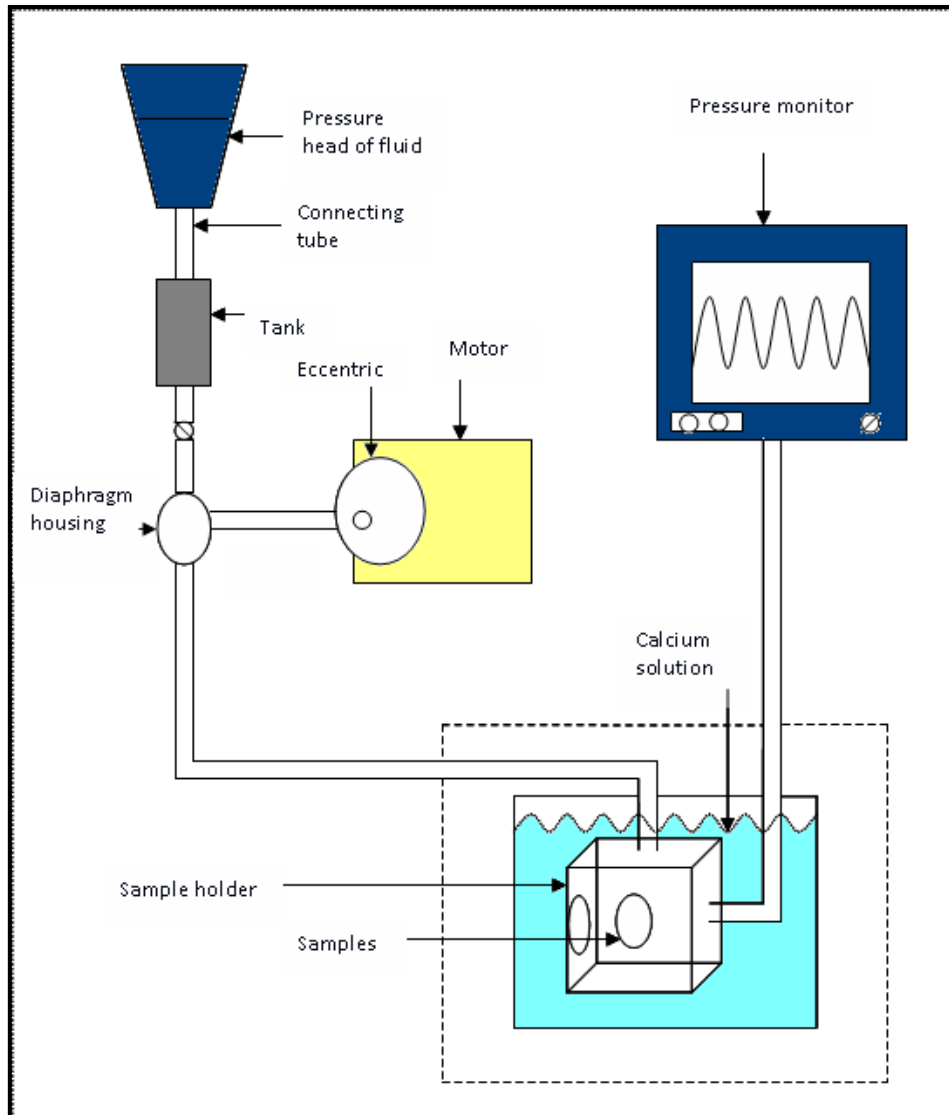


Figure 5.3: Schematic of the pulsatile flow circuit used in the experiment. Sample-holder connected to the pumping system and monitor. A valve controlling pressure and motor connected to eccentric and linked to diaphragm by connecting rod

The stent-grafts were subjected to an accelerated circumferential pulsatile fatigue test at 45-Hz. The inner side of the sample-holder chamber was filled with distilled water, in direct contact with the pumping system, exposing the samples to pulsatile mechanical stress. The solution tank and samples were placed in an incubator at 37° C and 5% CO₂ over the test period. We closely considered the solution to be used for perfusion. It would have been ideal to use blood however we felt it was unsuitable due to the need for long-term usage (more than one year), limited availability and potential for pump-related cell damage in the fatigue-testing experiment. Normal saline has been used predominantly in *in vivo* models and we did not think it would offer any advantage over distilled water. Phosphate-buffered saline has also been used in biological research but we did not use it due to concerns of bacterial growth, as it was not possible to keep the entire apparatus sterile for long periods of time as required in this experimental work.

Pressure head of fluid provided mean pressure to the system and was connected to a pump, which provided oscillatory pressure about the mean (i.e. pulse). A solenoid-operated valve controlled application of pressure to the specimens. The motor was operated by speed controller allowing it to run at 2500-rpm and was connected to an adjustable eccentric, which was linked to the diaphragm by a connecting rod. The eccentric could be adjusted to pump between 0-19 mm³ of fluid and the diaphragm pump was used to create pulsatile force for dynamic testing of samples. Leading down from the diaphragm was a connector, which was joined to a tube that was passed into a cell culture incubator (Hercell 150, Heraeus, USA) and was connected to the sample holder device. A small outlet in the sample holder device connected it by a small tube to a Datex-Engstrom Light monitor (Datex-Engstrom Division, Instrumentarium Corp., Finland). This was used to monitor the pressure of the pulsatile stress of the inside fluid of sample holder chamber during the test on a weekly basis.

5.2.3. Surface topography

Following completion, all stent-grafts were visually assessed for any damage to the polymer graft or nitinol wires.

5.2.3.1 Scanning electron microscopy

The fatigue-tested polymer and control sheets were dehydrated with ethanol/distilled water in increments of 10% ethanol at 41 °C and then freeze-dried for 2 days. Following this, sections of the nanocomposite were attached to aluminium stubs before being coated with gold using an SC500 (EM Scope) sputter coater. Next, a scanning electron microscope system (Philips SEM Model 501, Netherlands) was used to analyse 10 areas of the polymer sheets chosen at random for surface degradation namely pitting, fissuring, cracking¹⁷⁷ and crystalline segment shearing ('balding').

5.2.3.2 Fourier transform infra-red spectroscopy (FTIR)

The stent-graft sheets of POSS-PCU were subjected to infra-red spectrophotometric analysis to detect any sub-surface bond degradation. Pre and post fatigue test, using an ATR-FTIR analyser (FTIR-4200, Jasco, UK), the surfaces of the polymeric films were exposed to infra-red spectra of 4000–600 cm⁻¹ at 4 cm⁻¹ resolution with thirty scans per sample. The analysis was repeated 3 times and averaged. Both surfaces of polymer sheets were exposed at an incident angle of 30° and the subsequent spectrum was presented in relation to absorbance. The peaks present in these spectra represent the excitation of chemical bonds within the material as a result of applying infrared energy corresponding to the specific vibrational energy of that bond. Loss in intensity of the absorbance peaks is indicative of the degradation behavior of the material.

5.2.4 Compliance analysis

As described before¹⁷⁸ POSS-PCU grafts were placed in series within a flow circuit containing a solution with viscosity similar to blood (0.035-poise) pumped at 1-Hz and at mean pressures of 60 to 120-mmHg using a variable speed pump (BioMedicus, Minnetonka, MN, USA) in order to simulate arterial pulsation. The change in the diameter of the graft with respect to each cardiac cycle was measured at discrete sites along the stent-free graft wall at 90° to the long axis of the stent-graft. Segments of the graft were scanned with a specially adapted duplex colour-flow ultrasonography system (Pie 350; Pie Medical Systems, Maastricht, The Netherlands). A 7.5 MHz linear array probe was positioned directly over the segment under investigation. The change in induced radiofrequency signal received was then sampled over a 4 second interval. These data were then transferred to a personal computer for real-time display of displacement waveforms of the anterior and posterior graft walls. In this way, end-diastolic and end-systolic intraluminal diameters were determined automatically over the pulsatile cycle. Diametrical compliance (C) defined as the inverse of Petersen's elastic modulus $E_p^{147;148}$, and expressed as %/mm Hg $\times 10^{-2}$, was determined for each test segment at each mean pressure as follows:

$$C = (D_s - D_d / D_d) \times 10^4 / (P_s - P_d), \text{ where}$$

D_s and D_d are systolic and diastolic diameter, and P_s and P_d are systolic and diastolic pressure, respectively.

5.2.5. Mechanical resistance and elasticity

5.2.5.1 Radial stress-strain studies

An Instron 5565 tensometer equipped with a 500 N load cell was used to measure the radial strength of the POSS-PCU polymer. Sample thickness was measured using a micrometer and specimens loaded in the test machine (figure 5.4). This study is based on the ASTM D413 standard, to determine the force per unit width required to separate a rubber layer from a flexible substrate such as fabric, fibre, wire, or sheet metal (ASTM D413 2007). The adhesion strength is equal to the mean force recorded during the test.

The lower and upper machine grips clamped the polymer film, at a starting distance of 10-mm. The test was conducted with a crosshead displacement rate of 5-mm/min to a final length of 40-mm. Both stent-graft and control specimens were tested. The system was programmed to collect data relating static stress and static modulus as a function of strain (strain %). A stress–strain curve was plotted with strain/vessel wall distension on the x -axis and systolic pressure representing circumferential stress on the y -axis to understand the difference in biomechanical behaviour of fatigue-tested and control polymers and then to correlate this information with the classical Hookean laws.

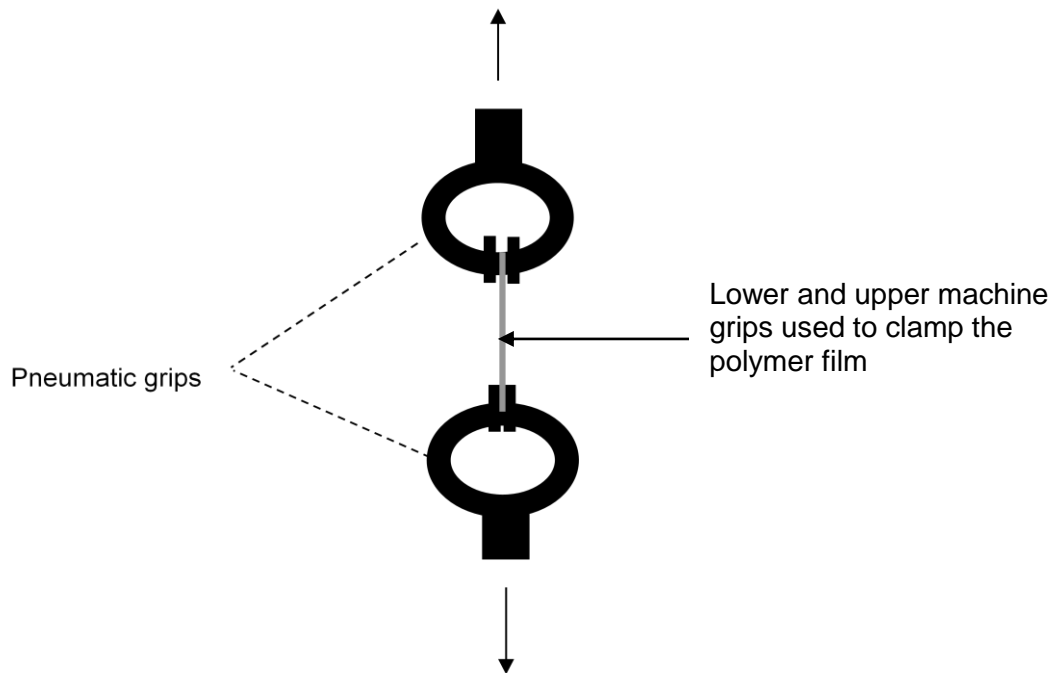


Figure 5.4: Schematic for stress-strain studies. The polymer film clamped in the pneumatic machine grips.

5.2.5.2 Linear elasticity

This investigation was performed using ASTM F703 methodology using ISO 37 dumbbell-shaped specimens (size type 3). Polymer tubes were opened to flat sheets and dumbbell shapes cut using a cutting machine. A 10-mm long portion was marked along the inner 20-mm length segment of the dumbbell and wall thickness was measured at three points along the 10-mm marked segment (at both ends and middle). The dumbbells were then attached to a tensometer. The marked segments were manually stretched to 200% (20mm), 400% (40mm) and 500% (50mm) lengths. The samples were left in the stretched position for 60 seconds, removed and allowed to relax for a further 60 seconds. The length of the marked segment was then measured and the percentage elastic deformation calculated for a total of six samples from each group using the following formula:

$$\left(\frac{\text{Length after Stretching}}{10} - 1 \right) \times 100$$

5.2.6 Thermo-mechanical resistance

5.2.6.1 Differential scanning calorimetry (DSC)

The POSS-PCU grafts pre and post-fatigue were studied by differential scanning calorimetry to determine whether the respective samples had undergone a significant change in glass transition temperature (T_g) and melting temperature (T_m) using a heat-flux differential scanning calorimeter (DSC-60 Shimadzu Ltd., Japan) in a dry nitrogen atmosphere equipped with a liquid nitrogen cooling unit.

Samples 20 mg in weight and 3 mm x 3 mm in size from different parts of the polymer were used for T_m and T_g measurements. The DSC was calibrated using an indium standard. The thermal cycle ranged from -50 °C to +280 °C at a heating rate of 10 °C/min. The glass transition T_g was calculated as inflection in the C_p change and all specimens were run three times. All samples were weighed pre- (W) and post-test (W') to confirm that there was no change in mass after melting.

5.2.6.2 Thermo-mechanical analysis (TMA)

Thermo-mechanical analysis (TMA) was performed using a Shimadzu TMA-50 analyser. Samples 4-mm × 4-mm were placed in a covered aluminium crucible. Previously the probe displacement had been set to zero on the crucible and lid. The sample in the crucible was then cooled to -100 °C to induce its glassy state. A static load (0.5-N) was applied to the sample and the initial displacement of the probe was measured giving the starting sample thickness. The sample was then linearly heated at 2 °C/min to 300 °C and the resulting displacement or sample compression (expressed as % of sample thickness) was plotted against temperature.

5.2.7. Acceptance criteria

The stent-graft was classified as “failed” if it met any one of the following:

1. At least one broken strut in the nitinol.
2. Cracks on SEM analysis of nitinol compared to any visible cracks in the control, a significant change being classified as failure.
3. Significant change in compliance.
4. Significant loss of mechanical strength evidenced by stress-strain and linear elasticity studies
5. Significant loss of thermo-mechanical resistance

5.2.8. Statistical Analysis

The data from each experiment obtained was plotted and analysed using GraphPad Prism 4 software (GraphPad, San Diego, CA, USA). The data are presented as means and standard deviation. Statistical analysis of tests was carried out using the student's t-test.

5.3 RESULTS

All four stent-grafts successfully completed the 400-million cycles equivalent to 10 years of cardiac cycles in an average human adult. The test parameters are outlined in table 5.1.

Table 5.1: Test parameters from fatigue-testing circuit

Physical parameter	Variable
Mock vessel dimensions (n=4)	Diameter: 25 mm Length: 25.28 ± 0.51 cm (mean \pm s.d.)
Test stent-grafts dimensions (n=4)	Diameter: 30 mm Length: 7.07 ± 0.14 cm
Control stent-graft dimensions (n=1)	Diameter: 30 mm Length: 7.1 cm
Temperature	$37 \pm 1^\circ\text{C}$
Pressures	Systolic pressure range: 65 to 112 mm Hg Diastolic pressure range: -32 to 8 mm Hg Pulse pressure: 94 ± 14 mm Hg

5.3.1. Surface topography

5.3.1.1 Visual inspection and scanning electron microscopy

The polymer graft appeared intact with no holes or leakage points on visual inspection (figure 5.5). The nitinol wire showed no breakage. SEM images confirmed these findings (figure 5.6). The POSS-PCU polymer showed smooth surface with flat areas and very few crystalline peaks, a consistent feature seen in all analysed samples. Post fatigue-testing, there was some wear and tear on the inner surface of POSS-PCU polymer (figure 5.6c) but there were no cracks, pits, fissures or balding. Similarly, the outer surface showed uniform covering over the nitinol stents (figure 5.6d) with no signs of failure.

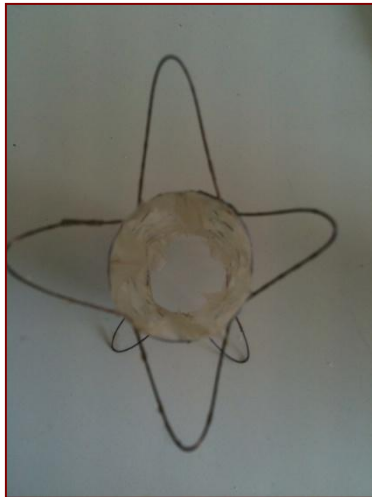
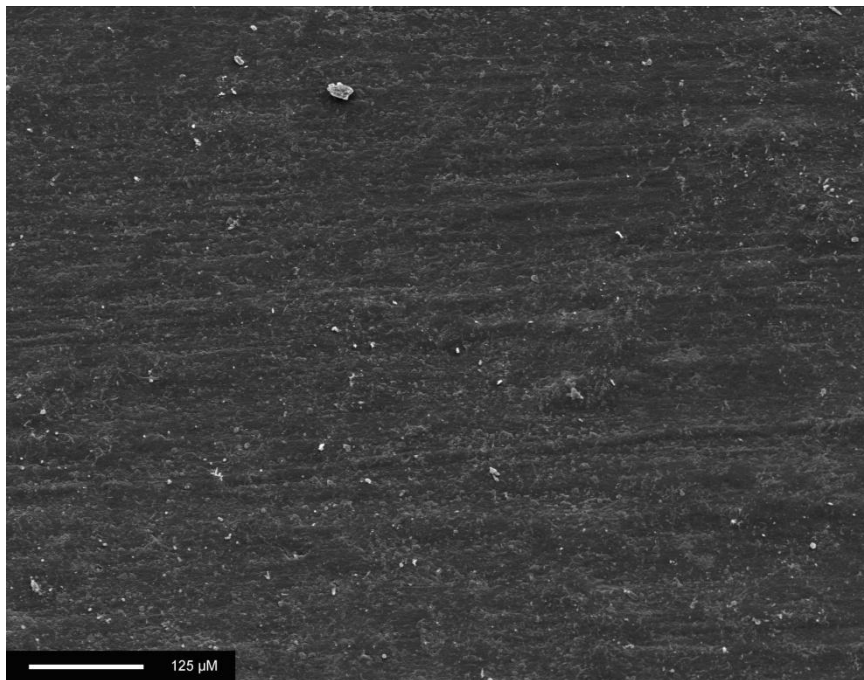
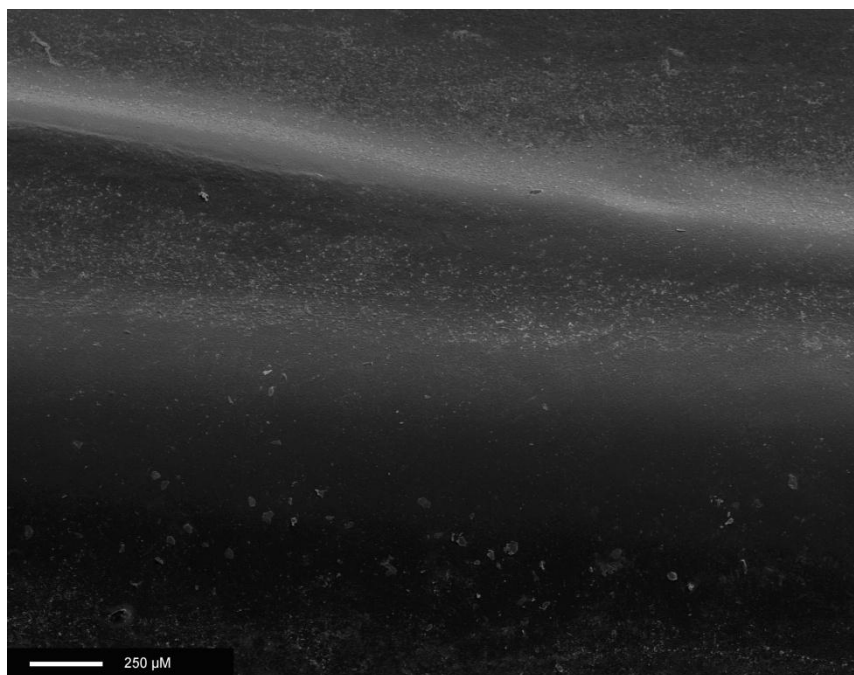


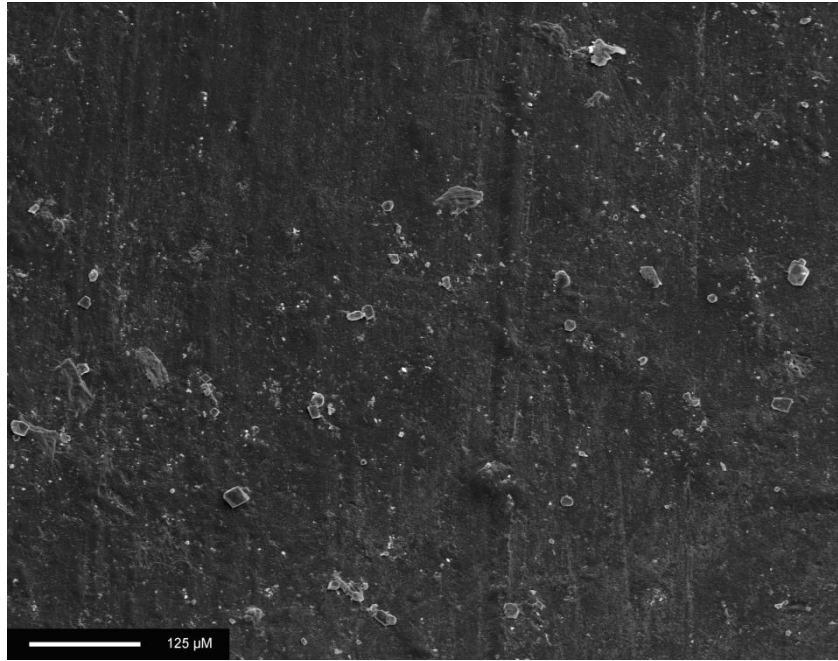
Figure 5.5: Images of the stent-grafts post-fatigue testing. Visual inspection revealed intact polymer and nitinol with no signs of breakage.



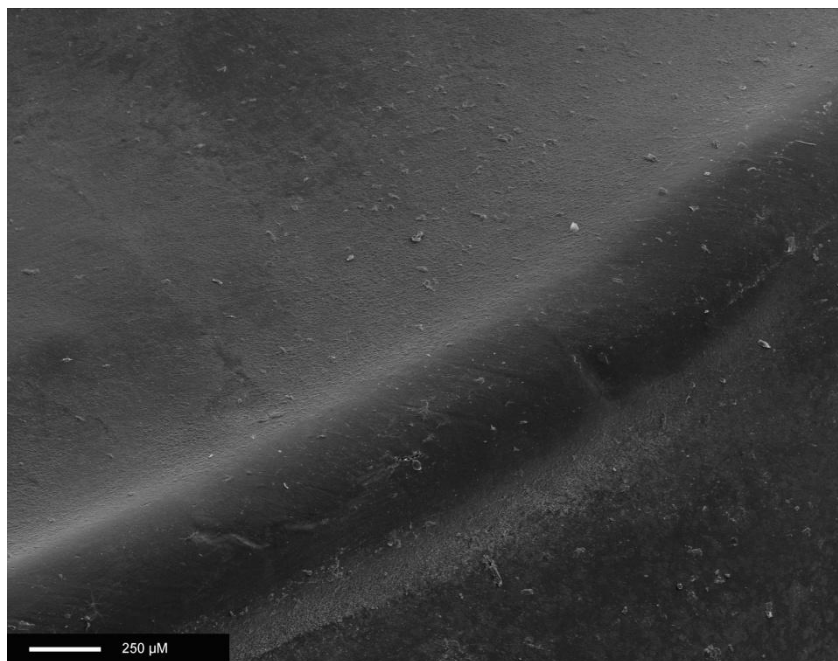
(a) Inner surface of control POSS-PCU



(b) Outer surface of control POSS-PCU (covering over the nitinol stent)



(c) Inner surface of fatigue-tested POSS-PCU



(d) Outer surface of fatigue-tested POSS-PCU with smooth covering over nitinol

Figure 5.6: Scanning electron microscopy images of stent-grafts (160X magnification). (a) Inner surface of zero-cycled control POSS-PCU (b) Outer surface of control POSS-PCU (c) Inner surface of fatigue-tested POSS-PCU (d) Outer surface of fatigue-tested POSS-PCU. No significant signs of degradation seen

5.3.1.2 Fourier transform infra-red spectroscopy (FTIR)

It was found that there were only small spectral differences between the pre and post fatigue test observed in Si-O (1111.76 cm^{-1} in control vs. 1105.01 cm^{-1} in fatigue-tested sample), NHCO (1738.51 cm^{-1} in control vs. 1728.87 cm^{-1} in fatigue-tested sample) and N-H (3324.68 cm^{-1} in control vs. 3327.57 cm^{-1} in fatigue-tested sample) bonds (figure 5.7 and figure 5.8). These differences were insignificant in terms of loss or gain of POSS-PCU chemical bonds for each bond wavelength as compared to control except the difference noted in the –NHCO- bonds (62% transmittance (1728.87 cm^{-1}) for fatigue-tested sample as compared to 47% (1738.51 cm^{-1}) for control). The increase in intensity of amine peak (N-H stretching) absorbance near 3300 cm^{-1} is likely to be the products of the biodegradation.

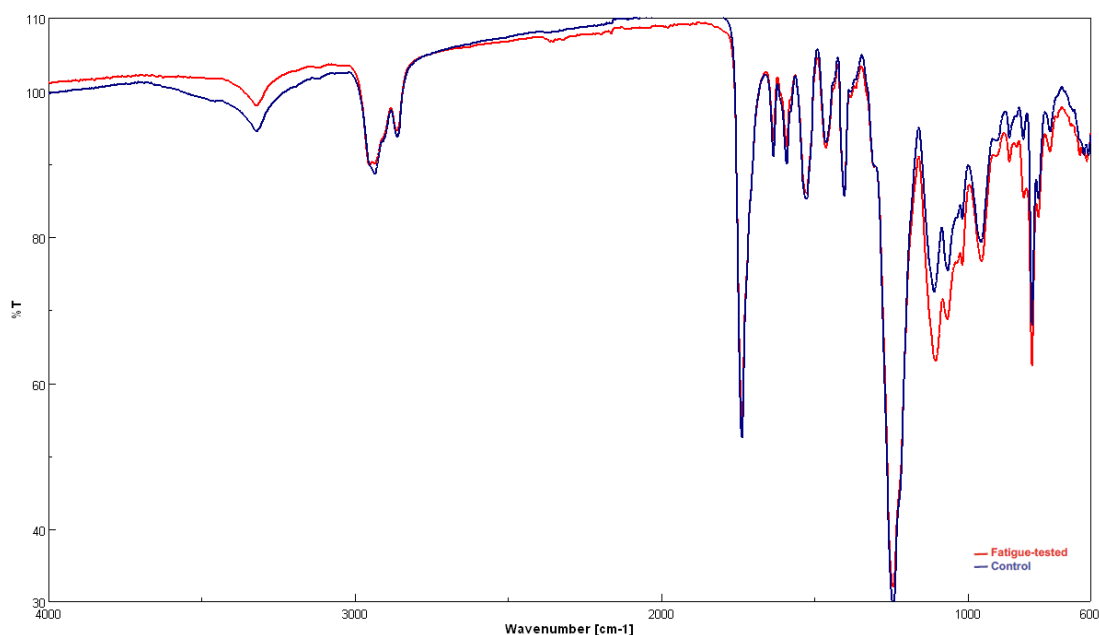


Figure 5.7: Fourier transform infrared spectroscopy (FTIR) curves for POSS-PCU (fatigue-tested and control). Wavelength on X-axis and % Transmittance on Y-axis

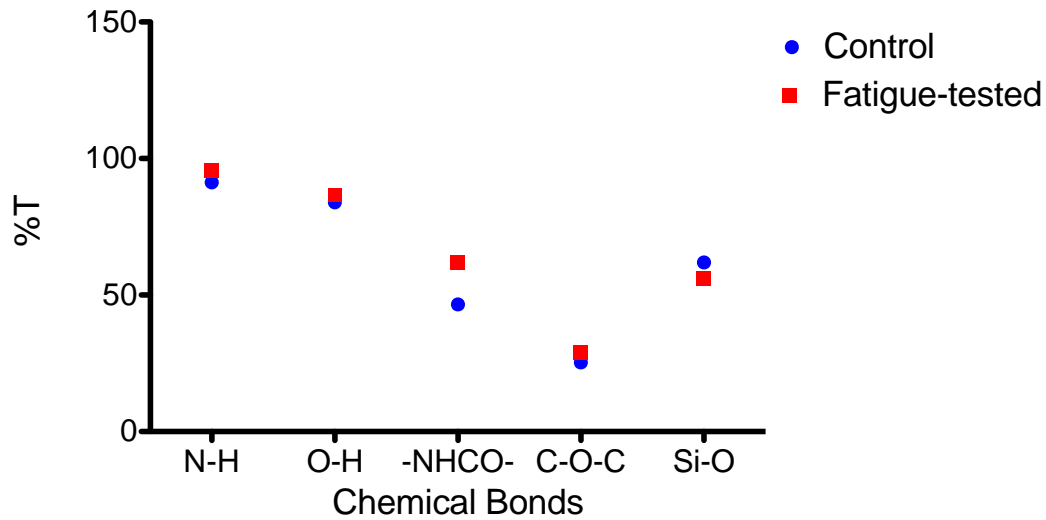


Figure 5.8: Comparison of the intensity of main bonds of fatigue-tested and control POSS-PCU by FTIR (% Transmittance based on their wavelengths)

5.3.2. Compliance analysis

The test parameters for the flow circuit are outlined in table 5.2. Compliance values for both fatigue-tested, 3.46 ± 1.27 (mean \pm S.D. $\%/mm\text{ Hg} \times 10^{-2}$), and control stent-grafts, 3.26 ± 0.65 ($\%/mm\text{ Hg} \times 10^{-2}$) across mean pressures of 60-120 mm Hg were not significantly different (mean difference 0.215 ± 0.286 , 95% confidence interval - 0.357 to 0.787, $P=.455$). (figures 5.9 and 5.10)

Table 5.2: Test parameters for flow circuit to measure compliance

Physical parameter	Variable
Mean pressure (mm Hg)	60-120
Pulse pressure	60.5 ± 0.8
Frequency of pulsatile cycle (Hz)	1
Mean flow rate (ml/min)	132 ± 24
Perfusate viscosity (poise)	0.035 ± 0.001

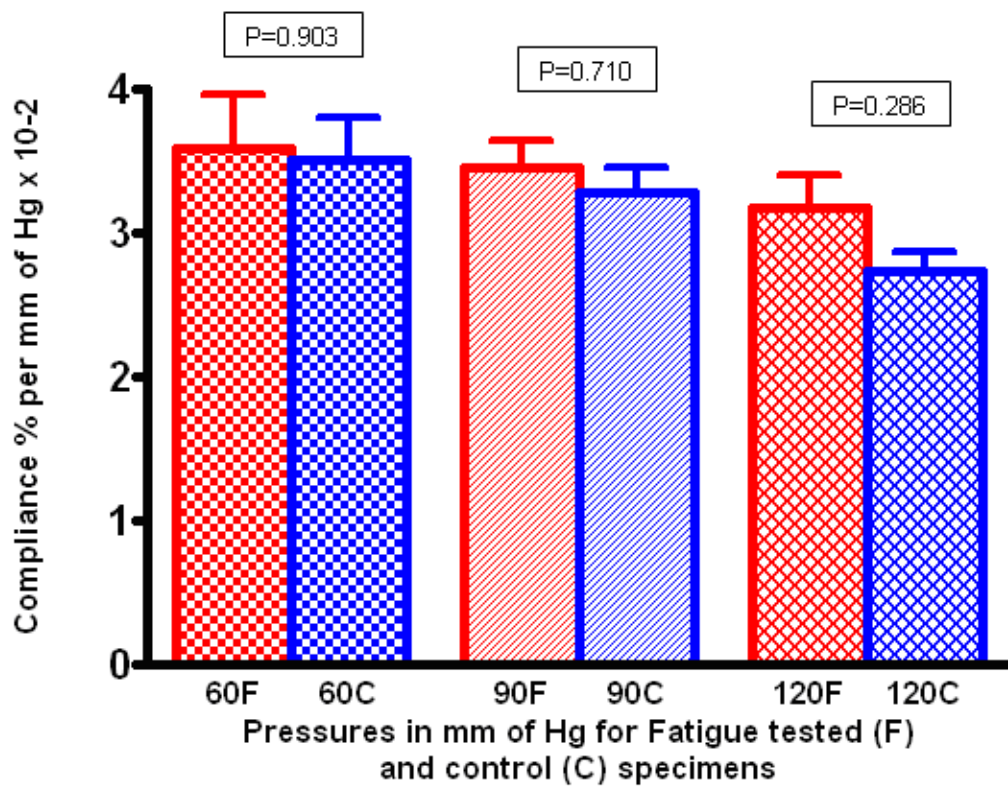


Figure 5.9: Compliance study results across mean pressure range 60-120 mm Hg. Columns represent mean values and error bars represent standard deviation. Fatigue-tested POSS-PCU in red and control POSS-PCU in blue

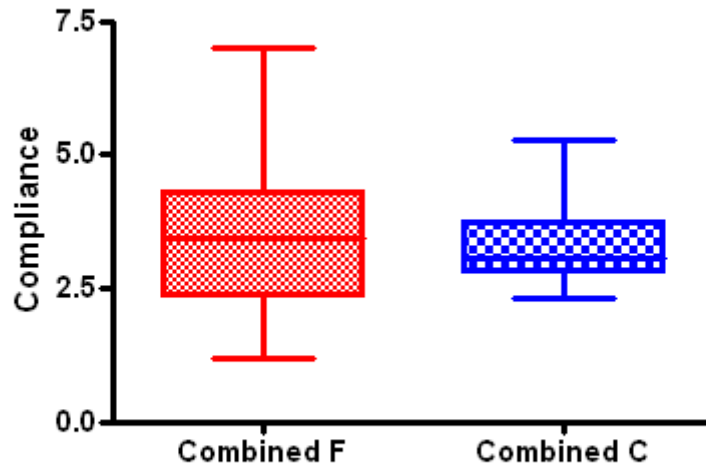


Figure 5.10: Combined compliance results of fatigue-tested (F) and control (C) specimens. Data presented as mean and error bars represent standard deviation

5.3.3. Mechanical strength and elasticity

5.3.3.1 Radial stress-strain studies

Stress–strain curves showed no significant difference in stress–strain behaviour between control and fatigue-tested grafts (table 5.3). This data shows that the soft segment of the polyurethane nanocomposite remains intact in spite of accelerated degradation as illustrated by the preservation of elasticity (figure 5.11).

Table 5.3: Radial stress-strain results

Test	Fatigue-tested polymer	Control polymer	P value
Thickness (mm)	0.169 ± 0.434	0.193 ± 0.0352	.360
Max Stress (MPa)	15.563 ± 4.487	20 ± 7.241	.197
Strain at Break (%)	477.176 ± 77.109	546.06 ± 82.759	.164
Stress at 50% strain (MPa)	3.970 ± 0.793	4.318 ± 0.877	.484
Stress at 100% strain (MPa)	5.806 ± 1.067	5.989 ± 1.191	.784
Stress at 200% strain (MPa)	8.201 ± 1.011	8.530 ± 1.571	.655
Stress at 300% strain (MPa)	10.351 ± 1.190	11.320 ± 2.202	.335
Stress at 500% strain (MPa)	18.863 ± 1.950	50.566 ± 2.909	.447

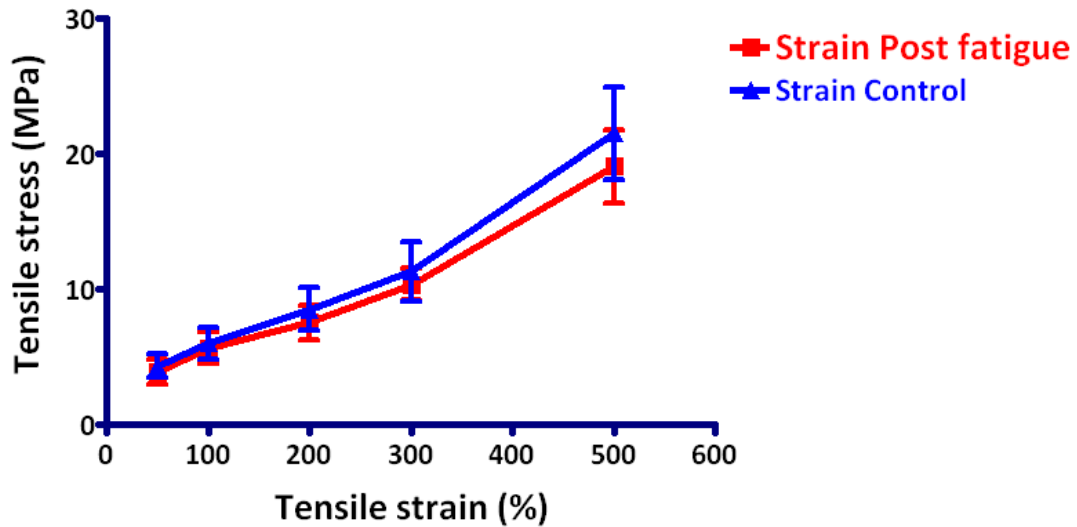


Figure 5.11: Stress-strain curve of fatigue-tested (F) and control (C) POSS-PCU. Data presented as mean and error bars represent standard deviation

5.3.3.2 Linear elasticity

Average lengths of 10mm length sections of dumbbell-shaped samples stretched by 200% (30mm), 300% (40mm) and 400% (50mm) are shown in table 5.4. As seen in figure 5.12, stretching samples up to 500% produced no significant difference with both polymers exhibiting similar elastic properties.

Table 5.4: Linear elasticity test results

Length Stretched	Tube	Average Length after stretching (mm)	Deformation
300% (30 mm)	F	10.9 mm	9%
	C	11.1 mm	11%
400% (40 mm)	F	11.3 mm	13%
	C	11.3 mm	13%
500% (50 mm)	F	11.8 mm	18%
	C	11.4 mm	13%

F – fatigue tested specimens, C – control specimens

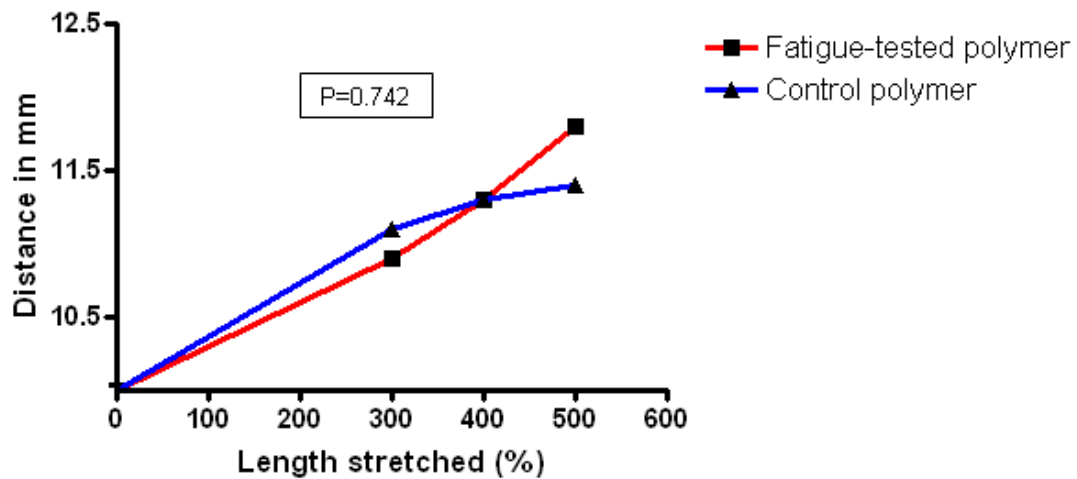


Figure 5.12: Linear elasticity test. Data presented as mean. Length stretched in % on X-axis and distance in mm on Y-axis

5.3.4. Thermo-mechanical resistance

5.3.4.1 Differential scanning calorimetry (DSC)

DSC scans of the fatigue-tested and control samples of POSS-PCU are illustrated in figure 5.13. DSC showed a systematic decrease in the glass transition exothermic peak temperature in the fatigue-tested sample compared with the control. The T_g value characteristic (long-range molecular movement within the soft segment domains) decreased for fatigue tested polymer from -25°C to -28°C compared to control. This phase transition is due to the onset of long-range coordinated molecular motion accompanied by a change in the free volume properties in the polymer. Because of the low weight average molecular weight (M_w), hard and soft segments were not long enough to form highly ordering soft and hard regions, so these polyurethanes showed amorphous state, without any melting endotherm observed in the DSC curves.

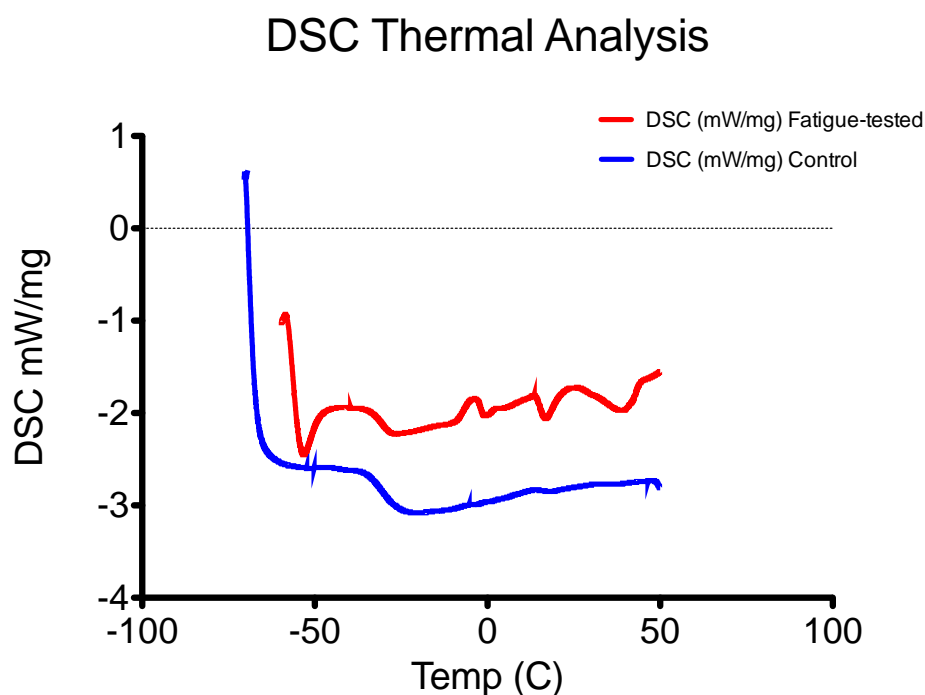


Figure 5.13: DSC thermal analysis curves of fatigue-tested and control POSS PCU specimens. Temperature in $^{\circ}\text{C}$ on X-axis and DSC in mW/mg on Y-axis

5.3.4.2 Thermo-mechanical analysis (TMA) (figure 5.14)

The TMA curves describe the behaviour of the material under load when heated from its glassy state. As the temperature increases the material softens as it goes through its glass transition temperature (T_g) with T_g measured by TMA showing a decrease in dimension change with the increase in temperature similar to the DSC results. Post fatigue testing there was a decrease of T_g up to 4 °C (decreased to -19.8°C for the fatigue test as compared to -24.1°C for the control).

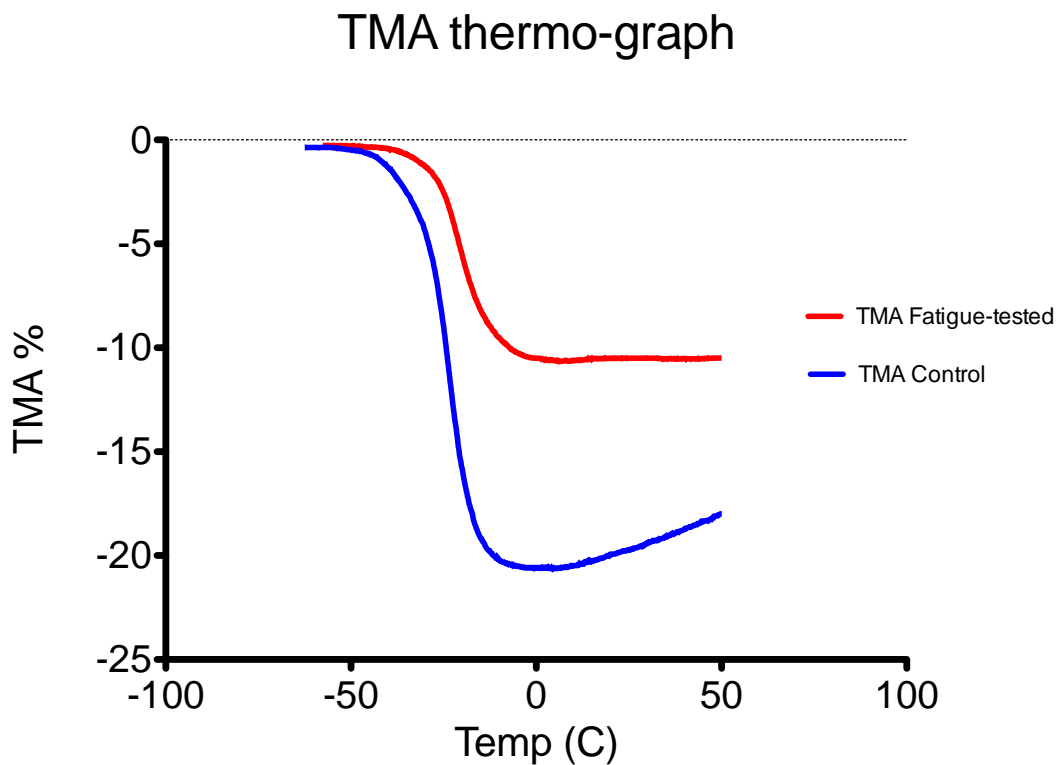


Figure 5.14: Typical TMA thermo-graph curve of POSS PCU (fatigue-tested and control specimens). Temperature in °C on X-axis and TMA (%) on Y-axis

5.4 DISCUSSION

The past 15 years have seen a gradual improvement in long-term stent-graft performance as designs evolved through the elimination of features associated with late failure and the replication of features associated with durable success¹⁷⁹. The Mintec (later called the Vanguard; Boston Scientific, Natick, MA) stent-graft suffered from every form of graft failure, including fabric erosion^{180;181}. The stent structure was held in alignment by polypropylene sutures, which fractured or untied. The resulting distortion of the stent and impingement of stent apices on fabric caused fabric erosion, type III endoleak, and rupture. Stronger sutures and tighter weaves have made current designs more stable, but none is free from occasional instances of graft failure¹⁸²⁻¹⁸⁴. So our aim was to develop a sutureless stent-graft using a graft material which has superior properties of compliance, antithrombogenicity, biostability and spontaneous endothelialisation^{170;171;185;186}. Accelerated durability testing validates fatigue analysis and evaluates failure modes such as fretting, abrasion and wear¹⁸⁷. So we performed this testing for the recommended duration to the equivalent of ten years of real-time use under pulsatile flow and physiologic loading that simulates blood pressure conditions in the human body.

Migration and endoleak are the most important factors in failure after EVAR¹⁸⁸. Our *in vitro* model was not designed to test migration of the stent-graft as we did not simulate the drag forces experienced by the stent-graft especially at the proximal end. The surface treatment and bonding with nitinol remained robust with no occurrence of wire breakage or obvious fractures. SEM images confirmed uniformity of polymer covering the nitinol surface.

Our FTIR results showed no difference in integrity of all major chemical bonds following exposure to fatigue, except for –NHCO– (indicative of the carbonyl segments of carbonate) bonds. The chemical changes caused by biodegradation can be from severe oxidation of the aliphatic soft segment, hydrolysis of the urethane bonds joining hard to soft segments, and significant hydrolysis of aliphatic hard segment. Hydrolysis and biodegradation of the aliphatic hard segment of polyurethane results in loss of absorbance in non-hydrogen-bonded carbonyl (1740-1718 cm⁻¹), urethane C-N (1231-1222 cm⁻¹), and urethane C-O-C (1080cm⁻¹) but amine absorbance (near 3300cm⁻¹). Hydrolysis of the hard segment also gives significant loss of hydrogen-bonded carbonyl absorbance (1702 cm⁻¹). Enhanced phase separation resulting from hydrolysis can also cause significant increase in hydrogen bonding (urea hydrogen-bonded absorbance at 1630 cm⁻¹). The absence of these changes in this study shows that no significant hydrolysis occurred in our sample.

The commonly used polymers ePTFE and Dacron are highly crystalline and stiff¹⁸⁹. After EVAR, the graft lying within the sac generates most of the wall movement by transmission of its own movement through the sac contents¹⁹⁰. To improve device longevity and reduce the risk of late rupture, it is important for the graft material to be resistant to structural failure and aneurysmal change. Compliance is a measure of the biomechanical properties of the graft with significant positive correlation between AAA compliance and risk of rupture¹⁹¹. So we measured compliance and our results confirmed that POSS-PCU shows resistance to failure from significant distension.

Mechanical strength of a polymer is a critical parameter for use in biomedical devices. Polyurethanes are the most compliant polymers and are natural choices; however they characteristically have poor resistance to degradation. To overcome this problem, our group have synthesized polyhedral oligomeric silsesquioxane integrated poly (carbonate-urea) urethane (POSS-PCU) nanocomposite to be biostable and biocompatible. In a recent study, it showed no signs of degradation after three years of

implantation in a sheep model¹⁹². We have used solid POSS PCU to develop a stent-graft system as we wanted it to be mechanically robust enough to withstand the forces it will be exposed to in an *in vivo* environment, whilst maintaining its compliance enough, which is a key parameter. An open walled, porous structure allows the mass transport of signalling molecules, nutrients and metabolic waste removal, all of which lead to improved adhesion and growth of endothelial cells and angiogenesis. However, this factor is more relevant in small diameter grafts. Following accelerated durability testing, mechanical strength is not lost as shown by the unchanged radial stress-strain curves. This data implies that the soft segment of the polyurethane nanocomposite remains intact in spite of the increased transmittance observed in carbonyl segment of carbonate (-NHCO-) on FTIR. This also correlates well with the observations on SEM. It has been noted in previous studies that a reduction in intensities of -NHCO- groups is due to degradation of polyurethane in coatings¹⁹³.

Previous studies of segmented polyurethane elastomers have demonstrated that their thermo-mechanical properties are markedly influenced by composition and morphological details¹⁹⁴. Morphological changes in polyurethanes are generally associated with changes in phase separation and subsequent crystallinity of hard and soft segment domains¹⁹⁵ which results in interchange between non-hydrogen bonded and hydrogen-bonded carbonyl and amide absorbance. Thermal analysis can be used to characterize the thermal behavior of the polyurethanes. DSC and TMA on fatigue-tested and control POSS-PCU determined the glass transition temperature (T_g) over which an amorphous polymer softens and loses its glass-like properties and assumes properties more commonly associated with rubber. The thermo-analysis of fatigue tested POSS-PCU showed essentially one characteristic thermo-tropic transition which was comparable to control samples. This result confirms that incorporation of the POSS nanomolecule in our polyurethane has conferred biostability and the probability of long term durability. The nano-engineering of POSS on the polymer surface means that the bulk of the polymer consists of PU molecules cross-linked by POSS nanocages, which

preserve radial elasticity¹⁹⁶ and enhances its resistance to degradation¹⁹⁷. Due to the protective layer of silica on the surface, POSS-PCU is even more resistant to degradation compared to PCU polyurethane.

Our study has limitations. This study showed no significant hydrolysis of the polymer however we used distilled water and obviously this analysis needs repetition in an in vivo model to confirm the resistance of POSS-PCU to hydrolysis and oxidation. We used straight configuration for the stent-graft instead of a bifurcated system and consequently, it was not possible to reproduce the axial or cyclic drag forces acting on the stent-graft to assess migration. Furthermore, hooks or barbs were not used for fixation. We aim to analysis this in the next stage of our work, which will involve implantation of the stent-graft in a large animal model. The exact nature of relationship of porous structure of POSS-PCU in large vessels like the aorta, with graft compliance and long-term durability needs to be further evaluated and this will be addressed in our future work.

5.5 CONCLUSION

Our study confirms that simulated physiological in vivo hydrodynamic loading has no significant degradative effect on an innovative sutureless stent-graft made from POSS-PCU nanocomposite polymer bonded to nitinol. The fundamental soft and hard segment domain chemistry of the poly (carbonate-urea) urethane polymer material did not change on exposure to fatigue. This study validates the use of POSS-PCU nanocomposite polymer as a durable graft material for endovascular stents. Sutureless technology incorporating nitinol stents proved to be robust with no separation over simulated 10 year cycle. This may allow development of durable stent-grafts with better compliance and antithrombogenicity, potentially at a lower cost. In the next two chapters, we have analysed the properties of the curved stent-graft.



Chapter 6

**A Nanocomposite Polymer Based Thoracic Endoprosthesis to Improve Aortic
Compliance Mismatch Following Endovascular Repair**

6.1 INTRODUCTION

Further to confirmation of durability and robustness of the sutureless stent-graft for AAA, we now wanted to evaluate the properties of the curved stent-graft. Our aim was to develop a stent-graft with superior compliance to presently used graft materials as compliance mismatch is a critical factor for thoracic aorta as discussed below.

Thoracic endovascular aortic aneurysm repair (TEVAR) has several advantages over open surgery which include decreased all-cause mortality at 30 days, reduced risk of paraplegia/paraparesis, reduction of renal dysfunction, transfusions, reoperation for bleeding, cardiac complications, neurologic complications, pneumonia, respiratory complications, reduced incidence of any complication, and shorter procedure time, and length of stay in intensive care unit or hospital^{198;199}. Thoracic endograft placement has been found to be efficacious and safe for use in the treatment of other pathologies such as type B aortic dissection, penetrating atherosclerotic ulcer, intramural haematoma, pseudoaneurysms, acute traumatic aortic disruption, and left subclavian artery aneurysms²⁰⁰⁻²⁰³ as well as ruptured thoracic aortic aneurysms²⁰⁴.

The proximal aorta is a highly compliant vessel, which reduces left ventricular workload and damps the propagated pressure wave²⁰⁵. It is the major contributor to total arterial compliance and an important determinant of cardiac afterload²⁰⁶. Ejection of the blood from the left ventricle is possible because the volume of the large arteries is able to increase in order to accommodate the ejected blood. This function is described as the "Windkessel property" of the aorta and the major conduit arteries and results in a considerable damping of the pressure wave and a significant reduction of cardiac afterload, enabling the heart to work efficiently near the optimum point on the Starling curve. Aortic reconstruction with a prosthetic non-compliant graft reduces this compliance and may have an adverse effect on cardiovascular haemodynamics, which in turn may lead to hypertension, cardiac hypertrophy and ischaemia, the development of vessel wall disease and thrombosis formation²⁰⁷⁻²⁰⁹.

Most currently available graft materials are stiff and poorly compliant. It has been estimated that woven Dacron graft is approximately 170 times stiffer than natural aorta²¹⁰. Compliance mismatch caused by surgical replacement of thoracic aorta with prosthetic grafts is well documented. The outcome of thoracic endografting is largely dependent upon the interaction of the endovascular device and the aortic wall at the zones of fixation. A tight, durable seal to isolate the aortic pathology from pressure and flow is the ultimate goal of these techniques. Failure to achieve this initial technical success or subsequent dilatation of the aorta at the landing zones leads to endoleak that compromises the integrity of the endovascular reconstruction. The extent to which the compliance mismatch²¹¹ induced by the insertion of the stent-graft might contribute to subsequent dilation is not known. The effect of using endografts of different design on thoracic aortic stiffness and compliance has been poorly studied. However, the development of more compliant prostheses, which match the host artery compliance, is expected to reduce the haemodynamic changes induced after their implantation.

We have presented an innovative design for a self-expanding thoracic stent-graft that incorporates a Nitinol alloy scaffold with a polyhedral oligomeric silsesquioxane (POSS) - poly (carbonate-urea) urethane (PCU) nanocomposite polymer (NP), chosen for its excellent biocompatibility and superior vascular properties. The polymer is hydrophobic and non-thrombogenic, and favours spontaneous endothelialisation²¹². It displays impressive anti-thrombogenic properties *in vitro* compared with expanded polytetrafluoroethylene (ePTFE), making it a promising biomaterial for cardiovascular applications²¹³. POSS-PCU is currently undergoing a range of clinical studies from small conduits for lacrimal duct treatment to nasal reconstruction in cancer patients to development of heart valve leaflets and small diameter bypass graft²¹⁴.

The main aim of this study was to develop “compliant” POSS-PCU Nitinol stent-graft for repair of thoracic aorta and the aortic arch that may result in better long-term durability and more effective endovascular repair.

6.2 METHODS

6.2.1 Material Properties for the Curved Stent-graft

The polymer development has been described in detail previously²¹⁵. We adopted similar method. In brief, polycarbonate polyol and trans-cyclohexanediolisobutyl silsesquioxane were placed in a reaction flask equipped with a stirrer under nitrogen. Next, the mixture was heated to dissolve the nanocage. To this was added methylene diisocyanate (MDI), and the reaction allowed to proceed at 70° C for 90 min to form a pre-polymer. Then N, N-dimethylacetamide (DMAC) was added. Chain extension of the pre-polymer was carried out by the addition of ethylenediamine and diethylamine in DMAC. 1-Butanol in DMAC was added to the mixture to form a 2% polyhedral oligomeric silsesquioxane–poly (carbonate urea) urethane (POSS–PCU) solution. All chemicals and reagents were purchased from Aldrich (Gillingham, UK). The typical mechanical properties of POSS-PCU used are outlined in table 6.1

Test	Method	Typical Value
Maximum Tensile Strength (Mpa)	ISO 37	71
Elongation at Break (%)	ISO 37	691
Tensile Stress at 50% Strain (Mpa)	ISO 37	4.62
Tensile Stress at 100% Strain (Mpa)	ISO 37	6.95
Tensile Stress at 200% Strain (Mpa)	ISO 37	13.24
Tensile Stress at 300% Strain (Mpa)	ISO 37	23.00
Young's Tensile Modulus 10-25mm (Mpa)	ISO 37	5.45
Tear Strength (N/mm)	ISO 34	96
Tensile Set	ASTM F 703	

Table 6.1: Typical Mechanical Properties of POSS-PCU

Tensile tests carried out to ISO 37, Specimen size type 3, Crosshead speed 100 mm/min

on an Instron 5565

Tear Strength carried out to ISO 34, Angle test piece with nick, Crosshead speed

500mm/min on an Instron 5565

Elongation measured at the grips

6.2.2 Design of a Curved Stent-graft for Thoracic Aorta and Aortic Arch

As discussed earlier, a curved mould was developed from a three-dimensional printer using dimensions from patient magnetic resonance imaging data. The curved mould was used to develop a silicone mandrel in four components. A thin layer of polymer, approximately 50 μg in thickness was applied over the mandrel with all four components joined together by a long screw. The polymer was allowed to dry and placed in an oven at 60°C for 2 hours. Now previously laser-cut nitinol rings were placed over the polymer layer at equal distance. A second polymer layer of similar thickness was applied and heat-treated as above. A further third layer of polymer was applied, aiming to achieve a thickness of 150 μg . Finally, the stent-graft with the mandrel was placed in an oven overnight at 60°C for 12 hours. It was removed and allowed to cool down for 4 hours. The polymer was carefully peeled off the mandrel and the components were separated by unscrewing.

6.2.3 Stent-graft Control

We used the Gore Tag stent-graft (W. L. Gore & Associates, Flagstaff, AZ), which was the first FDA-approved stent-graft, as control. It is comprised of an expanded polytetrafluoroethylene (ePTFE) graft with an outer self-expanding nitinol support structure.

6.2.4 Flow Phantom

As used earlier, we have utilised the flow circuit for assessing the dynamic behaviour of stent-grafts²¹⁶. The flow model comprised of a variable-speed electromagnetic centrifugal pump (Bio Medicus, Minnetonka, MN, USA), flexible plastic tubing and a fluid reservoir (figure 6.1). A previously developed governable flow waveform conditioner was cited in series with the circuit and used to generate arterial flow waveforms. Instantaneous flow rate was measured using a 6-mm tubular flow probe connected to a Transonic Medical flowmeter system (HT207; Transonic Medical System, Ithaca, NY, USA). Serial intraluminal pressure measurements were made at discrete sites along the stent-grafts using a Millar Mikro-tip catheter transducer (Millar Instruments, Houston, Texas, USA) introduced via a Y-connection port. A gas mixture of 95% oxygen and 5% carbon dioxide was bubbled through the fluid reservoir and the perfusate was maintained at 37°C via a heat exchanger (Portex, Hythe, UK). Pressure was varied by increasing the level of fluid reservoir above the graft segment and by varying the diameter of outflow resistance sited distally to the grafts. All outputs were fed into a commercial analogue-to-digital data acquisition recording system (ADC/MacLab; AD Instruments, Hastings, UK).

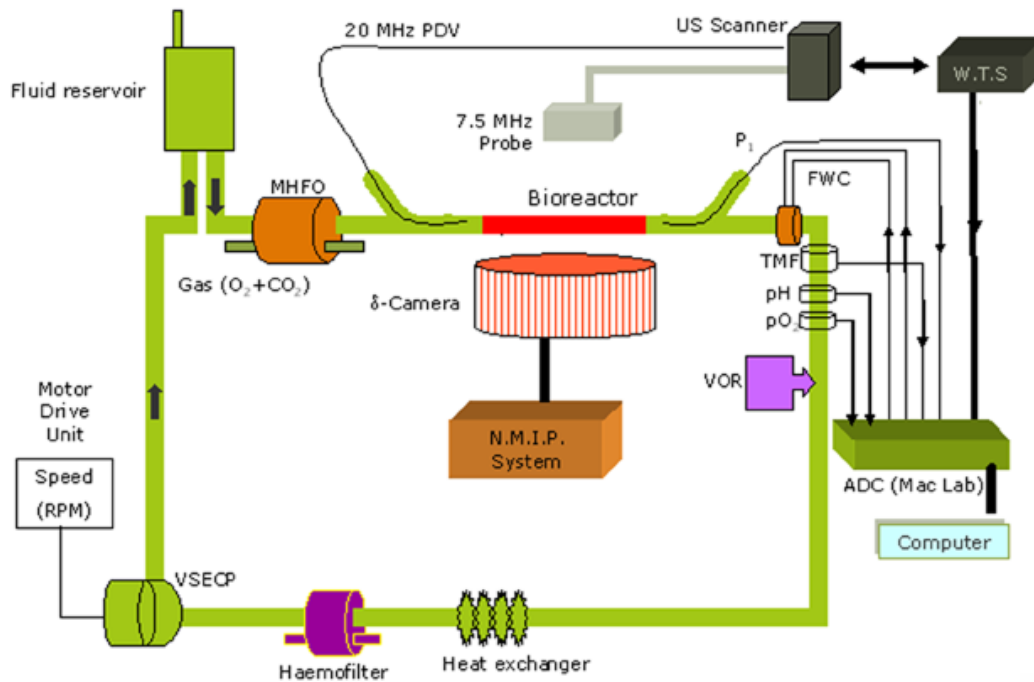


Figure 6.1: Diagrammatic representation of the flow model used for measurement of compliance and elastic stiffness index. ADC, analogue-to-digital data acquisition recording system; FWC, flow waveform conditioner; MHFO, maxima hollow fibre oxygenator (Medtronic, Anaheim, CA, USA); P1 and P2, Millar Mikro-tip pressure transducer; TMF, Transonic Medical flowmeter system; VSECP, variable-speed electromagnetic centrifugal pump; WTS, wall-tracking system

6.2.5 Measurement of Vessel Wall Movement

The change in vessel wall diameter with respect to each cardiac cycle was measured at discrete sites along the graft, with measurements taken in the sagittal plane at 90° to the long axis of the graft. The stent-grafts were scanned with a specially adapted, duplex colour-flow ultrasonography system (Wall Track; Pie Medical Systems). This system allowed the measurement of vessel wall movement over time by automatically tracking assigned points of the induced radiofrequency signal deemed to be representative of the anterior and posterior arterial walls. A detailed description of the system has been published elsewhere^{145;217}. Briefly, a 7.5-MHz linear array probe was immersed in the bath and positioned directly over the segment under investigation. The M-mode cursor was positioned at the midpoint of each test segment and perpendicular to the direction of flow; the change in induced radiofrequency signal received from the vessel walls was then sampled over time. These data were then transferred to a personal computer for real-time display of the displacement waveforms of the anterior and posterior artery walls. In this way, end-diastolic and end-systolic intra-luminal diameters were determined automatically over the pulsatile cycle (figure 6.2).

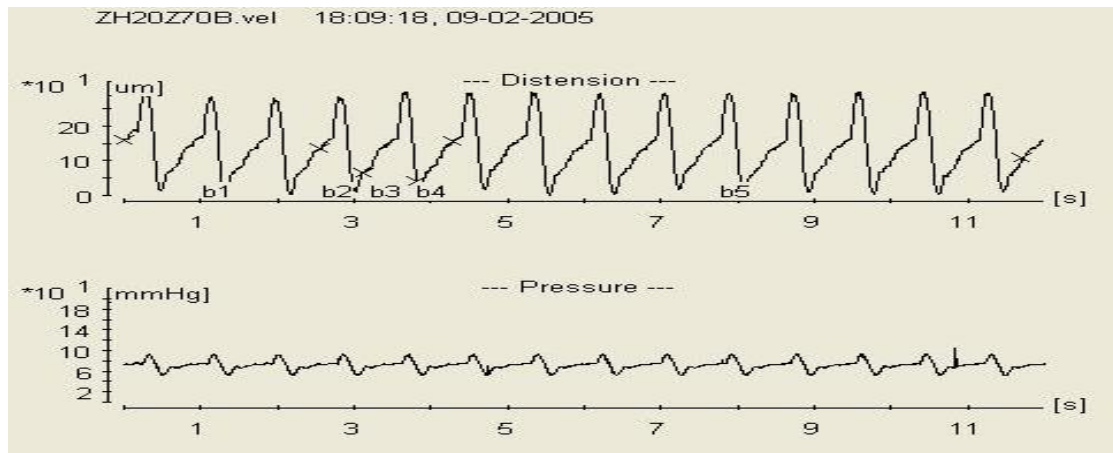


Figure 6.2: Distension-time curve generated by wall-tracking system. The Y-axis is represented by Distention in μm on the graph above and Pressure in mm of Hg in the graph below. The time in seconds is on X-axis for both the graphs

6.2.6 Haemodynamic and Arterial Parameters

The solution used for perfusion was made using 8% low molecular weight Dextran (molecular weight 77000-Da; Sigma-Aldrich, Poole, UK) added to a solution of M199 (minimum essential medium), 20% fetal bovine serum, 7.5% sodium bicarbonate (Sigma-Aldrich), 200-mmol L-glutamine (Gibco BRL; Life Technologies, Paisley, UK), penicillin 10000-units/ml and streptomycin 10-mg/ml, buffered at pH 7.20 ± 0.01 . The viscosity of this medium has previously been determined to approach that of whole human blood (Low-Shear 30; Contraves, Zurich, Switzerland)²¹⁸. Viscosity of the perfusion solution was determined and was calibrated with a cone-plate viscometer at 0.035 poise. This was facilitated by using 8% low molecular weight Dextran in the nutrient solution. Measurements were made using a near-constant pulse pressure over a range of mean pressures (table 6.1). For each mean pressure and test segment, three measurements of wall movement were made, and the experiment was repeated six times.

Physical Parameter	ePTFE stent-graft	NP stent-graft
Mean Pressure (mm Hg)	30-100	30-100
Pulse Pressure (mm Hg)	49±6	49±6
Flow rate ml/min	140 ± 25	132 ± 24
Perfusate temperature (°C)	37	37
Perfusate viscosity (poise)	0.035	0.035

Table 6.1: Typical Flow Circuit haemodynamic values (mean ± SD)

6.2.7 Statistical Analysis

The data from each experiment obtained were plotted and analysed using GraphPad Prism 4 software (GraphPad, San Diego, CA, USA). Grouped data are presented as mean ± SD (standard deviation). The unpaired Student's t-test was used for statistical comparison of the two stent-grafts. Only p values < 0.05 were considered significant.

6.3 RESULTS

6.3.1 Stent-graft Design

The NP stent-graft had uniform thickness of $150.7 \pm 6.6 \mu\text{g}$ and in its fully expanded shape, with diameter of 30 mm, matched curvature of aortic arch and descending thoracic aorta (figure 6.3). The inner side of the stent-graft was covered with a smooth layer of polymer (figure 6.4). Upon folding, the stent-graft was first straightened in a way that some polymer partly covered onto the nearest nitinol ring. Then, the stent-graft was easily folded as a traditional straight stent-graft because the nitinol rings are positioned in a way that the peaks of a nitinol ring point to the valleys of the adjacent nitinol ring. The folded stent-graft can be delivered to the aorta just as the traditional stent-graft does.



Figure 6.3: A fully expanded curved stent-graft from POSS-PCU NP bonded to nitinol and having curvature similar to aortic arch

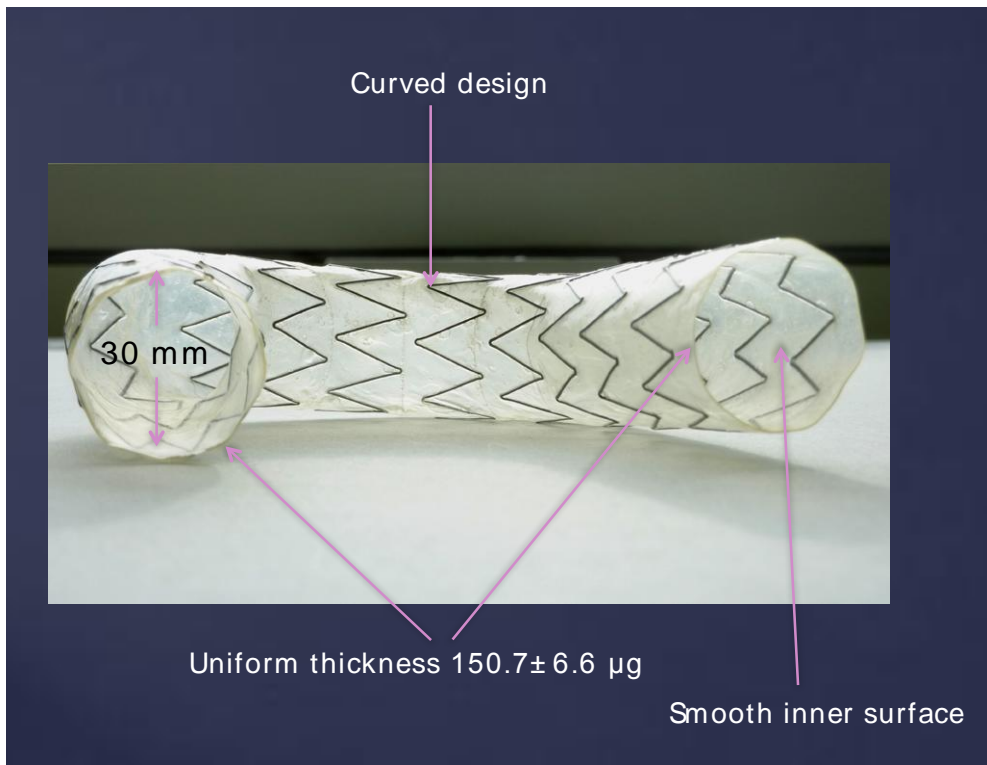


Figure 6.4: The smooth inner surface of the stent-graft with uniform thickness and curved design

6.3.2 Compliance Measurement

Compliance is a tool used to measure distensibility of the artery. Diametrical compliance (C) defined as the inverse of Petersen's elastic modulus $E_p^{147;148}$, and expressed as $\%/mm \text{ Hg} \times 10^{-2}$, was determined for each test segment at each mean pressure as follows:

$$C = (D_s - D_d / D_d) \times 10^4 / (P_s - P_d)$$

Here C is the compliance value of the stent-graft at a particular cross-section. D_s and D_d are systolic and diastolic diameter, and P_s and P_d are systolic and diastolic pressure, respectively. The compliance of the stent-grafts was measured at four locations. When

the stent-grafts were inserted in the model, triphasic flow was seen in all of the measurements with no difference in flow waveforms. The haemodynamic and arterial parameters were nearly consistent for both the stent-grafts.

The compliance results are shown in figure 6.5. The mean compliance of the ePTFE stent-graft was 2.3 ± 0.95 (95% CI 1.7-2.9) %/mm Hg X 10^{-2} . The mean compliance of the NP stent-graft was significantly better at 3.3 ± 0.61 (95% CI 3.0-3.5) %/mm Hg X 10^{-2} (P=0.0003).

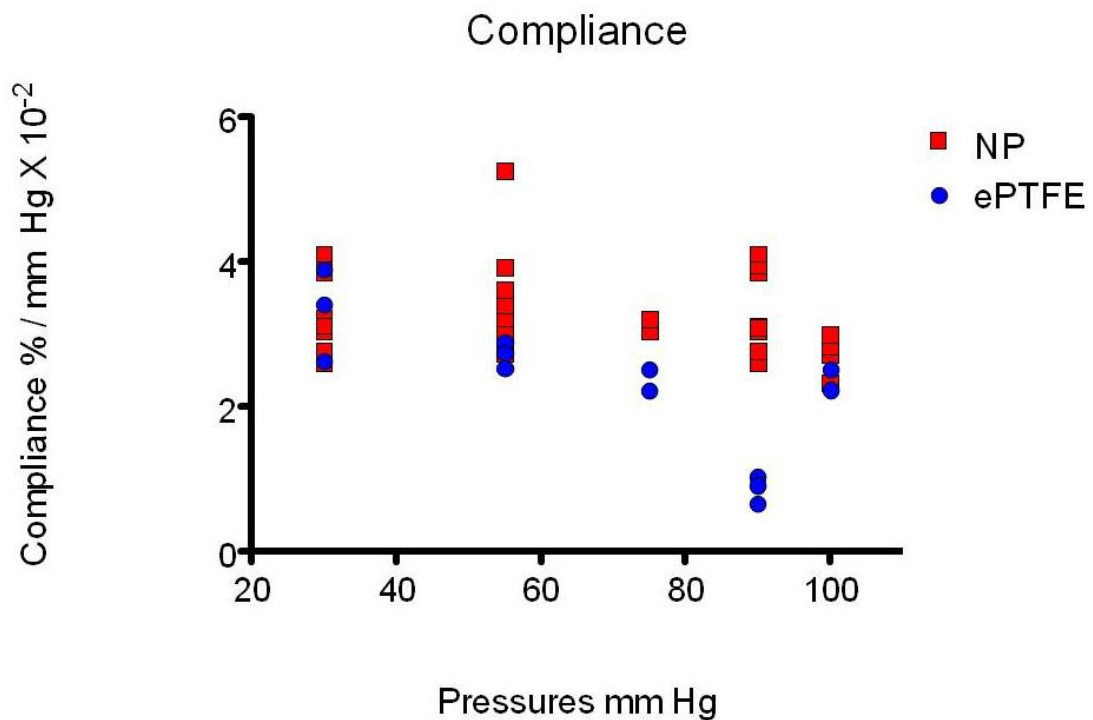


Figure 6.5: Compliance results. Data presented as mean values. Pressures in mm Hg on X-axis and Compliance in %/mm Hg x 10^{-2} on Y-axis

6.3.3 Stiffness Index

Arterial stiffness is one of the primary attributes of vasculopathy, involving several mechanisms and results in damaged arterial compliance²¹⁹. Arterial wall stiffness index, β as formulated by Kawasaki *et al*²²⁰, and utilised as a cardiovascular risk factor, was calculated using the following equation.

$$\beta = [\log_e (P_s/P_d)] \times D_d / (D_s - D_d)$$

The results of stiffness index measurement are shown in figure 6.6. The ePTFE stent-graft was significantly more stiff as compared to the NP stent-graft [β 92.7 ± 46.1 (95% CI 64.9-121) vs. β 39.1 ± 5.91 (95% CI 36.9-41.3); $P < 0.0001$]. The stiffness index-mean pressure curves were generated using non-linear regression (single phase exponential decay model). For both the stent-grafts, stiffness index was observed to behave in a non-linear fashion in response to elevation in mean perfusion pressure. It was observed that for NP stent-graft the stiffness remained nearly constant; however, the ePTFE stent-graft was significantly stiffer at physiological pressures.

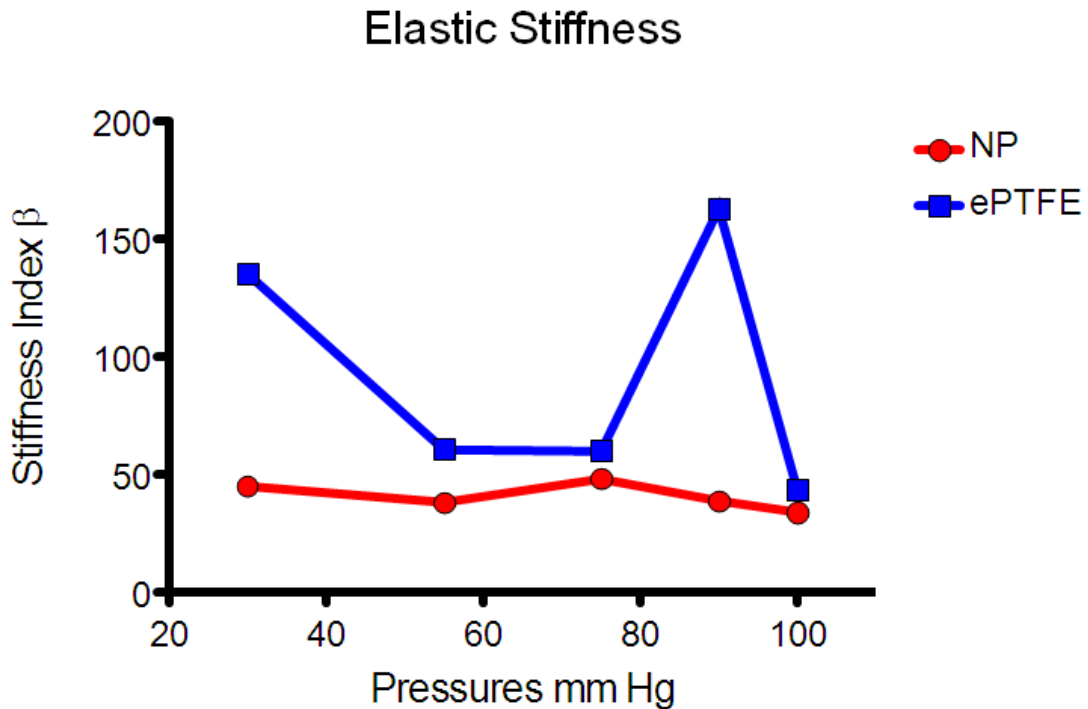


Figure 6.6: Elastic Stiffness Index Results. Data presented as mean values. Pressures in mm Hg on X-axis and Elastic stiffness index β on Y-axis

6.4 DISCUSSION

Our results confirm superior compliance profile of an innovative stent-graft based on POSS-PCU nanocomposite polymer, as compared to an ePTFE-based FDA-approved stent-graft in current clinical use. Using an *in vitro* flow phantom in a simulated physiological environment, we were also able to demonstrate that POSS-PCU stent-graft is significantly less stiff.

There have been studies on aortic compliance assessment after abdominal aortic aneurysm repair and it has been shown that stent-graft design alters aortic stiffness and elastic modulus at several sites after endograft implantation, which may have serious consequences for endograft efficacy and durability²²¹. The implantation of endovascular devices in the proximal descending aorta has been shown to increase left ventricular afterload²²². These changes may have long-term consequences especially in younger patients undergoing stenting for traumatic disruption of the aorta, patients with coronary artery disease and in patients with reduced left ventricular systolic reserve. Although, careful quantification of the interaction *in vivo* is required to characterise this response, information regarding endograft-aortic wall interaction from imaging following endografting has suggested that ‘compliance-matched’ stent-grafts may result in better long-term durability and more effective endovascular repair²²³. Haemodynamic studies have shown changes after endografting were similar in magnitude to open interposition grafts. The insertion of Dacron prosthesis in the descending aorta during the repair of traumatic disruption has been shown to increase characteristic impedance (stiffness) of the ascending aorta and this can potentially reduce cardiac efficiency and may predispose to the development of left ventricular hypertrophy^{224;225}. Simulated reduced aortic compliance by banding has been shown to significantly increase characteristic and input impedance, a significant decrease in systemic arterial compliance and a subsequent increase in systolic and pulse pressures leading to left ventricular hypertrophy²⁰⁶. Reduced compliance caused by endografting may have similar effects and so, having a better compliance-matched stent-graft can help improve the long-term durability of this procedure.

Arterial stiffness is one of the primary attributes of vasculopathy, involving several mechanisms and has been suggested as a strong independent predictor of cardiovascular disease²²⁶. The stent-grafts in current clinical use are based on either ePTFE (Tag), woven polyester (Zenith TX2) or monofilament polyester (Talent). As shown in our results, ePTFE is stiffer than POSS-PCU and this may have clinical

implications by having adverse structural and functional changes, however this statement is purely hypothetical and further research is necessary to support this.

6.5 LIMITATIONS

There are some limitations. We have studied the effect of graft material but the effects of other factors on stent-graft compliance such as intraluminal thrombus in the aneurysm sac are not factored. The non-Newtonian behaviour of blood has not been considered. The pressure range that we used included a maximum mean pressure of 100 mm Hg and confirmation of findings at higher pressure range possible in clinical situations is essential. At present, our study cannot model any long-term effects that a rigid stent-graft might have on vascular haemodynamics.

6.6 CONCLUSIONS

We present an innovative curved stent-graft, based on a new biomaterial for endovascular repair of thoracic aorta, which matches the curvature of aortic arch and can be used to develop fenestrated or branched devices in the future. In an *in vitro* model over a range of pressures, it shows superior compliance profile and is less stiff in comparison to graft material in current clinical use in thoracic endografts. Although, this research is still in infancy, we believe that with improvement in physiological and haemodynamic properties of stent-grafts, clinical management of patients with thoracic aortic pathologies and stent-graft design can be vastly improved in the future.

Our future work will be aimed at analysing the imaging properties of the stent-graft on exposure to flow, especially with magnetic resonance imaging to confirm its compatibility.



Chapter 7

**Magnetic Resonance Signal Attenuation and Image Artefact Testing of a
Nanocomposite Polymer Nitinol Thoracic Stent-graft**

7.1 INTRODUCTION

The curved stent-graft developed from POSS-PCU bonded to Nitinol and matching the conformability of aortic arch has shown superior compliance profile with better elastic stiffness as compared to ePTFE used in some of the current devices. For thoracic stent-grafts, it is important to assess compatibility with imaging modalities, particularly magnetic resonance imaging (MRI) and this has been highlighted in this chapter.

As already described in the earlier chapters, the curved design combines deployable structure technology to improve the folding efficiency and performance of the device *in vivo*. The scaffold geometry is designed similar to the aortic vessel. The new technology allows pre-forming of the angulation of the host aortic arch into the device and due to the bonding of the graft around the metal skeleton, we hypothesize that it reduces the risk of mechanical stress-related disruption, which can help in reducing the incidence of kinking, migration, and endoleak. Because of the folding technology, a more flexible and potentially narrower gauge delivery system can be employed but most importantly device can be constructed so that once deployed it will be inherently stronger, more stable and have the degree of angulation tailored to the individual patient. There is also scope to include branch grafts in the folded metal structure to incorporate the major vessels. Such a device has the potential to treat many more patients with this increasingly common condition in our ageing population. It will reduce the need to occlude or reconstruct the great vessels thus significantly reducing complications and risk of operative death associated with hybrid procedures.

Magnetic Resonance Imaging (MRI) is increasingly being used for assessment and follow-up of patients with aortic disease. It has the advantage over other imaging modalities such as computed tomography, of being able to give anatomical and functional information in a single scan. MRI has superior soft tissue contrast and can be used to assess the quality of endovascular repair, by assessment of device positioning and device to wall apposition. Gadolinium contrast agents (used in MRI) are less nephrotoxic compared with iodinated agents and this may improve survival in patients with poor renal function following endovascular aneurysm repair (EVAR).²²⁷ Application of MRI can be compromised by poor visibility of the device, susceptibility artefacts introduced by the stent or severe signal reduction by radio-frequency shielding. The safety and compatibility of devices within the magnetic field is one of the key parameters in aortic stent-graft development. The Food and Drug Administration (FDA) therefore recommends that stent-grafts undergo MRI assessment prior to clinical use.

The objectives of this study were to assess MRI characteristics of POSS-PCU and Nitinol thoracic stent-graft including image artefacts and flow velocity measurement in a dedicated *in vitro* aortic phantom.

7.2 METHODS

7.2.1. Magnetic Resonance Imaging (MRI) assessment

All images were acquired on a 3T MR scanner (Achieva, Philips Healthcare, Best, The Netherlands) with a 32-element coil. Initial survey and reference scans obtained localisation images and coil sensitivity maps respectively. Comparison was made with a commercially available Valiant stent-graft (Medtronic, Minneapolis, MN) which is based on polyester graft fabric sutured to a self-expanding nitinol wire stent.

7.2.1.1 Static Fluid MRI Signal Assessment

Medtronic and NP stent-grafts were scanned separately in a glass cylindrical container filled with water dosed with 10mL gadopentetate dimeglumine (Magnevist, Bayer Healthcare, Germany) to observe stationary signal attenuation (figure 7.1).

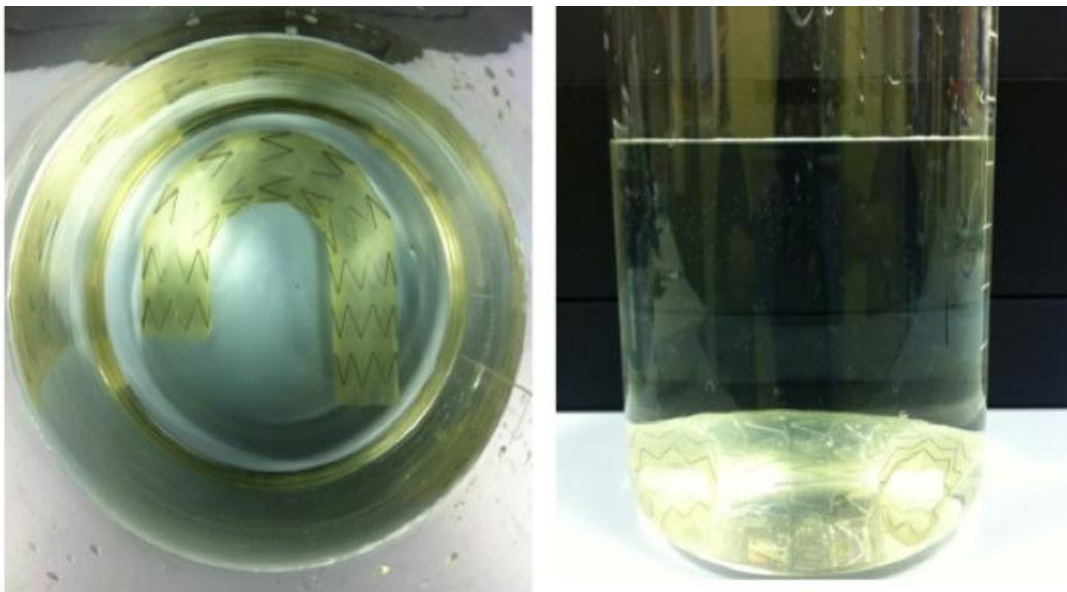


Figure 7.1: Phantom setup for NP stent-graft. Stent-grafts were scanned separately in a glass cylindrical container filled with water dosed with 10mL gadopentetate dimeglumine

Isotropic three-dimensional (3D) T1-weighted Fast Field Echo (FFE) images were acquired using the following scan parameters: FOV: 200x200 mm², acquired voxel size: 1.0x1.0x1.0 mm³, flip angle 9°, TR/TE: 4.2/1.9 ms.

Image data were analysed using commercially available software (Philips ViewForum, Best, The Netherlands). The amount of artefact generated by the devices was assessed and graded by RC using a three-point grading scale:

Grade 1: Severe artefacts with poor visualisation of the device;

Grade 2: Minor artefacts;

Grade 3: Excellent visualisation and delineation of device details²²⁸.

Potential signal shielding from inside the device was assessed by placement of a region of interest inside and outside the centre of each stent-graft and calculation of percentage signal loss within each stent-graft lumen.

7.2.1.2 Flow Encoded MRI Signal Assessment

A steady flow phantom was set up using a large elevated fluid reservoir to a large empty tank at floor level. Water was transmitted from the elevated reservoir to the lower tank via a ($\frac{1}{2}$ ØID X $\frac{5}{8}$ " ØOD) Tygon (Cole-Parmer Instrument Co. Ltd., London, UK) tube conduit passing into the scanner and out again. The stent-grafts were positioned around the tubing with the tubing orientation such that both stent-grafts had an uncovered section of Tygon tube running beside it at the same position to the static magnetic field (B_0) for comparison (baseline) (figure 7.2). Before commencing each flow encoded scan, the tube was unclamped and the flow allowed to develop for at least five seconds. Image slices were positioned perpendicular to the stent and tubing. 2D through-plane phase contrast images were acquired using the following scan parameters: FOV: $250 \times 250 \text{ mm}^2$, slice thickness: 10mm, acquired voxel size: $1.0 \times 1.0 \text{ mm}^2$, flip angle 10° , venc 150cm/s, TR/TE: 5.2/2.9 ms, retrospective ECG-gating, temporal resolution 45ms, NSA: 1. Prior to analysis the data were corrected for eddy currents and Maxwell phase offsets.

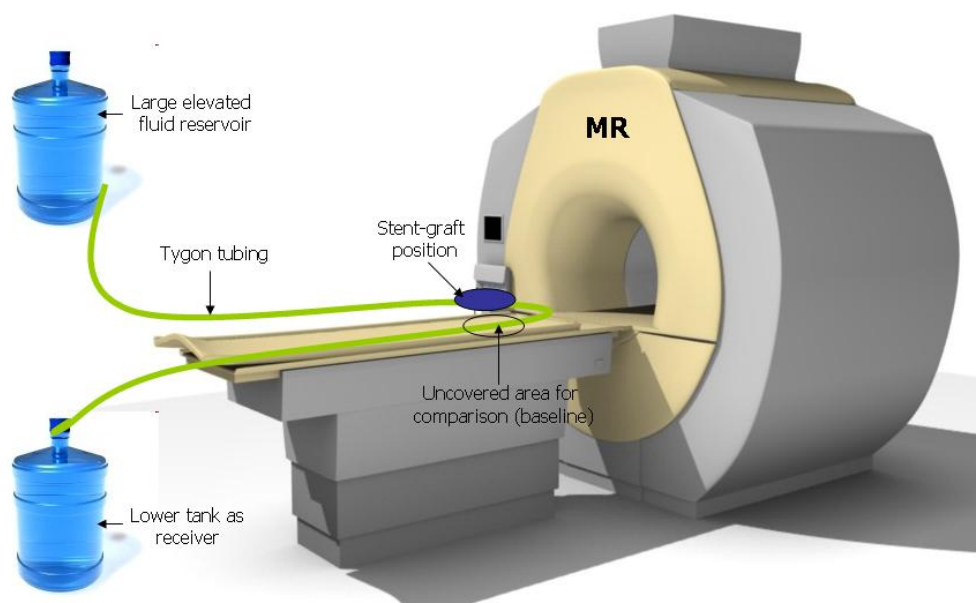


Figure 7.2: Schematic diagram illustrating the MRI flow phantom setup. Large elevated fluid reservoir connected to fluid tank on the floor using Tygon tubing. Stent-grafts positioned as shown with corresponding uncovered tubing for baseline comparison

Image data were analysed using commercially available software (Philips ViewForum, Best, The Netherlands). A region of interest was created using semi-automatic segmentation within the lumen of each stent and the corresponding uncovered tubing in each image set. All voxels within the contour were evaluated and by integration over all time phases the amount of water passing through each contour per second was calculated (flow).

7.2.3. Statistical analysis

All statistical tests were performed using Graphpad for Prism 5 (La Jolla, CA, USA). Normalisation of data was used for baseline correction. The comparison was done using unpaired t-test and p-value <0.05 was considered significant.

7.3 RESULTS

7.3.1 Stent-graft Design

The NP stent-graft had uniform thickness of $150.7 \pm 6.6 \mu\text{g}$ and in its fully expanded shape, with diameter of 30 mm, matched curvature of aortic arch and descending thoracic aorta. Upon folding, the stent-graft was first straightened in a way that some polymer partly covered onto the nearest nitinol ring. Then, the stent-graft was easily folded as a traditional straight stent-graft because the nitinol rings are positioned in a way that the peaks of a nitinol ring point to the valleys of the adjacent nitinol ring. The folded stent-graft can be delivered to the aorta just as the traditional stent-graft does.

7.3.2 Subjective data analysis for image artefact testing

Imaging results of the endograft and its lumen on the 3D T1-weighted MR images showed that both Medtronic and NP stent-grafts had no significant susceptibility artefacts affecting the image quality. There was no image distortion and the nitinol struts could be easily distinguished. There was minimal signal attenuation within the lumen of Medtronic stent-graft but none on NP stent-graft (figures 7.3 and 7.4). No significant susceptibility artefacts affecting the image quality were seen and the nitinol struts could be easily distinguished. The artefacts were graded as 3 on most occasions

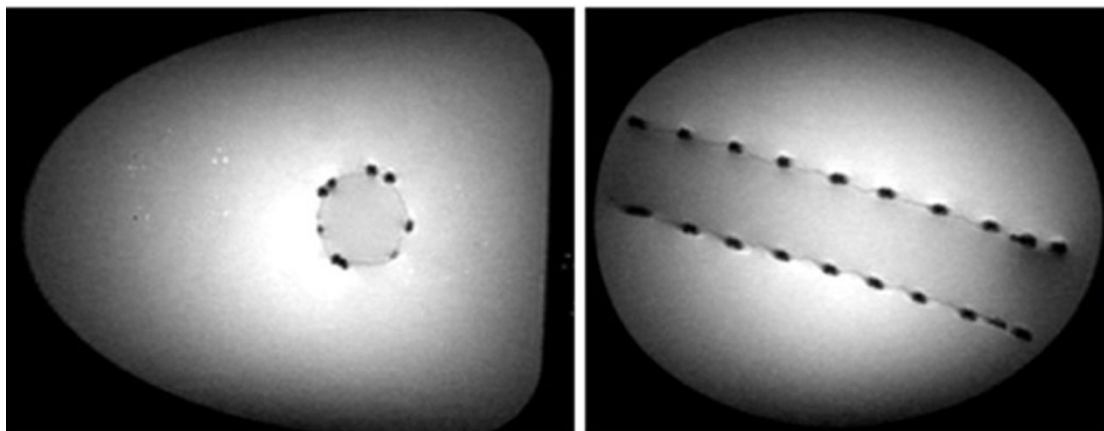


Figure 7.3: MR static images for Medtronic Valiant™ stent-graft. Minimal susceptibility artefacts were seen, however the image quality was good

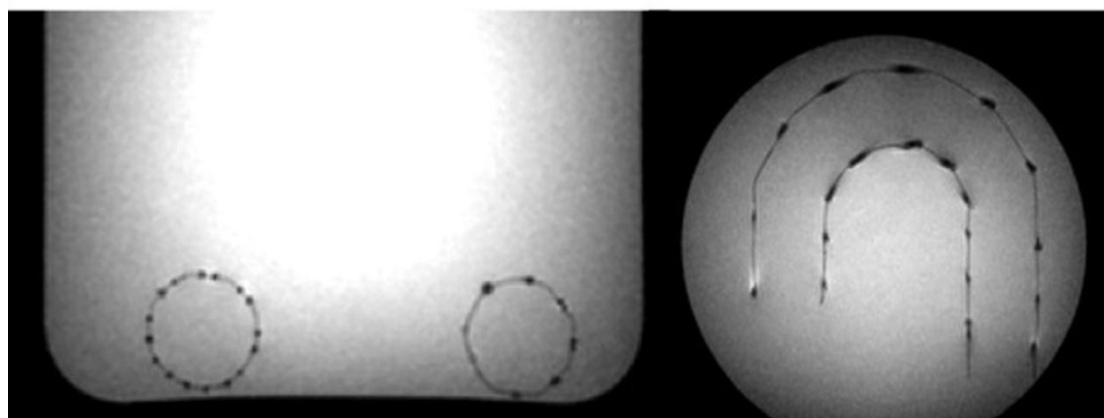


Figure 7.4: MR static images for NP stent-graft. No significant susceptibility artefacts affecting imaging quality were seen

7.3.3 Objective data analysis for signal magnitude on image artefact testing

The signal inside and outside the Medtronic stent-graft was 644.2 (SD 36.2) and 659.6 (SD 85.8) respectively. The percentage signal attenuation for this device was 2.39%. The signal inside and outside the NP stent-graft was 1561.7 (SD 31.2) and 1595.5 (SD 40.8) respectively. The percentage signal attenuation for this device was 2.16%. Selected slices of the high-resolution datasets demonstrated the individual amount of RF signal shielding of the stent-grafts (figures 7.5 and 7.6). There was no relevant signal attenuation within the lumen of Medtronic and NP stent-grafts. There was no regional signal enhancement. Quantitative assessment of RF signal caging showed that the percentage attenuation was around 2-10%, for the Medtronic stent-graft and only 0-2% for NP stent-graft. Small variations in the attenuation score might be due to a different location of the measurement regions of interest (ROIs) relative to the position of the surface coils (inherent spatial signal variations).

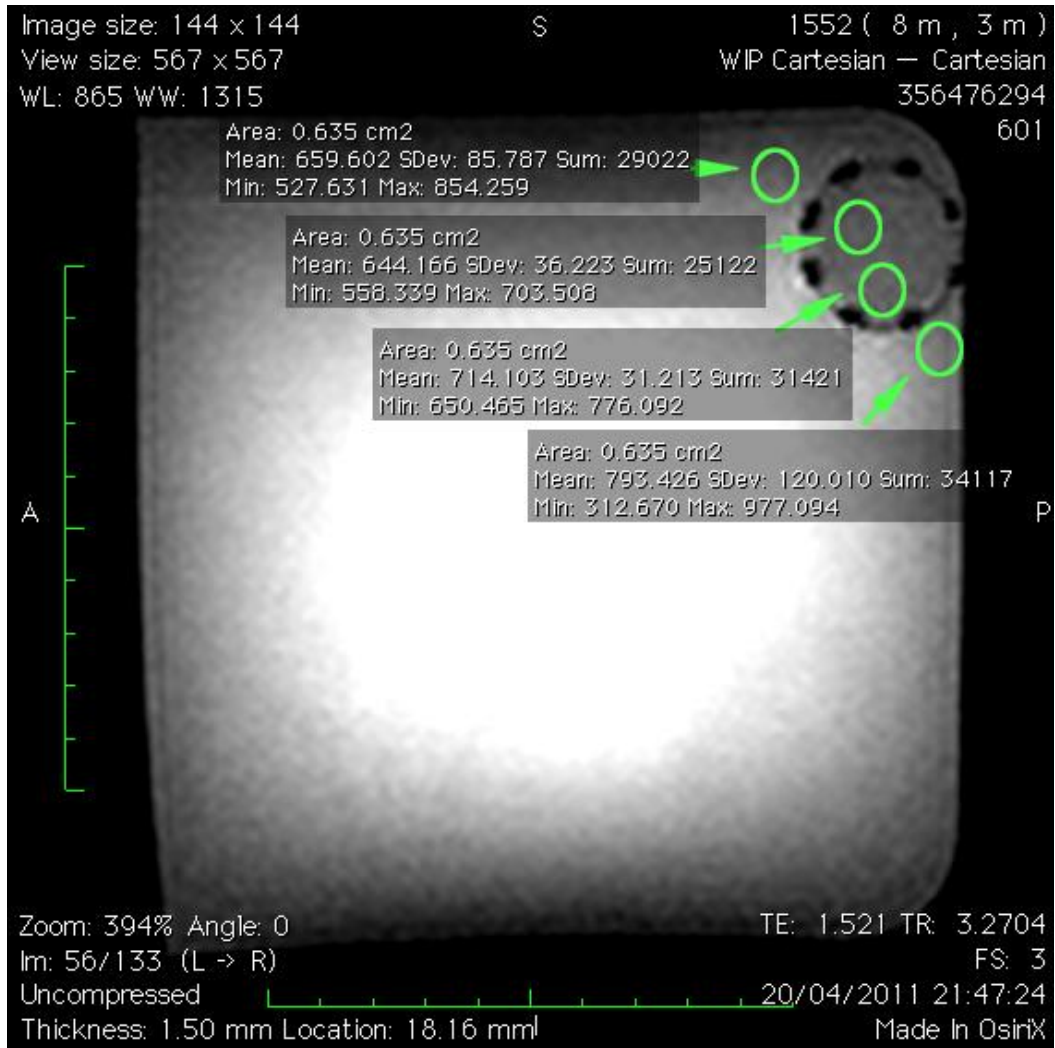


Figure 7.5: Axial slice from Medtronic Valiant™ stent-graft showing signal magnitude inside and outside used to calculate % signal attenuation

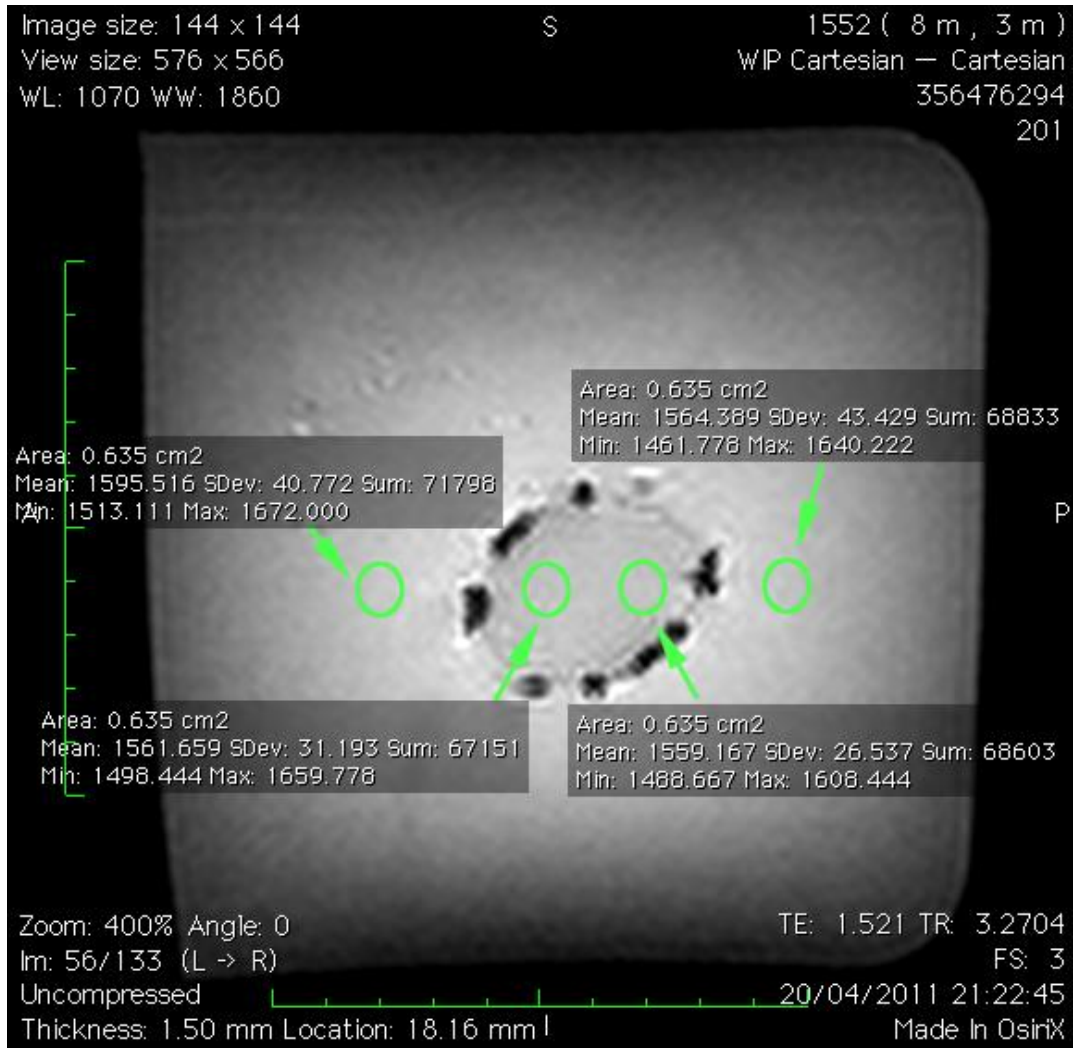


Figure 7.6: Axial slice from NP stent-graft showing signal magnitude inside and outside used to calculate % signal attenuation

7.3.4 Analysis of flow measurement

In MRI velocity attenuation study, steady flow phantom was set at mean flow rate of 105.3 ml/sec and mean velocity of 79.5 cm/sec. Following normalisation of the data, the flow in the Medtronic stent-graft was 102 ± 2.27 ml/sec with no significant difference to baseline (104 ± 1.98 ml/sec; $P=0.892$). Flow through the NP stent-graft was 99.8 ± 2.4 which was not different to baseline (104 ± 0.96 ml/sec; $P=0.176$). There was no significant difference in flow between Medtronic and NP stent-grafts (102 ± 2.27 vs. 99.8 ± 2.4 ml/sec; $P=0.328$). As shown above, the velocity attenuation in the NP stent-graft was 4.6% as compared to 1.9% in Medtronic stent-graft (figure 7.7).

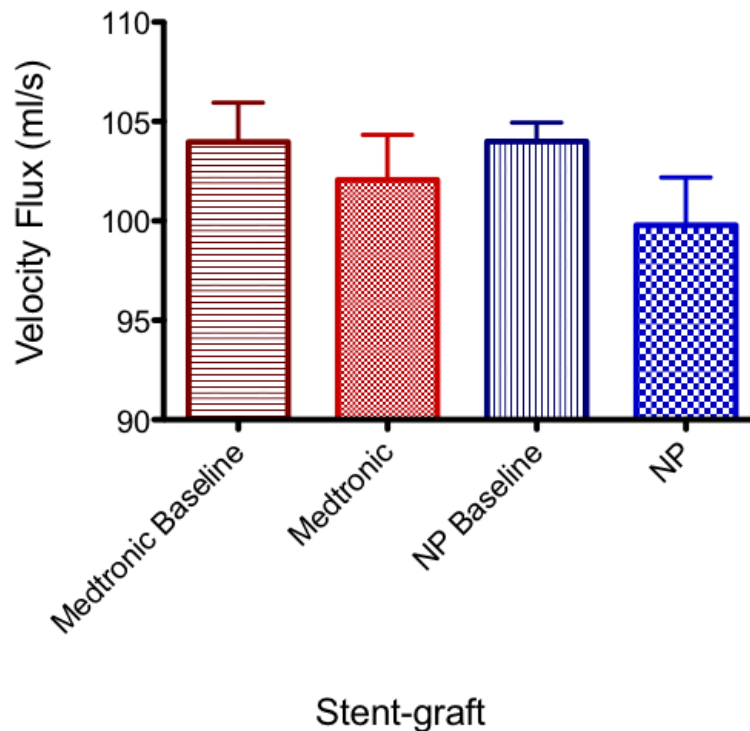


Figure 7.7: Velocity flux comparison for Medtronic and NP stent-grafts. Columns represent mean values and error bars represent standard deviation

7.4 DISCUSSION

We have designed an innovative sutureless stent-graft for endovascular repair of thoracic aorta and our results confirm the feasibility and compatibility of its assessment using MRI. This stent-graft has a unique curved shape with a potential to have branches and promise of use in the repair of aortic arch. Endovascular prostheses currently in use are not designed for the treatment of arch pathologies²²⁹, where blood flow generates high forces, the aorta moves through a wide excursion with every pulse, and temporary flow interruption can lead to stroke or cardiac arrest²³⁰. Therefore, incomplete alignment, type 1 endoleaks and retrograde type A dissections may occur.

These can be potentially avoided by our curved design simulating accurate aortic dimensions and a hybrid approach can be replaced by complete endovascular intervention. Furthermore, this stent-graft is based on a nanocomposite polymer having properties of compliance, antithrombogenicity and spontaneous endothelialisation, superior to presently used Dacron and Polytetrafluoroethylene (PTFE).

MRI has been incorporated into diagnostic routine for the assessment of aortic abnormalities and several studies have suggested that MRI may be superior to standard techniques for detecting endoleaks during follow-up, as well as for evaluation of aneurysm sac exclusion and graft patency. The application of MRI in patients with endovascular stent-grafts has limitations. The image quality may be compromised by susceptibility artefacts introduced by the stent material²³¹ or severe signal reduction in the stent-graft due to radio-frequency (RF) shielding of the mesh²³². The Food and Drug Administration (FDA) therefore recommends that stent-grafts undergo MRI assessment prior to clinical use because safety issues such as RF heating and dislocation must be carefully considered²³³. In direct comparison to CT, MRI has proven to provide all relevant information required for follow-up of endoluminally treated abdominal aortic aneurysm with superior performance in the assessment of thrombus reorganisation²³⁴ and inferior performance in the identification of stent fracture²³⁵.

Our study has shown that the novel NP stent-graft is not associated with any relevant susceptibility artefacts or relevant RF signal loss within the stent-graft lumen. RF shielding effects depend on stent material and wall geometry. Our results of no significant RF shielding for nitinol based stent-grafts are comparable to previous studies²³⁶. The shielding effects vary substantially with the orientation of a stent. Consequently, the shielding effects need to be confirmed following implantation in humans. However, this should not pose a problem considering the negligible susceptibility and shielding effects exhibited by Nitinol stents.

Our results did show difference in velocity attenuation between two stent-grafts to some extent, however it did not significantly affect appreciation of graft's exterior or interior. The detectability of in-stent stenosis can be affected by overall attenuation inside the stent but this is more relevant in smaller stents. In these stents, flow patency has to be assessed proximally and beyond the stent where arterial flow signal could be seen. However, in thoracic stents, with high systolic velocities and flow volumes with larger stent diameter, in-stent flow measurements are unlikely to be significantly affected. The findings of our investigation and previous studies suggest that nitinol stent-grafts do not cause any major artefact that could significantly influence flow measurements²³⁷.

MR-safe is defined by ASTM as a device which when used in an MRI environment under specified conditions, has demonstrated to present no additional risk to the patient or other individual but may affect the quality of the diagnostic information. No additional risk to the patient due to stent movement, dislodgement or migration using an MRI system with a static magnetic field of 3.0T or less is expected²³⁸. Another potential safety hazard associated with MRI examinations is the possibility of localised increases in the radiofrequency Specific Absorption Rate (SAR) near metallic implants. The local electric field can be amplified, especially if the implants are composed of long conducting structures that potentially can couple

significantly with RF energy of the body coil²³⁹. This might lead to excessive tissue heating. These resonance effects, however, occur only when the length of implants exceeds one half of the RF wavelength²⁴⁰. For endografts, that are small as compared to RF wavelength (<20 cm in length, as used in this study), RF resonance is considered unlikely²⁴¹, so no significant heating of these devices is expected. Accordingly, this testing is not essential. Furthermore, for Valiant stent-graft, the whole-body averaged SAR of 3.0 W/kg for 15 minutes exposure to MRI will produce a maximum temperature increase of only 0.7 °C, which is considered physiologically inconsequential and does not pose additional risk to the patient²⁴².

This study has limitations. Although, the image artefacts have been addressed, the safety and compatibility concerning magnetically induced displacement force and torque and RF heating remains to be proven, before the device can be classified as MR-safe. The flow rate probably wasn't consistently at exactly 100 ml/s; we didn't assess the amount of signal loss and artefacts with different device orientations and we have assessed at 3T magnetic strength only. Another limitation might be that we did not perform an *in vivo* analysis. However, the purpose of this study was to assess the accuracy in relation to our gold standard, i.e. a stent-graft in current clinical use. Because in addition to graft material, stent diameter and pulsatility of flow, other haemodynamic parameters including viscosity and compliance of arteries affect the distortion of magnetic field, our results will need to be confirmed in an *in vivo* model.

7.5 CONCLUSION

MRI is likely to be an integral part of follow-up after implantation of thoracic endografts. Since flow in arch and descending thoracic aorta exhibits very high systolic velocities and flow volumes it is an especially challenging environment. The knowledge gain on blood flow alterations within aortic stent-grafts could be used to identify risk factors for later stent-graft failure as well as to improve stent-graft design. We have designed a stent-graft from NP that does not display any relevant material-induced artefacts on MRI. On flow assessment, signal attenuation is comparable with commercial device. The small difference noted was statistically insignificant and is unlikely to be of any clinical implication. These properties are important in developing this stent-graft, sutureless, compliant, durable and made from biocompatible and antithrombogenic polymer, for future clinical use. In future, we aim to perform haemodynamic testing to further improve the stent-graft design and confirm its properties in an *in vivo* model. Our work will also involve making a branched device for branches of the aortic arch in addition to assessment of folding profile and deployment.



Chapter 8

Discussion, Conclusion and Future work

8.1 DISCUSSION

The key findings of this work are:

- a) We have developed aortic stent-grafts using surface-modified nitinol bonded to a nanocomposite polymer based on polyhedral oligomeric silsesquioxane (POSS) – poly carbonate-urea urethane (PCU). Using several modifications, the prototype for infra-renal abdominal aortic aneurysm (AAA) repair has been optimised.
- b) The stent-graft utilises deployable structures technology and has shown folding efficiency similar to current devices with a potential to develop delivery systems for future percutaneous insertion.
- c) Using similar principles, we have also developed an innovative design for a thoracic stent-graft which is conformable to the aortic arch anatomy. This device can be further modified to have fenestrations and branches.
- d) We have developed an aortic model for physiological analysis of endografts and shown superiority to presently used models.
- e) Through extensive in vitro analysis, our results show that the sutureless technology proved to be durable and robust on exposure to fatigue equivalent to 10 years of use in human body in an accelerated simulated physiological environment. This test was carried out based on FDA recommendations.
- f) On in vitro testing, the POSS PCU stent-graft showed superior compliance and elastic stiffness profile in comparison to ePTFE-based stent-graft in current clinical use.
- g) Finally, the curved stent-graft showed comparable properties to current device in magnetic resonance signal attenuation analysis in a dedicated in vitro flow phantom. There were no significant artefacts affecting the visibility or image quality.

8.1.1 Endovascular stent-grafts

The long-term durability of EVAR remains a concern and the potential for adverse events related to endograft migration, endoleak or endograft failure requires lifelong surveillance. The data on longer-term benefits are less clear, with no obvious survival advantage and an expense of increased reintervention rates, and additional costs²⁴³.

The endograft technology needs to advance further with next-generation devices and novel properties to address these shortcomings and subsequently lead to further widespread adaptation of this treatment modality.

The use of TEVAR in thoracic aortic pathology is a rapidly developing field that carries many promises for the future on multiple fronts. Current devices will definitely become more developed and new devices will be introduced. It is important to develop devices which are more flexible and can conform better to the aorta, specifically in the hostile aortic arch environment as well as other tortuous areas. Also, the development of branched devices will expand the utility of the technology in covering more pathologies and treating them in a more effective manner.

8.1.2 Contemporary graft materials

The endografts in current clinical use are mainly made from either thin woven polyester (Dacron) or ePTFE. Sac enlargement after endovascular aneurysm repair (EVAR), without evidence of endoleak, has been attributed largely to endotension or material porosity. The first-generation Gore ExcluderTM graft allowed serous transudate contributing to continued sac pressurisation. AneuRxTM grafts had a higher incidence of microleaks, or persistent transgraft blood flow, occurring through the thin graft material. The ExcluderTM and AneuRxTM devices modified their graft material in 2004 with

reduced permeability²⁴⁴. Stent and graft materials have different mechanical properties and any repetitive movement between them may damage the fabric. Stronger sutures and tighter weaves have made current designs more stable, but none is yet free from fabric graft failure²⁴⁵.

With the availability of new materials, reducing mismatch in aortic stiffness and compliance may become important in future EVAR grafts. Indeed, some differences in presently used materials have already been observed by van Herwaarden and colleagues finding differences in compliance between Gore ExcluderTM and Medtronic TalentTM stent-grafts at the level of aneurysm neck²⁴⁶. In the next decade, we can expect continuing improvements in device design. Plasmid-loaded cationised gelatin (CG) hydrogel-coated stent-grafts have been proposed offering transduction of therapeutic genes into the vascular wall facilitating the biologic healing between the aorta and graft²⁴⁷. Novel graft materials need to be developed and tested, which have the potential to deliver compliance, antithrombogenicity, and biocompatibility to provide better configurations and reduce the risk of complications.

8.1.3 POSS-PCU nanocomposite polymer as graft material

Our group has developed a family of nanocomposite polymers for biomedical applications. Polyhedral oligomeric silsesquioxane–poly(carbonate urea)urethane (POSS–PCU) is a biostable, durable and has displayed impressive anti-thrombogenic properties in vitro compared with ePTFE, making it a promising biomaterial for cardiovascular applications²⁴⁸⁻²⁵¹. Polyurethanes are composed of hard and soft segments, incompatibility between which, results in microphase separation. This behaviour infers tough, viscoelastic response, that is ideal for vascular applications. Biostability is achieved by incorporation of a biologically stable soft segment group made up of polycarbonate molecules to form a PCU. The material's surface properties

are defined by POSS groups that are covalently bonded to the polymer backbone. These nanoparticle pendant groups modify the material's surface morphology making it resistant to thrombus formation and they are also suitable for chemically modification to promote endothelialisation.

8.1.4 Metallic stent designs in modern endografts and folding efficiency

The Zenith FlexTM and Zenith TX2TM devices are constructed with a frame of self-expanding stainless steel Z-stents. The PowerlinkTM is created with self-expanding cobalt-chromium stents that form the inner structure of the device. All the other stent-grafts involve a metal skeleton made from Nickel-Titanium commonly referred as Nitinol. This material is chosen for its ability to elastically recover large strains and thereby, expand from the delivery catheter and conform to geometry of the host artery. The material's high elasticity also infers good flexibility, critical for navigation and deployment in tortuous vessels. Several different nitinol stent designs have been used. The AneuRxTM uses diamond shaped nitinol rings for high radial strength required to achieve fixation without active anchoring barbs. The ExcluderTM is composed of nitinol wire construct in helical configuration. The TalentTM uses nitinol springs and the EndurantTM has M-shaped stents.

Our design is based on principle of compact packaging of a tubular structure, by carefully designed creases that behave as line hinges. We have used a folding pattern composed of a number of rows of rectangular elements. Each repeated element comprised of hill and valley fold lines that allow it to collapse efficiently to a minimal volume. The advantage of this configuration includes forming a scaffold structure arranged so that each support hoop is opposing the next, so that when this structure is collapsed, an efficient folding can be achieved. Our stent design is similar to the ExcluderTM, the EndurantTM, and the TalentTM devices but different to the AneuRxTM. We analysed the folding efficiency by feeding it through a reducing funnel and into

sheath that was heat shrunk to constrain the device in its folded condition. A collapsed diameter of 6.5 mm was achieved from an expanded diameter of 31.1 mm. This corresponded to a reduction ratio of 4.8. The prototype's folding ratio compared favourably with Talent™ stent-graft¹³⁵. Moreover, improvements to the packing and sheathing systems used should make it possible to reduce the packaged diameter to less than 4mm, thereby making it suitable for percutaneous insertion.

8.1.5 Bonding versus suturing of graft material to metal skeleton

The Excluder™ and Powerlink™ have sutureless designs. All the other stent-grafts involve suturing of the graft material to metal exoskeleton. Similarly, for thoracic endografts, the Tag™ design does not involve any sutures.

We have used a sutureless design for endografts using nitinol, which has been surface-modified. Chemical treatment induces a chemical bond between the POSS-PCU polymer and the substrate. This approach requires a metal substrate which has an oxide layer that can enhance the polymer coating bond strength²⁵². This oxide layer was achieved using a variety of chemical, thermal and electrochemical pre-treatment methods^{253;254}. The results have shown three-fold increase in the bond-strength between the graft material and nitinol²⁵⁵.

8.1.6 Physiological model for in vitro testing

Many investigators have undertaken in vivo studies into specific aspects of preoperative and post operative AAA's using silicone rubber or latex AAA models²⁵⁶⁻²⁵⁹. The most important component in any in vitro study should be the AAA model itself. These models should be reproducible, have consistent material properties, consistent thickness and be physiological in behaviour.

There are a number of important considerations when attempting to develop models with physiological properties. Creating materials with a similar stress-strain response to aortic tissue may not lead to models that behave similar to the vessel itself. Because of this, the compliance (or stiffness) of arteries has become the attribute which researchers attempt to mimic^{258;260}. The manufacturing methods for creating both idealised and realistic AAA models have been previously reported^{258;260;261}. The abdominal aorta is surrounded by visceral organs, abdominal muscle and the spine which undoubtedly influence its deformation under pressure²⁶². So it is important that in vitro models engineer a degree of “over-compliance” to buffer subsequent tissue-induced stiffening effect.

Our aim was to develop a new model which has superior compliance to the presently used models. In order to assess the compliance of aorta, we used porcine aortas and measured their compliance. We know from previous pulsatile flow studies that there are several regions with oscillating shear stress on the posterior aortic wall opposite the superior mesenteric artery and downstream the right renal artery. Although, it was not possible to factor this in our model, we measured compliance at several areas including the juxta-renal aorta, close to the bifurcation and at the level of main branches. Our results confirmed that the new model had superior compliance and elastic stiffness profile and presently available latex model can fail at physiological pressures. Previous similar reports from other groups have analysed compliance of AAA models, however they analysed the effect of intra-luminal thrombus on compliance^{263;264}. This was not essential in our study as we used non-aneurysmal aorta. Furthermore, our main aim was to develop a model for long-term in vitro fatigue analysis of endovascular stent-grafts. Our model was developed with physiological properties and this can be further utilised for careful design of realistic AAA geometries in the future.

8.1.7 Long-term fatigue and durability analysis

In the next stage of our work, the long-term durability of the stent-graft using the new physiological model was analysed. The first commercially available stent-grafts were unable to withstand the haemodynamic forces of the vascular environment. The past 15 years have seen a gradual improvement in long-term stent-graft performance as designs evolved through the elimination of features associated with late failure and the replication of features associated with durable success. Any new stent-graft should be tested to failure in a realistic model of the endovascular environment. Computational techniques, such as finite element analysis, enable to map the distribution of strain and stress as a basis for estimates of stent life. Accelerated fatigue testing subjects prototypes of the stent-graft, or its components, to cyclical deformation at rates far higher than the human pulse, the goal being to compress the effects of years in the human circulation into a few months of testing²⁶⁵. Clinical manifestations of stent-graft instability often present long after the stent-graft is inserted, and the lessons of clinical experience take a long time to become evident. As a result, the interactive cycle of device evolution, from design to failure and redesign was quick to correct the causes of early failure, but slow to correct sources of late failure. By the time a late-occurring problem was identified, acknowledged, and corrected, many patients had already been treated using stent-grafts that were destined to fail^{45;49;266}.

Due to these factors, the FDA, which has the regulatory authority, recommends testing new stent-grafts for duration equivalent to 10 years in human body. The aorta and all its contents are in constant motion. Cyclical loading, unloading, and deformation causes work hardening and fracture of stents at sites of localised stress, strain, surface irregularities, and asymmetric loading. As discussed earlier, nitinol is the material of choice for many stents because it is versatile, easy to form, and magnetic resonance imaging compatible. Unfortunately, nitinol stents are fracture-prone. So it was important to confirm the durability of nitinol after surface

modification. Our results show that the bonding of POSS-PCU with nitinol remained robust with no occurrence of device failure on completion of accelerated fatigue testing.

Long-term graft performance is of vital importance as now more and more patients are being offered endovascular aortic repair even in a younger age group. In previously reported work, suture-generated holes in the graft fabric were seen in virtually all explanted AneuRx™ stent-grafts⁶¹. These holes were not generally large enough to cause a type III endoleak, but they did cause worrisome pressurisation and dilatation of the aneurysm⁵¹, leading to the substitution of a tighter weave graft fabric for the loose woven fabric of the original design. Our results confirmed the durability of POSS-PCU on exposure to long-term cyclic loading. There was no significant change in its essential properties. The radial strength, elasticity and thermo-mechanical strength were preserved. More importantly, there was no significant change in its compliance. Loss of compliance after implantation has been a known factor associated with polyurethane grafts. So with POSS backbone in our nanocomposite polymer, more biostability is achieved.

8.1.8 The curved design: the first step towards a new branched endograft

Despite expanding indications for stent-grafting to more proximal lesions in the aortic arch, technical and anatomic difficulties persist, caused by the inflexible structure of most tubular stent-grafts and their inability to conform to the curved aortic arch²⁶⁷. Several articles have reported inadequate stent-graft apposition along the inner curve of the arch resulting in type I endoleaks and stent-graft collapse²⁶⁸⁻²⁷¹. Current thoracic stent-grafts are straight and semi-rigid due to their segmentation. Several techniques have been tried to improve conformability including in situ bending²⁷² or in situ fenestrations²⁷³.

We utilised the aortic arch dimensions from real patient magnetic resonance imaging data to develop a curved design. The graft thickness for POSS-PCU used was approximately 150 μg and because of its elastic properties, it can be easily conformed into the desired shape. A better proximal apposition of the device at the inner curve of the aortic arch can be potentially achieved that may prevent early and late stent-graft related complications. Although, still in infancy, this design is promising as there is a potential to add fenestrations and branches which will make complete endovascular repair of aortic arch pathologies feasible, obviating the need for extra-anatomic bypass.

8.1.9 Improving compliance mismatch: POSS-PCU versus ePTFE

Studies show that TAA compliance is closely associated with many factors among which the implantation of the stent-graft is the most important²⁷⁴. Before stent-graft implantation, the elastic TAA wall receives direct impact from the pulsatile blood. Hence, it has strong motion behaviour before TEVAR, and the compliance value is high. After TEVAR, part of the pulse energy is absorbed by the stent-graft directly, and the stagnant blood as well as the soft intra-luminal thrombus serve as excellent buffer. Therefore, the compliance value after TEVAR is much smaller than the one before TEVAR²⁷⁵. Compliance mismatch in the proximal aorta can potentially reduce cardiac efficiency and may predispose to the development of left ventricular hypertrophy. “Compliance-matched” stent-grafts can help avoid this problem, although there is lack of significant evidence for this hypothesis due to limited published work. Dacron and ePTFE in presently used stent-grafts are inherently stiff with poor compliance. Our results confirm superior profile of POSS-PCU stent-graft as compared to commercial device based on ePTFE in current clinical use. We hope to be able confirm translation of this superior property in a suitable in vivo model. If successful, this can address limitation of current graft materials and help in making TEVAR a more effective and durable procedure.

8.1.10 Magnetic Resonance Imaging conditioning: mandatory in new designs

For adequate evaluation of treatment success after EVAR, several specific items should be monitored: the effectiveness of aneurysm sac exclusion, graft patency, graft migration, and graft integrity. Several recent studies have shown magnetic resonance imaging (MRI) and magnetic resonance angiography (MRA) techniques are more sensitive for endoleak detection than standard computed tomographic angiography (CTA).

One possible disadvantage of MRI techniques is that the endografts have to be MRI compatible, so a major potential problem is the presence of metallic components in the endografts. Metallic structures can produce artefacts that may considerably degrade image quality. Following stent-graft implantation, MRI image artefacts can extend throughout the anatomical region containing the device. This can obscure the view of immediately adjacent anatomical structures. The MRI compatibility of the POSS-PCU nitinol stent-graft was confirmed by absence of significant artefacts that could potentially degrade the diagnostic value of the images. The findings of our investigation and previous studies suggest that nitinol stent-grafts do not cause any major artefact that could significantly influence flow measurements^{276;277}. The surface-modification protocol applied in our stent-graft did not affect its MRI properties. In a dedicated in vitro aortic flow phantom, the results were comparable to a commercially available stent-graft.

8.2 CONCLUSIONS AND FUTURE WORK

This work describes a basic science/engineering project with clear implications for clinical application of aortic endografts. Combining deployable structures technology with advanced biomaterial provides exciting possibilities for improving stent-graft design. A sutureless device with an efficient folding pattern has been developed for

repair of abdominal aortic aneurysms. Similarly, a conformable anatomically accurate stent-graft is developed which matches the curvature of human aortic arch. We have developed a physiologically relevant aortic model for long-term fatigue analysis and confirmed the durability of the sutureless design. The POSS-PCU graft bonding with nitinol skeleton remains robust with no signs of failure after 10 years of equivalent usage in an accelerated in vitro environment with simulated physiological conditions. Several essential properties of POSS-PCU nanocomposite polymer remain unaltered. The developed stent-grafts are MRI-compatible and show superior compliance and elastic stiffness profile as compared to presently used devices.

Based on positive results from this work, the following recommendations are made for future

- a) POSS-PCU needs further characterisation for use in stent-grafts. Future work should be directed at determining the optimum thickness of the graft material to ensure folding efficiency, mechanical strength and compliance. In addition, the ends of the polymer tube are vital as type I endoleak can occur if the material is thin and forms an internal flap allowing the blood to flow through the aneurysm sac.
- b) The stent-grafts proposed in this project are based on solid POSS-PCU. Several current devices use material with pores, which would allow tissue cellular infiltration. Porous POSS-PCU has been utilised to develop small diameter bypass grafts in addition to several other cardiovascular devices. The implication of using porous as opposed to solid POSS-PCU on its biomechanical properties in the stent-graft design needs further evaluation.
- c) The addition of fenestrations and branches to the curved device is essential to make it suitable for clinical use.

- d) Several variants to which the stent-graft is exposed in vivo cannot be factored in bench testing. The biostability of the sutureless design and its properties, especially the effects of oxidation and hydrolysis need confirmation in a suitable animal model.

The modern design of aortic stent-grafts is very complex. In addition to the properties of stent and graft materials, which are evaluated in this experimental work, axial migration force at the proximal attachment which changes with variations in pressure, angulation, and tortuosity, is a critical parameter in stent-graft development. Deployment using packing and sheathing systems needs to be considered. Due to the complexity involved, further evaluation and design development may be more appropriate by partnership with a current device-manufacturing company.

REFERENCES

- (1) Komarneni S. Nanocomposites. *Journal of Materials Chemistry* 1992; 2(12):1219-1230.
- (2) Fu BX, Gelfer MY, Hsiao BS, Phillips S, Viers B, Blanski R et al. Physical gelation in ethylene-propylene copolymer melts induced by polyhedral oligomeric silsesquioxane (POSS) molecules. *Polymer* 2003; 44(5):1499-1506.
- (3) Oaten M, Choudhury NR. Silsesquioxane-urethane hybrid for thin film applications. *Macromolecules* 2005; 38(15):6392-6401.
- (4) Ghanbari H, de Mel A, Seifalian AM. Cardiovascular application of polyhedral oligomeric silsesquioxane nanomaterials: a glimpse into prospective horizons. *International Journal of Nanomedicine* 2011; 6:775-786.
- (5) Kannan RY, Salacinski HJ, Sales KM, Butler PE, Seifalian AM. The endothelialization of polyhedral oligomeric silsesquioxane nanocomposites: an in vitro study. *Cell Biochem Biophys* 2006; 45(2):129-136.
- (6) Alcorn HG, Wolfson SK, Jr., Sutton-Tyrrell K, Kuller LH, O'Leary D. Risk factors for abdominal aortic aneurysms in older adults enrolled in The Cardiovascular Health Study. *Arterioscler Thromb Vasc Biol* 1996; 16(8):963-970.
- (7) British Heart Foundation. Factfile: Abdominal aortic aneurysm. 2005.
Ref Type: Report
- (8) NICE technology appraisal guidance 167. Endovascular stent-grafts for the treatment of abdominal aortic aneurysms. 2009.
Ref Type: Report
- (9) Krupski WC, Rutherford RB. Update on open repair of abdominal aortic aneurysms: the challenges for endovascular repair. *J Am Coll Surg* 2004; 199(6):946-960.
- (10) Darling RC, Messina CR, Brewster DC, Ottinger LW. Autopsy Study of Unoperated Abdominal Aortic-Aneurysms - Case for Early Resection. *Circulation* 1977; 56(3):161-164.
- (11) Rinckenbach S, Hassani O, Thaveau F, Bensimon Y, Jacquot X, Tally SE et al. Current outcome of elective open repair for infrarenal abdominal aortic aneurysm. *Ann Vasc Surg* 2004; 18(6):704-709.

- (12) Faries PL, Dayal R, Rhee J, Trocciola S, Kent KC. Stent graft treatment for abdominal aortic aneurysm repair: recent developments in therapy. *Current Opinion in Cardiology* 2004; 19(6):551-557.
- (13) Huber TS, Wang JG, Derrow AE, Dame DA, Ozaki CK, Zelenock GB et al. Experience in the United States with intact abdominal aortic aneurysm repair. *Journal of Vascular Surgery* 2001; 33(2):304-310.
- (14) Williamson WK, Nicoloff AD, Taylor LM, Jr., Moneta GL, Landry GJ, Porter JM. Functional outcome after open repair of abdominal aortic aneurysm. *J Vasc Surg* 2001; 33(5):913-920.
- (15) Perkins JMT, Magee TR, Hands LJ, Collin J, Galland RB, Morris PJ. Prospective evaluation of quality of life after conventional abdominal aortic aneurysm surgery. *European Journal of Vascular and Endovascular Surgery* 1998; 16(3):203-207.
- (16) Volodos NL, Karpovich IP, Troyan VI, Kalashnikova Y, Shekhanin VE, Ternyuk NE et al. Clinical experience of the use of self-fixing synthetic prostheses for remote endoprosthetics of the thoracic and the abdominal aorta and iliac arteries through the femoral artery and as intraoperative endoprosthesis for aorta reconstruction. *Vasa Suppl* 1991; 33:93-95.
- (17) Parodi JC, Palmaz JC, Barone HD. Transfemoral intraluminal graft implantation for abdominal aortic aneurysms. *Ann Vasc Surg* 1991; 5(6):491-499.
- (18) Brewster DC, Jones JE, Chung TK, LaMuraglia GM, Kwolek CJ, Watkins MT et al. Long-term outcomes after endovascular abdominal aortic aneurysm repair: the first decade. *Ann Surg* 2006; 244(3):426-438.
- (19) Chaudhury MH, inventors. Method for performing aneurysm repair. patent U.S. Patent Number 4,140,126. 1979 1979.
- (20) Kornberg E, inventors. Aortic graft device and method for performing an intraluminal abdominal aortic aneurysm repair. patent U.S. Patent Number 4,562,596. 1986 1986.
- (21) Kornberg E, inventors. Device and method for performing an intraluminal abdominal aortic aneurysm repair. patent U.S. Patent Number 4,617,932. 1986 1986.
- (22) Lazarus HM, inventors. Intraluminal graft device, system and method. patent U.S. Patent Number 4,787,899. 1988 1988.

- (23) Lazarus HM. Endovascular Grafting for the Treatment of Abdominal Aortic-Aneurysms. *Surgical Clinics of North America* 1992; 72(4):959-968.
- (24) Chuter TAM, Donayre C, Wendt G. Bifurcated Stent-Grafts for Endovascular Repair of Abdominal Aortic-Aneurysm - Preliminary Case-Reports. *Surgical Endoscopy-Ultrasound and Interventional Techniques* 1994; 8(7):800-802.
- (25) Hagen B, Harnoss BM, Trabhardt S, Ladeburg M, Fuhrmann H, Franck C. Self-Expandable Macroporous Nitinol Stents for Transfemoral Exclusion of Aortic-Aneurysms in Dogs - Preliminary-Results. *Cardiovascular and Interventional Radiology* 1993; 16(6):339-342.
- (26) Rutherford RB, Krupski WC. Current status of open versus endovascular stent-graft repair of abdominal aortic aneurysm. *J Vasc Surg* 2004; 39(5):1129-1139.
- (27) Carpenter JP, Anderson WN, Brewster DC, Kwolek C, Makaroun M, Martin J et al. Multicenter pivotal trial results of the Lifepath System for endovascular aortic aneurysm repair. *J Vasc Surg* 2004; 39(1):34-43.
- (28) Zarins CK. The US AneuRx Clinical Trial: 6-year clinical update 2002. *Journal of Vascular Surgery* 2003; 37(4):904-908.
- (29) Matsumura JS, Brewster DC, Makaroun MS, Naftel DC. A multicenter controlled clinical trial of open versus endovascular treatment of abdominal aortic aneurysm. *Journal of Vascular Surgery* 2003; 37(2):262-271.
- (30) Greenberg RK, Chuter TAM, Sternbergh C, Fearnot NE. Zenith AAA endovascular graft: Intermediateterm results of the US multicenter trial. *Journal of Vascular Surgery* 2004; 39(6):1209-1218.
- (31) Carpenter JP. Multicenter trial of the PowerLink bifurcated system for endovascular aortic aneurysm repair. *J Vasc Surg* 2002; 36(6):1129-1137.
- (32) Saratzis N, Melas N, Saratzis A, Lazarides J, Ktenidis K, Tsakiliotis S et al. Anaconda aortic stent-graft: single-center experience of a new commercially available device for abdominal aortic aneurysms. *J Endovasc Ther* 2008; 15(1):33-41.
- (33) Stehr A, Schnitzbauer AA, Steinbauer MG, Topel I, Pfister K, Schlitt HJ et al. Early experience shows rapid shrinking of abdominal aortic aneurysms after endovascular treatment with Anaconda device. *Vasa* 2007; 36(3):199-204.

- (34) Criado FJ, Fairman RM, Becker GJ. Talent LPS AAA stent graft: Results of a pivotal clinical trial. *Journal of Vascular Surgery* 2003; 37(4):709-715.
- (35) Arko FR, Filis KA, Seidel SA, Gonzalez J, Lengle SJ, Webb R et al. How many patients with infrarenal aneurysms are candidates for endovascular repair? The Northern California experience. *J Endovasc Ther* 2004; 11(1):33-40.
- (36) Iezzi R, Cotroneo AR. Endovascular repair of abdominal aortic aneurysms: CTA evaluation of contraindications. *Abdom Imaging* 2006; 31(6):722-731.
- (37) Carpenter JP, Baum RA, Barker CF, Golden MA, Mitchell ME, Velazquez OC et al. Impact of exclusion criteria on patient selection for endovascular abdominal aortic aneurysm repair. *J Vasc Surg* 2001; 34(6):1050-1054.
- (38) Velazquez OC, Larson RA, Baum RA, Carpenter JP, Golden MA, Mitchell ME et al. Gender-related differences in infrarenal aortic aneurysm morphologic features: issues relevant to Ancure and Talent endografts. *J Vasc Surg* 2001; 33(2 Suppl):S77-S84.
- (39) Wolf YG, Tillich M, Lee WA, Rubin GD, Fogarty TJ, Zarins CK. Impact of aortoiliac tortuosity on endovascular repair of abdominal aortic aneurysms: evaluation of 3D computer-based assessment. *J Vasc Surg* 2001; 34(4):594-599.
- (40) PTCA.org. Boston Scientific Announces Acquisition of TriVascular, Inc. 2005.
Ref Type: Report
- (41) Carpenter JP. Midterm results of the multicenter trial of the powerlink bifurcated system for endovascular aortic aneurysm repair. *J Vasc Surg* 2004; 40(5):849-859.
- (42) Diethrich EB. AAA stent grafts: current developments. *J Invasive Cardiol* 2001; 13(5):383-390.
- (43) Malina M, Lindblad B, Ivancev K, Lindh M, Malina J, Brunkwall J. Endovascular AAA exclusion: will stents with hooks and barbs prevent stent-graft migration? *J Endovasc Surg* 1998; 5(4):310-317.
- (44) Sternbergh WC, III, Money SR, Greenberg RK, Chuter TA. Influence of endograft oversizing on device migration, endoleak, aneurysm shrinkage, and aortic neck dilation: results from the Zenith Multicenter Trial. *J Vasc Surg* 2004; 39(1):20-26.

- (45) Zarins CK, Bloch DA, Crabtree T, Matsumoto AH, White RA, Fogarty TJ. Stent graft migration after endovascular aneurysm repair: importance of proximal fixation. *J Vasc Surg* 2003; 38(6):1264-1272.
- (46) Benharash P, Lee JT, Abilez OJ, Crabtree T, Bloch DA, Zarins CK. Iliac fixation inhibits migration of both suprarenal and infrarenal aortic endografts. *J Vasc Surg* 2007; 45(2):250-257.
- (47) French JR, Simring DV, Merrett N, Thursby P. Aorto-enteric fistula following endoluminal abdominal aortic aneurysm repair. *Anz Journal of Surgery* 2004; 74(5):397-399.
- (48) Sampaio SM, Panneton JM, Mozes G, Andrews JC, Noel AA, Kalra M et al. AneuRx device migration: incidence, risk factors, and consequences. *Ann Vasc Surg* 2005; 19(2):178-185.
- (49) Tonnessen BH, Sternbergh WC, III, Money SR. Mid- and long-term device migration after endovascular abdominal aortic aneurysm repair: a comparison of AneuRx and Zenith endografts. *J Vasc Surg* 2005; 42(3):392-400.
- (50) Fogarty TJ, Arko FR, Zarins CK. Endograft technology: highlights of the past 10 years. *J Endovasc Ther* 2004; 11 Suppl 2:II192-II199.
- (51) Zarins CK, Bloch DA, Crabtree T, Matsumoto AH, White RA, Fogarty TJ. Aneurysm enlargement following endovascular aneurysm repair: AneuRx clinical trial. *J Vasc Surg* 2004; 39(1):109-117.
- (52) Jacobs TS, Won J, Gravereaux EC, Faries PL, Morrissey N, Teodorescu VJ et al. Mechanical failure of prosthetic human implants: A 10-year experience with aortic stent graft devices. *Journal of Vascular Surgery* 2003; 37(1):16-26.
- (53) Jacobs T, Teodorescu V, Morrissey N, Carroccio A, Ellozy S, Minor M et al. The endovascular repair of abdominal aortic aneurysm: an update analysis of structural failure modes of endovascular stent grafts. *Semin Vasc Surg* 2003; 16(2):103-112.
- (54) Wales L, Dunckley M, Bohm N, Kwok T, Bratby M, Morgan R et al. Device-specific outcomes following endovascular aortic aneurysm repair. *Eur J Vasc Endovasc Surg* 2008; 36(6):661-667.
- (55) Buth J, Harris PL, van MC, Fransen G. The significance and management of different types of endoleaks. *Semin Vasc Surg* 2003; 16(2):95-102.

- (56) Bernhard VM, Mitchell RS, Matsumura JS, Brewster DC, Decker M, Lamparello P et al. Ruptured abdominal aortic aneurysm after endovascular repair. *J Vasc Surg* 2002; 35(6):1155-1162.
- (57) van Marrewijk CJ, Fransen G, Laheij RJ, Harris PL, Buth J. Is a type II endoleak after EVAR a harbinger of risk? Causes and outcome of open conversion and aneurysm rupture during follow-up. *Eur J Vasc Endovasc Surg* 2004; 27(2):128-137.
- (58) van MC, Buth J, Harris PL, Norgren L, Nevelsteen A, Wyatt MG. Significance of endoleaks after endovascular repair of abdominal aortic aneurysms: The EUROSTAR experience. *J Vasc Surg* 2002; 35(3):461-473.
- (59) Rayt HS, Sandford RM, Salem M, Bown MJ, London NJ, Sayers RD. Conservative management of type 2 endoleaks is not associated with increased risk of aneurysm rupture. *Eur J Vasc Endovasc Surg* 2009; 38(6):718-723.
- (60) Gorich J, Rilinger N, Sokiranski R, Kramer S, Schutz A, Sunder-Plassmann L et al. Embolization of type II endoleaks fed by the inferior mesenteric artery: Using the superior mesenteric artery approach. *Journal of Endovascular Therapy* 2000; 7(4):297-301.
- (61) Zarins CK, Arko FR, Crabtree T, Bloch DA, Ouriel K, Allen RC et al. Explant analysis of AneuRx stent grafts: relationship between structural findings and clinical outcome. *J Vasc Surg* 2004; 40(1):1-11.
- (62) Biebl M, Hakaim AG, Oldenburg WA, Klocker J, McKinney JM, Paz-Fumagalli R. Management of a large intraoperative type IIIb endoleak in a bifurcated endograft-a case report. *Vasc Endovascular Surg* 2005; 39(3):267-271.
- (63) Faries PL, Cadot H, Agarwal G, Kent C, Hollier LH, Marin ML. Management of endoleak after endovascular aneurysm repair: Cuffs, coils, and conversion. *Journal of Vascular Surgery* 2003; 37(6):1155-1161.
- (64) Rashid ST, Salacinski HJ, Fuller BJ, Hamilton G, Seifalian AM. Engineering of bypass conduits to improve patency. *Cell Proliferation* 2004; 37(5):351-366.
- (65) Guidoin R, Douville Y, Basle MF, King M, Marinov GR, Traore A et al. Biocompatibility studies of the anaconda stent-graft and observations of nitinol corrosion resistance. *Journal of Endovascular Therapy* 2004; 11(4):385-403.

- (66) Kamineni R, Heuser RR. Abdominal aortic aneurysm: a review of endoluminal treatment. *J Interv Cardiol* 2004; 17(6):437-445.
- (67) Gilling-Smith G, Brennan J, Harris P, Bakran A, Gould D, McWilliams R. Endotension after endovascular aneurysm repair: definition, classification, and strategies for surveillance and intervention. *J Endovasc Surg* 1999; 6(4):305-307.
- (68) Lin PH, Bush RL, Katzman JB, Zemel G, Puente OA, Katzen BT et al. Delayed aortic aneurysm enlargement due to endotension after endovascular abdominal aortic aneurysm repair. *Journal of Vascular Surgery* 2003; 38(4):840-842.
- (69) Conti JC, Strobe ER. Radial compliance of natural and mock arteries: how this property defines the cyclic loading of deployed vascular stents. *Biomed Sci Instrum* 2002; 38:163-172.
- (70) Criado FJ, Wilson EP, Fairman RM, bul-Khoudoud O, Wellons E. Update on the talent aortic stent-graft: A preliminary report from United States phase I and II trials. *Journal of Vascular Surgery* 2001; 33(2):S146-S149.
- (71) Hinchliffe RJ, Macierewicz J, Hopkinson BR. Early results of a flexible bifurcated endovascular stent-graft (Aorfix). *Journal of Cardiovascular Surgery* 2004; 45(4):285-291.
- (72) Kramer SC, Seifarth H, Pamler R, Fleiter T, Gorich J. Geometric changes in aortic endografts over a 2-year observation period. *Journal of Endovascular Therapy* 2001; 8(1):34-38.
- (73) Gotman I. Characteristics of metals used in implants. *Journal of Endourology* 1997; 11(6):383-389.
- (74) Heintz C, Riepe G, Birken L, Kaiser E, Chakfe N, Morlock M et al. Corroded nitinol wires in explanted aortic endografts: An important mechanism of failure? *Journal of Endovascular Therapy* 2001; 8(3):248-253.
- (75) Guidoin R, Marois Y, Douville Y, King MW, Castonguay M, Traore A et al. First-generation aortic endografts: Analysis of explanted stenter devices from the EUROSTAR registry. *Journal of Endovascular Therapy* 2000; 7(2):105-122.
- (76) White JG, Mulligan NJ, Gorin DR, D'Agostino R, Yucel EK, Menzoian JO. Response of normal aorta to endovascular grafting: a serial histopathological study. *Arch Surg* 1998; 133(3):246-249.

- (77) Shi Q, Wu MH, Onuki Y, Ghali R, Hunter GC, Johansen KH et al. Endothelium on the flow surface of human aortic Dacron vascular grafts. *J Vasc Surg* 1997; 25(4):736-742.
- (78) McPhee J, Eslami MH, Arous EJ, Messina LM, Sehanzer A. Endovascular treatment of ruptured abdominal aortic aneurysms in the United States (2001-2006): A significant survival benefit over open repair is independently associated with increased institutional volume. *Journal of Vascular Surgery* 2009; 49(4):817-826.
- (79) van Herwaarden JA, Muhs BE, Vincken KL, van Prehn J, Teutelink A, Bartels LW et al. Aortic compliance following EVAR and the influence of different endografts: determination using dynamic MRA. *J Endovasc Ther* 2006; 13(3):406-414.
- (80) Long A, Rouet L, Vitry F, Albertini JN, Marcus C, Clement C. Compliance of abdominal aortic aneurysms before and after stenting with tissue doppler imaging: evolution during follow-up and correlation with aneurysm diameter. *Ann Vasc Surg* 2009; 23(1):49-59.
- (81) Alankar S, Barth MH, Shin DD, Hong JR, Rosenberg WR. Aortoduodenal fistula and associated rupture of abdominal aortic aneurysm after endoluminal stent graft repair. *J Vasc Surg* 2003; 37(2):465-468.
- (82) Alimi YS, Chakfe N, Rivoal E, Slimane KK, Valerio N, Riepe G et al. Rupture of an abdominal aortic aneurysm after endovascular graft placement and aneurysm size reduction. *J Vasc Surg* 1998; 28(1):178-183.
- (83) Bertges DJ, Villeda ER, Makaroun MS. Aortoenteric fistula due to endoleak coil embolization after endovascular AAA repair. *J Endovasc Ther* 2003; 10(1):130-135.
- (84) Heikkinen L, Valtonen M, Lepantalo M, Saimanen E, Jarvinen A. Infrarenal endoluminal bifurcated stent graft infected with *Listeria monocytogenes*. *Journal of Vascular Surgery* 1999; 29(3):554-556.
- (85) Norgren L, Jernby B, Engellau L. Aortoenteric fistula caused by a ruptured stent-graft: A case report. *Journal of Endovascular Surgery* 1998; 5(3):269-272.
- (86) Velazquez OC, Carpenter JP, Baum RA, Barker CF, Golden M, Criado F et al. Perigraft air, fever, and leukocytosis after endovascular repair of abdominal aortic aneurysms. *Am J Surg* 1999; 178(3):185-189.

- (87) Elkouri S, Blair JF, Therasse E, Oliva VL, Bruneau L, Soulez G. Aortoduodenal fistula occurring after type II endoleak treatment with coil embolization of the aortic sac. *Journal of Vascular Surgery* 2003; 37(2):461-464.
- (88) Ghosh J, Murray D, Khwaja N, Murphy MO, Halka A, Walker MG. Late infection of an endovascular stent graft with septic embolization, colonic perforation, and aortoduodenal fistula. *Ann Vasc Surg* 2006; 20(2):263-266.
- (89) Lyden SP, Tanquilut EM, Gavin TJ, Adams JE. Aortoduodenal Fistula after Abdominal Aortic Stent Graft Presenting with Extremity Abscesses. *Vascular* 2005; 13(5):305-308.
- (90) Ratchford EV, Morrissey NJ. Aortoenteric fistula: a late complication of endovascular repair of an inflammatory abdominal aortic aneurysm. *Vasc Endovascular Surg* 2006; 40(6):487-491.
- (91) Sharif MA, Lee B, Lau LL, Ellis PK, Collins AJ, Blair PH et al. Prosthetic stent graft infection after endovascular abdominal aortic aneurysm repair. *J Vasc Surg* 2007; 46(3):442-448.
- (92) Tiesenhausen K, Hessinger M, Konstantiniuk P, Tomka M, Baumann A, Thalhammer M et al. Surgical conversion of abdominal aortic stent-grafts--outcome and technical considerations. *Eur J Vasc Endovasc Surg* 2006; 31(1):36-41.
- (93) Daugherty M, Shearer GR, Ernst CB. Primary Aortoduodenal Fistula - Extra-Anatomic Vascular Reconstruction Not Required for Successful Management. *Surgery* 1979; 86(3):399-401.
- (94) Saratzis N, Saratzis A, Melas N, Ktenidis K, Kiskinis D. Aortoduodenal fistulas after endovascular stent-graft repair of abdominal aortic aneurysms: single-center experience and review of the literature. *J Endovasc Ther* 2008; 15(4):441-448.
- (95) Chaikof EL, Blankensteijn JD, Harris PL, White GH, Zarins CK, Bernhard VM et al. Reporting standards for endovascular aortic aneurysm repair. *J Vasc Surg* 2002; 35(5):1048-1060.
- (96) Cho JS, Dillavou ED, Rhee RY, Makaroun MS. Late abdominal aortic aneurysm enlargement after endovascular repair with the Excluder device. *J Vasc Surg* 2004; 39(6):1236-1241.

- (97) Mennander A, Pimenoff G, Heikkinen M, Partio T, Zeitlin R, Salenius JP. Nonoperative approach to endotension. *Journal of Vascular Surgery* 2005; 42(2):194-198.
- (98) Abbruzzese TA, Kwolek CJ, Brewster DC, Chung TK, Kang J, Conrad MF et al. Outcomes following endovascular abdominal aortic aneurysm repair (EVAR): an anatomic and device-specific analysis. *J Vasc Surg* 2008; 48(1):19-28.
- (99) Brewster DC. Presidential address: What would you do if it were your father? Reflections on endovascular abdominal aortic aneurysm repair. *Journal of Vascular Surgery* 2001; 33(6):1139-1147.
- (100) Hobo R, Laheij RJF, Buth J. The influence of aortic cuffs and iliac limb extensions on the outcome of endovascular abdominal aortic aneurysm repair. *Journal of Vascular Surgery* 2007; 45(1):79-85.
- (101) Hobo R, Buth J. Secondary interventions following endovascular abdominal aortic aneurysm repair using current endografts. A EUROSTAR report. *Journal of Vascular Surgery* 2006; 43(5):896-902.
- (102) Greenhalgh RM, Brown LC, Kwong GPS, Powell JT, Thompson SG. Comparison of endovascular aneurysm repair with open repair in patients with abdominal aortic aneurysm (EVAR trial 1), 30-day operative mortality results: randomised controlled trial. *Lancet* 2004; 364(9437):843-848.
- (103) Prinssen M, Verhoeven ELG, Buth J, Cuypers PWM, van Sambeek MRHM, Balm R et al. A randomized trial comparing conventional and endovascular repair of abdominal aortic aneurysms. *New England Journal of Medicine* 2004; 351(16):1607-1618.
- (104) Schermerhorn ML, O'Malley AJ, Jhaveri A, Cotterill P, Pomposelli F, Landon BE. Endovascular vs. open repair of abdominal aortic aneurysms in the Medicare population. *N Engl J Med* 2008; 358(5):464-474.
- (105) MacMillan DP, Chaikof EL. Surgical conversion after endovascular aortic repair. In: Pierce WH, Matsumura JS, Yao JST, editors. *Trends in vascular surgery*. Evanston, IL: Greenwood Academic; 2004. 317-324.
- (106) Giles KA, Pomposelli F, Hamdan A, Wyers M, Jhaveri A, Schermerhorn ML. Decrease in total aneurysm-related deaths in the era of endovascular aneurysm repair. *J Vasc Surg* 2009; 49(3):543-550.

- (107) Drury D, Michaels JA, Jones L, Ayiku L. Systematic review of recent evidence for the safety and efficacy of elective endovascular repair in the management of infrarenal abdominal aortic aneurysm. *British Journal of Surgery* 2005; 92(8):937-946.
- (108) Greenberg RK, Chuter TAM, Cambria RP, Sternbergh WC, Fearnot NE. Zenith abdominal aortic aneurysm endovascular graft. *Journal of Vascular Surgery* 2008; 48(1):1-9.
- (109) Tanski W, III, Fillinger M. Outcomes of original and low-permeability Gore Excluder endoprosthesis for endovascular abdominal aortic aneurysm repair. *J Vasc Surg* 2007; 45(2):243-249.
- (110) Smith S, Mountcastle S, BurrIDGE A, Dodson TF, Salam AA, Kasirajan K et al. A single-institution experience with the AneuRx Stent Graft for endovascular repair of abdominal aortic aneurysm. *Ann Vasc Surg* 2008; 22(2):221-226.
- (111) Connors MS, Sternbergh WC, Carter G, Tonnessen BH, Yoselevitz M, Money SR. Endograft migration one to four years after endovascular abdominal aortic aneurysm repair with the AneuRx device: A cautionary note. *Journal of Vascular Surgery* 2002; 36(3):476-482.
- (112) Arko FR, Murphy EH. Endovascular aneurysm repair utilizing the AneuRx and Talent stent grafts. *Perspect Vasc Surg Endovasc Ther* 2008; 20(2):120-128.
- (113) Brown LC, Greenhalgh RM, Kwong GP, Powell JT, Thompson SG, Wyatt MG. Secondary interventions and mortality following endovascular aortic aneurysm repair: device-specific results from the UK EVAR trials. *Eur J Vasc Endovasc Surg* 2007; 34(3):281-290.
- (114) Waasdorp EJ, de Vries JP, Hobo R, Leurs LJ, Buth J, Moll FL. Aneurysm diameter and proximal aortic neck diameter influence clinical outcome of endovascular abdominal aortic repair: a 4-year EUROSTAR experience. *Ann Vasc Surg* 2005; 19(6):755-761.
- (115) Wang GJ, Carpenter JP. The Powerlink system for endovascular abdominal aortic aneurysm repair: six-year results. *J Vasc Surg* 2008; 48(3):535-545.
- (116) Greenhalgh RM, Brown LC, Epstein D, Kwong GPS, Powell JT, Sculpher MJ et al. Endovascular aneurysm repair and outcome in patients unfit for open repair of abdominal aortic aneurysm (EVAR trial 2): randomised controlled trial. *Lancet* 2005; 365(9478):2187-2192.

- (117) Schermerhorn ML, Finlayson SR, Fillinger MF, Buth J, van MC, Cronenwett JL. Life expectancy after endovascular versus open abdominal aortic aneurysm repair: results of a decision analysis model on the basis of data from EUROSTAR. *J Vasc Surg* 2002; 36(6):1112-1120.
- (118) Hua HT, Cambria RP, Chuang SK, Stoner MC, Kwolek CJ, Rowell KS et al. Early outcomes of endovascular versus open abdominal aortic aneurysm repair in the National Surgical Quality Improvement Program-Private Sector (NSQIP-PS). *Journal of Vascular Surgery* 2005; 41(3):382-389.
- (119) Becquemin JP, Kelley L, Zubilewicz T, Desgranges P, Lapeyre M, Kobeiter H. Outcomes of secondary interventions after abdominal aortic aneurysm endovascular repair. *J Vasc Surg* 2004; 39(2):298-305.
- (120) Biancari F, Ylonen K, Anttila V, Juvonen J, Ronsi P, Satta J et al. Durability of open repair of infrarenal abdominal aortic aneurysm: a 15-year follow-up study. *J Vasc Surg* 2002; 35(1):87-93.
- (121) Angle N, Dorafshar AH, Moore WS, Quinones-Baldrich WJ, Gelabert HA, Ahn SS et al. Open versus endovascular repair of abdominal aortic aneurysms: what does each really cost? *Ann Vasc Surg* 2004; 18(5):612-618.
- (122) Dryjski M, O'Brien-Irr MS, Hassett J. Hospital costs for endovascular and open repair of abdominal aortic aneurysm. *Journal of the American College of Surgeons* 2003; 197(1):64-70.
- (123) Blankensteijn JD, De Jong SECA, Prinssen M, van der Ham AC, Buth J, van Sterkenburg SMM et al. Two-year outcomes after conventional or endovascular repair of abdominal aortic aneurysms. *New England Journal of Medicine* 2005; 352(23):2398-2405.
- (124) Hopkins R, Bowen J, Campbell K, Blackhouse G, De RG, Novick T et al. Effects of study design and trends for EVAR versus OSR. *Vasc Health Risk Manag* 2008; 4(5):1011-1022.
- (125) Castelli P, Caronno R, Piffaretti G, Tozzi M, Lagana D, Carrafiello G et al. Ruptured abdominal aortic aneurysm: endovascular treatment. *Abdom Imaging* 2005; 30(3):263-269.
- (126) Alsac JM, Desgranges P, Kobeiter H, Becquemin JP. Emergency endovascular repair for ruptured abdominal aortic aneurysms: feasibility and comparison of early results with conventional open repair. *Eur J Vasc Endovasc Surg* 2005; 30(6):632-639.

- (127) Hechelhammer L, Lachat ML, Wildermuth S, Bettex D, Mayer D, Pfammatter T. Midterm outcome of endovascular repair of ruptured abdominal aortic aneurysms. *Journal of Vascular Surgery* 2005; 41(5):752-757.
- (128) Punshon G, Vara DS, Sales KM, Kidane AG, Salacinski HJ, Seifalian AM. Interactions between endothelial cells and a poly(carbonate-silsesquioxane-bridge-urea)urethane. *Biomaterials* 2005; 26(32):6271-6279.
- (129) Haidopoulos M, Turgeon S, Sarra-Bournet C, Laroche G, Mantovani D. Development of an optimized electrochemical process for subsequent coating of 316 stainless steel for stent applications. *Journal of Materials Science-Materials in Medicine* 2006; 17(7):647-657.
- (130) Mazumder MM, De S, Trigwell S, Ali N, Mazumder MK, Mehta JL. Corrosion resistance of polyurethane-coated Nitinol cardiovascular stents. *Journal of Biomaterials Science-Polymer Edition* 2003; 14(12):1351-1362.
- (131) Haidopoulos M, Turgeon S, Sarra-Bournet C, Laroche G, Mantovani D. Development of an optimized electrochemical process for subsequent coating of 316 stainless steel for stent applications. *J Mater Sci Mater Med* 2006; 17(7):647-657.
- (132) Liu XP, Wang YN, Yang DZ, Qi M. The effect of ageing treatment on shape-setting and superelasticity of a nitinol stent. *Materials Characterization* 2008; 59(4):402-406.
- (133) Koski K, Holsa J, Ernoult J, Rouzaud A. The connection between sputter cleaning and adhesion of thin solid films. *Surface & Coatings Technology* 1996; 80(1-2):195-199.
- (134) Bakhshi R, Edirisinghe MJ, Darbyshire A, Ahmad Z, Seifalian AM. Electrohydrodynamic Jetting Behaviour of Polyhedral Oligomeric Silsesquioxane Nanocomposite. *Journal of Biomaterials Applications* 2009; 23(4):293-309.
- (135) Kwolek CJ, Fairman R. Update on thoracic aortic endovascular grafting using the medtronic talent device. *Semin Vasc Surg* 2006; 19(1):25-31.
- (136) Zhang C, Zhang N, Wen X. Synthesis and characterization of biocompatible, degradable, light-curable, polyurethane-based elastic hydrogels. *J Biomed Mater Res A* 2007; 82(3):637-650.
- (137) Kannan RY, Salacinski HJ, Odlyha M, Butler PE, Seifalian AM. The degradative resistance of polyhedral oligomeric silsesquioxane nanocore integrated polyurethanes: an in vitro study. *Biomaterials* 2006; 27(9):1971-1979.

- (138) Kannan RY, Salacinski HJ, Sales KM, Butler PE, Seifalian AM. The endothelialization of polyhedral oligomeric silsesquioxane nanocomposites: an in vitro study. *Cell Biochem Biophys* 2006; 45(2):129-136.
- (139) de MA, Punshon G, Ramesh B, Sarkar S, Darbyshire A, Hamilton G et al. In situ endothelialization potential of a biofunctionalised nanocomposite biomaterial-based small diameter bypass graft. *Biomed Mater Eng* 2009; 19(4-5):317-331.
- (140) Kraft KA, Fei DY, Shao X, Chang YY, Arena R. Improved aortic stiffness assessment in the elderly using a one-dimensional fluid displacement MR method. *J Magn Reson Imaging* 2006; 24(3):603-610.
- (141) Flecher EM, Curry JW, Joudinaud TM, Kegel CL, Weber PA, Duran CM. Coronary flow obstruction in percutaneous aortic valve replacement. An in vitro study. *Eur J Cardiothorac Surg* 2007; 32(2):291-294.
- (142) van 't V, Buth J, Merckx M, Tonino P, van den BH, Pijls N et al. Biomechanical properties of abdominal aortic aneurysms assessed by simultaneously measured pressure and volume changes in humans. *J Vasc Surg* 2008; 48(6):1401-1407.
- (143) Walker RD, Smith RE, Sherriff SB, Wood RF. Latex vessels with customized compliance for use in arterial flow models. *Physiol Meas* 1999; 20(3):277-286.
- (144) Giudiceandrea A, Seifalian AM, Krijgsman B, Hamilton G. Effect of prolonged pulsatile shear stress in vitro on endothelial cell seeded PTFE and compliant polyurethane vascular grafts. *Eur J Vasc Endovasc Surg* 1998; 15(2):147-154.
- (145) Hoeks APG. Non-invasive study of the local mechanical arterial characteristics in humans. In: Safa ME, O'Rourke MFO, editors. *The Arterial System in Hypertension*. Dordrecht, Netherlands: Kluwer Academic Publishers; 1993. 119-134.
- (146) Tai NR, Giudiceandrea A, Salacinski HJ, Seifalian AM, Hamilton G. In vivo femoropopliteal arterial wall compliance in subjects with and without lower limb vascular disease. *J Vasc Surg* 1999; 30(5):936-945.
- (147) Peterson LH, Jenesen RE, Parnell J. Mechanical properties of arteries in vivo. *Circulation Research* 8, 622-639. 1960.
Ref Type: Generic

- (148) Seifalian AM, Hawkes DJ, Giudiceandrea A, McNeill J, Cochester A, Hamilton G. A novel technique of blood flow and compliance measurement using digital subtraction angiography. In: Greenhalgh RM, editor. *Vascular Imaging for Surgeons*. London: WB Saunders; 1995. 51-70.
- (149) Kawasaki T, Sasayama S, Yagi S, Asakawa T, Hirai T. Noninvasive Assessment of the Age-Related-Changes in Stiffness of Major Branches of the Human Arteries. *Cardiovascular Research* 1987; 21(9):678-687.
- (150) Winer BJ, Brown DR, Michels KM. *Statistical principles in Experimental Design*. 3rd ed. New York: McGraw-Hill; 1991.
- (151) Caro CG, Pedley TJ, Schroter RC, Seed WA. *Solid mechanics and the properties of blood vessel walls. The mechanics of the circulation*. Oxford: Oxford University Press; 1978. 86-105.
- (152) Lye CR, Sumner DS, Hokanson DE, Strandness DE, Jr. The transcutaneous measurement of the elastic properties of the human saphenous vein femoropopliteal bypass graft. *Surg Gynecol Obstet* 1975; 141(6):891-895.
- (153) O'Rourke M. Arterial compliance and wave reflection. *Arch Mal Coeur* 84, 45-48. 1991.
Ref Type: Generic
- (154) Lye CR, Sumner DS, Hokanson DE, Strandness DE, Jr. The transcutaneous measurement of the elastic properties of the human saphenous vein femoropopliteal bypass graft. *Surg Gynecol Obstet* 1975; 141(6):891-895.
- (155) Abbott WM, Megerman J, Hasson JE, L'Italien G, Warnock DF. Effect of compliance mismatch on vascular graft patency. *J Vasc Surg* 1987; 5(2):376-382.
- (156) Hermeling E, Hoeks AP, Winkens MH, Waltenberger JL, Reneman RS, Kroon AA et al. Noninvasive assessment of arterial stiffness should discriminate between systolic and diastolic pressure ranges. *Hypertension* 2010; 55(1):124-130.
- (157) Burton AC. Relationship of structure to function of the tissues of the wall of blood vessels. *Physiol Rev* 34, 619-642. 1954.
Ref Type: Generic
- (158) ROACH MR, Burton AC. The reason for the shape of the distensibility curves of arteries. *Can J Biochem Physiol* 1957; 35(8):681-690.

- (159) Abbott WM, Megerman J, Hasson JE, L'Italien G, Warnock DF. Effect of compliance mismatch on vascular graft patency. *J Vasc Surg* 1987; 5(2):376-382.
- (160) Santiago EJ, Chatamra K, Taylor DE. Haemodynamic aspects of lower limb arterial reconstruction using Dacron and Goretex prostheses. *Ann R Coll Surg Engl* 1981; 63(4):253-256.
- (161) Long A, Rouet L, Vitry F, Albertini JN, Marcus C, Clement C. Compliance of abdominal aortic aneurysms before and after stenting with tissue doppler imaging: evolution during follow-up and correlation with aneurysm diameter. *Ann Vasc Surg* 2009; 23(1):49-59.
- (162) Gawenda M, Knez P, Winter S, Jaschke G, Wassmer G, Schmitz-Rixen T et al. Endotension is influenced by wall compliance in a latex aneurysm model. *Eur J Vasc Endovasc Surg* 2004; 27(1):45-50.
- (163) Sonesson B, Hansen F, Stale H, Lanne T. Compliance and diameter in the human abdominal aorta--the influence of age and sex. *Eur J Vasc Surg* 1993; 7(6):690-697.
- (164) Wada T, Fujishiro K, Fukumoto T, Yamazaki S. Relationship between ultrasound assessment of arterial wall properties and blood pressure. *Angiology* 1997; 48(10):893-900.
- (165) Sarkar S, Burriesci G, Wojcik A, Aresti N, Hamilton G, Seifalian AM. Manufacture of small calibre quadruple lamina vascular bypass grafts using a novel automated extrusion-phase-inversion method and nanocomposite polymer. *Journal of Biomechanics* 2009; 42(6):722-730.
- (166) Hofstra L, Willigers JM, Huvers FC, Schaper NC, Kester AD, Kitslaar PJ et al. Short-term variation in the elastic properties of a muscular artery in humans. *Clin Sci (Lond)* 1994; 86(5):567-574.
- (167) Greenhalgh RM, Brown LC, Powell JT, Thompson SG, Epstein D, Sculpher MJ. Endovascular versus Open Repair of Abdominal Aortic Aneurysm. *New England Journal of Medicine* 2010; 362(20):1863-1871.
- (168) Zhang Y, Sun H, Chen C. Superhard cubic BC₂N compared to diamond. *Phys Rev Lett* 2004; 93(19):195504.

- (169) Kannan RY, Salacinski HJ, Odlyha M, Butler PE, Seifalian AM. The degradative resistance of polyhedral oligomeric silsesquioxane nanocore integrated polyurethanes: An in vitro study. *Biomaterials* 2006; 27(9):1971-1979.
- (170) de MA, Punshon G, Ramesh B, Sarkar S, Darbyshire A, Hamilton G et al. In situ endothelialization potential of a biofunctionalised nanocomposite biomaterial-based small diameter bypass graft. *Biomed Mater Eng* 2009; 19(4-5):317-331.
- (171) Kannan RY, Salacinski HJ, Sales KM, Butler PE, Seifalian AM. The endothelialization of polyhedral oligomeric silsesquioxane nanocomposites: an in vitro study. *Cell Biochem Biophys* 2006; 45(2):129-136.
- (172) Sarkar S, Burriesci G, Wojcik A, Aresti N, Hamilton G, Seifalian AM. Manufacture of small calibre quadruple lamina vascular bypass grafts using a novel automated extrusion-phase-inversion method and nanocomposite polymer. *Journal of Biomechanics* 2009; 42(6):722-730.
- (173) US Food and Drug Administration. Non-clinical tests and recommended labeling for intravascular stents and associated delivery systems: guidance for industry and FDA Staff. 2005. US Department of Health and Human Services: Food and Drug Administration, Center for Devices and Radiological Health.
Ref Type: Report
- (174) Salacinski HJ, Handcock S, Seifalian AM, inventors. Polymer for use in conduits and medical devices. patent WO2005070998. 2005 2005.
- (175) Bakhshi R, Darbyshire A, Evans JE, You Z, Lu J, Seifalian AM. Polymeric coating of surface modified nitinol stent with POSS-nanocomposite polymer. *Colloids Surf B Biointerfaces* 2011; 86(1):93-105.
- (176) Kwolek CJ, Fairman R. Update on thoracic aortic endovascular grafting using the medtronic talent device. *Semin Vasc Surg* 2006; 19(1):25-31.
- (177) Wiggins MJ, Wilkoff B, Anderson JM, Hiltner A. Biodegradation of polyether polyurethane inner insulation in bipolar pacemaker leads. *J Biomed Mater Res* 2001; 58(3):302-307.
- (178) Tai NR, Salacinski HJ, Edwards A, Hamilton G, Seifalian AM. Compliance properties of conduits used in vascular reconstruction. *Br J Surg* 2000; 87(11):1516-1524.

Bibliography

- (179) Chuter TA. Durability of endovascular infrarenal aneurysm repair: when does late failure occur and why? *Semin Vasc Surg* 2009; 22(2):102-110.
- (180) Beebe HG, Cronenwett JL, Katzen BT, Brewster DC, Green RM. Results of an aortic endograft trial: impact of device failure beyond 12 months. *J Vasc Surg* 2001; 33(2 Suppl):S55-S63.
- (181) Guidoin R, Marois Y, Douville Y, King MW, Castonguay M, Traore A et al. First-generation aortic endografts: analysis of explanted Stentor devices from the EUROSTAR Registry. *J Endovasc Ther* 2000; 7(2):105-122.
- (182) Jacobs TS, Won J, Gravereaux EC, Faries PL, Morrissey N, Teodorescu VJ et al. Mechanical failure of prosthetic human implants: a 10-year experience with aortic stent graft devices. *J Vasc Surg* 2003; 37(1):16-26.
- (183) Brown KE, Heyer KS, Matsumura JS, Eskandari MK. Late Type III endoleak and graft failure of an Ancure stent-graft. *J Vasc Interv Radiol* 2008; 19(10):1506-1508.
- (184) Wanhainen A, Nyman R, Eriksson MO, Bjorck M. First report of a late type III endoleak from fabric tears of a Zenith stent graft. *J Vasc Surg* 2008; 48(3):723-726.
- (185) Tai NR, Salacinski HJ, Edwards A, Hamilton G, Seifalian AM. Compliance properties of conduits used in vascular reconstruction. *Br J Surg* 2000; 87(11):1516-1524.
- (186) Sarkar S, Sales KM, Hamilton G, Seifalian AM. Addressing thrombogenicity in vascular graft construction. *J Biomed Mater Res B Appl Biomater* 2007; 82(1):100-108.
- (187) US Food and Drug Administration. Non-clinical tests and recommended labeling for intravascular stents and associated delivery systems: guidance for industry and FDA Staff. 2005. US Department of Health and Human Services: Food and Drug Administration, Center for Devices and Radiological Health.
Ref Type: Report
- (188) Thomas B, Sanchez L. Proximal migration and endoleak: impact of endograft design and deployment techniques. *Semin Vasc Surg* 2009; 22(3):201-206.
- (189) Kannan RY, Salacinski HJ, Odlyha M, Butler PE, Seifalian AM. The degradative resistance of polyhedral oligomeric silsesquioxane nanocore integrated polyurethanes: An in vitro study. *Biomaterials* 2006; 27(9):1971-1979.

- (190) Sekhri AR, Lees WR, Adiseshiah M. Measurement of aortic compliance in abdominal aortic aneurysms before and after open and endoluminal repair: preliminary results. *J Endovasc Ther* 2004; 11(4):472-482.
- (191) Vorp DA. Biomechanics of abdominal aortic aneurysm. *Journal of Biomechanics* 2007; 40(9):1887-1902.
- (192) Kannan RY, Salacinski HJ, Ghanavi JE, Narula A, Odlyha M, Peirovi H et al. Silsesquioxane nanocomposites as tissue implants. *Plastic and Reconstructive Surgery* 2007; 119(6):1653-1662.
- (193) Wang ZY, Liu FC, Han EH, Ke W, Luo SZ. Effect of ZnO nanoparticles on anti-aging properties of polyurethane coating. *Chinese Science Bulletin* 2009; 54(19):3464-3472.
- (194) Salacinski HJ, Odlyha M, Hamilton G, Seifalian AM. Thermo-mechanical analysis of a compliant poly(carbonate-urea)urethane after exposure to hydrolytic, oxidative, peroxidative and biological solutions. *Biomaterials* 2002; 23(10):2231-2240.
- (195) McCarthy SJ, Meijs GF, Mitchell N, Gunatillake PA, Heath G, Brandwood A et al. In-vivo degradation of polyurethanes: transmission-FTIR microscopic characterization of polyurethanes sectioned by cryomicrotomy. *Biomaterials* 1997; 18(21):1387-1409.
- (196) Kannan RY, Salacinski HJ, Edirisinghe MJ, Hamilton G, Seifalian AM. Polyhedral oligomeric silsesquioxane-polyurethane nanocomposite microvessels for an artificial capillary bed. *Biomaterials* 2006; 27(26):4618-4626.
- (197) Kannan RY, Salacinski HJ, Odlyha M, Butler PE, Seifalian AM. The degradative resistance of polyhedral oligomeric silsesquioxane nanocore integrated polyurethanes: An in vitro study. *Biomaterials* 2006; 27(9):1971-1979.
- (198) Cheng D, Martin J, Shennib H, Dunning J, Muneretto C, Schueler S et al. Endovascular aortic repair versus open surgical repair for descending thoracic aortic disease a systematic review and meta-analysis of comparative studies. *J Am Coll Cardiol* 2010; 55(10):986-1001.
- (199) Gopaldas RR, Huh J, Dao TK, Lemaire SA, Chu D, Bakaeen FG et al. Superior nationwide outcomes of endovascular versus open repair for isolated descending thoracic aortic aneurysm in 11,669 patients. *J Thorac Cardiovasc Surg* 2010; 140(5):1001-1010.

- (200) D'Souza S, Duncan A, Aguila F, Oderich G, Ricotta J, Kalra M et al. TEVAR for non-aneurysmal thoracic aortic pathology. *Catheter Cardiovasc Interv* 2009; 74(5):783-786.
- (201) Adams JD, Angle JF, Matsumoto AH, Peeler BB, Arslan B, Cherry KJ et al. Endovascular repair of the thoracic aorta in the post-FDA approval era. *J Thorac Cardiovasc Surg* 2009; 137(1):117-123.
- (202) Hughes GC, Daneshmand MA, Swaminathan M, Nienaber JJ, Bush EL, Husain AH et al. "Real world" thoracic endografting: results with the Gore TAG device 2 years after U.S. FDA approval. *Ann Thorac Surg* 2008; 86(5):1530-1537.
- (203) Botta L, Buttazzi K, Russo V, Parlapiano M, Gostoli V, Di Bartolomeo R et al. Endovascular repair for penetrating atherosclerotic ulcers of the descending thoracic aorta: early and mid-term results. *Ann Thorac Surg* 2008; 85(3):987-992.
- (204) Gopaldas RR, Dao TK, Lemaire SA, Huh J, Coselli JS. Endovascular versus open repair of ruptured descending thoracic aortic aneurysms: A nationwide risk-adjusted study of 923 patients. *J Thorac Cardiovasc Surg* 2011.
- (205) Guyton AC. Cardiac output, venous return, and their regulations. In: Guyton AC, editor. *Textbook of Medical Physiology*. 8 ed. Philadelphia, Saunders; 1991. 221-233.
- (206) Ioannou CV, Morel DR, Katsamouris AN, Katranitsa S, Startchik I, Kalangos A et al. Left ventricular hypertrophy induced by reduced aortic compliance. *J Vasc Res* 2009; 46(5):417-425.
- (207) Ioannou CV, Stergiopoulos N, Katsamouris AN, Startchik I, Kalangos A, Licker MJ et al. Hemodynamics induced after acute reduction of proximal thoracic aorta compliance. *Eur J Vasc Endovasc Surg* 2003; 26(2):195-204.
- (208) Morita S, Asou T, Kuboyama I, Harasawa Y, Sunagawa K, Yasui H. Inelastic vascular prosthesis for proximal aorta increases pulsatile arterial load and causes left ventricular hypertrophy in dogs. *J Thorac Cardiovasc Surg* 2002; 124(4):768-774.
- (209) Quaglini V, Villa T, Migliavacca F, Carmo M, Settembrini P, Contro R et al. An in vitro methodology for evaluating the mechanical properties of aortic vascular prostheses. *Artif Organs* 2002; 26(6):555-564.

- (210) Kinley CE, Marble AE. Compliance: a continuing problem with vascular grafts. *J Cardiovasc Surg (Torino)* 1980; 21(2):163-170.
- (211) Back M, Kopchok G, Mueller M, Cavaye D, Donayre C, White RA. Changes in arterial wall compliance after endovascular stenting. *J Vasc Surg* 1994; 19(5):905-911.
- (212) Kannan RY, Salacinski HJ, Sales KM, Butler PE, Seifalian AM. The endothelialization of polyhedral oligomeric silsesquioxane nanocomposites - An in vitro study. *Cell Biochemistry and Biophysics* 2006; 45(2):129-136.
- (213) Kannan RY, Salacinski HJ, De Groot J, Clatworthy I, Bozec L, Horton M et al. The antithrombogenic potential of a polyhedral oligomeric silsesquioxane (POSS) nanocomposite. *Biomacromolecules* 2006; 7(1):215-223.
- (214) Ahmed M, Ghanbari H, Cousins BG, Hamilton G, Seifalian AM. Small calibre polyhedral oligomeric silsesquioxane nanocomposite cardiovascular grafts: Influence of porosity on the structure, haemocompatibility and mechanical properties. *Acta Biomater* 2011.
- (215) Kannan RY, Salacinski HJ, Odlyha M, Butler PE, Seifalian AM. The degradative resistance of polyhedral oligomeric silsesquioxane nanocore integrated polyurethanes: an in vitro study. *Biomaterials* 2006; 27(9):1971-1979.
- (216) Desai M, Ahmed M, Darbyshire A, You Z, Hamilton G, Seifalian AM. An aortic model for the physiological assessment of endovascular stent-grafts. *Ann Vasc Surg* 2011; 25(4):530-537.
- (217) Tai NR, Giudiceandrea A, Salacinski HJ, Seifalian AM, Hamilton G. In vivo femoropopliteal arterial wall compliance in subjects with and without lower limb vascular disease. *J Vasc Surg* 1999; 30(5):936-945.
- (218) Giudiceandrea A, Seifalian AM, Krijgsman B, Hamilton G. Effect of prolonged pulsatile shear stress in vitro on endothelial cell seeded PTFE and compliant polyurethane vascular grafts. *Eur J Vasc Endovasc Surg* 1998; 15(2):147-154.
- (219) Seo J, Choi D, Rienmueller R, Lim JG, Chang Y, Lee J. Suggestion for a new image-based aortic wall stiffness evaluation technique: arterial wall stiffness index. *Int J Cardiovasc Imaging* 2009; 25 Suppl 1:83-94.

- (220) Kawasaki T, Sasayama S, Yagi S, Asakawa T, Hirai T. Noninvasive Assessment of the Age-Related-Changes in Stiffness of Major Branches of the Human Arteries. *Cardiovascular Research* 1987; 21(9):678-687.
- (221) van Herwaarden JA, Muhs BE, Vincken KL, van Prehn J, Teutelink A, Bartels LW et al. Aortic compliance following EVAR and the influence of different endografts: determination using dynamic MRA. *J Endovasc Ther* 2006; 13(3):406-414.
- (222) Dobson G, Flewitt J, Tyberg JV, Moore R, Karamanoglu M. Endografting of the descending thoracic aorta increases ascending aortic input impedance and attenuates pressure transmission in dogs. *Eur J Vasc Endovasc Surg* 2006; 32(2):129-135.
- (223) Dobson G, Flewitt J, Tyberg JV, Moore R, Karamanoglu M. Endografting of the descending thoracic aorta increases ascending aortic input impedance and attenuates pressure transmission in dogs. *Eur J Vasc Endovasc Surg* 2006; 32(2):129-135.
- (224) Kim SY, Hinkamp TJ, Jacobs WR, Lichtenberg RC, Posniak H, Pifarre R. Effect of an inelastic aortic synthetic vascular graft on exercise hemodynamics. *Ann Thorac Surg* 1995; 59(4):981-989.
- (225) Morita S, Asou T, Kuboyama I, Harasawa Y, Sunagawa K, Yasui H. Inelastic vascular prosthesis for proximal aorta increases pulsatile arterial load and causes left ventricular hypertrophy in dogs. *J Thorac Cardiovasc Surg* 2002; 124(4):768-774.
- (226) O'Rourke MF, Staessen JA, Vlachopoulos C, Duprez D, Plante GE. Clinical applications of arterial stiffness; definitions and reference values. *Am J Hypertens* 2002; 15(5):426-444.
- (227) Wisniowski B, Barnes M, Jenkins J, Boyne N, Kruger A, Walker PJ. Predictors of outcome after elective endovascular abdominal aortic aneurysm repair and external validation of a risk prediction model. *J Vasc Surg* 2011.
- (228) Eggebrecht H, Zenge M, Ladd ME, Erbel R, Quick HH. In vitro evaluation of current thoracic aortic stent-grafts for real-time MR-guided placement. *Journal of Endovascular Therapy* 2006; 13(1):62-71.
- (229) Schoder M, Lammer J, Czerny M. Endovascular Aortic Arch Repair: Hopes and Certainties. *European Journal of Vascular and Endovascular Surgery* 2009; 38(3):255-261.

- (230) Chuter TAM, Buck DG, Schneider DB, Reilly LM, Messina LM. Development of a branched stent-graft for endovascular repair of aortic arch aneurysms. *Journal of Endovascular Therapy* 2003; 10(5):940-945.
- (231) Merkle EM, Klein S, Kramer SC, Wisianowsky C. MR angiographic findings in patients with aortic endoprostheses. *American Journal of Roentgenology* 2002; 178(3):641-648.
- (232) Klemm T, Duda S, Machann J, Seekamp-Rahn K, Schnieder L, Claussen CD et al. MR imaging in the presence of vascular stents: A systematic assessment of artifacts, for various stent orientations, sequence types, and field strengths. *Journal of Magnetic Resonance Imaging* 2000; 12(2):606-615.
- (233) Engellau L, Larsson EM, Albrechtsson U, Jonung T, Ribbe E, Thorne J et al. Magnetic resonance imaging and MR angiography of endoluminally treated abdominal aortic aneurysms. *European Journal of Vascular and Endovascular Surgery* 1998; 15(3):212-219.
- (234) Engellau L, Larsson EM, Albrechtsson U, Jonung T, Ribbe E, Thorne J et al. Magnetic resonance imaging and MR angiography of endoluminally treated abdominal aortic aneurysms. *European Journal of Vascular and Endovascular Surgery* 1998; 15(3):212-219.
- (235) Merkle EM, Klein S, Wisianowsky C, Boll DT, Fleiter TR, Pamler R et al. Magnetic resonance imaging versus multislice computed tomography of thoracic aortic endografts. *Journal of Endovascular Therapy* 2002; 9:2-3.
- (236) Wang Y, Truong TN, Yen C, Bilecen D, Watts R, Trost DW et al. Quantitative evaluation of susceptibility and shielding effects of nitinol, platinum, cobalt-alloy, and stainless steel stents. *Magnetic Resonance in Medicine* 2003; 49(5):972-976.
- (237) Rengier F, Delles M, Weber TF, Bockler D, Ley S, Kauczor HU et al. In vitro validation of flow measurements in an aortic nitinol stent graft by velocity-encoded MRI. *Eur J Radiol* 2011; 80(1):163-167.
- (238) Health Canada. SUMMARY BASIS OF DECISION (SBD) VALIANT® THORACIC STENT GRAFT with XCELERANT® DELIVERY SYSTEM. Medtronic Inc. [Application Number 122390. Licence Number 77678]. 4-3-2009.
Ref Type: Generic

- (239) Eggebrecht H, Zenge M, Ladd ME, Erbel R, Quick HH. In vitro evaluation of current thoracic aortic stent-grafts for real-time MR-guided placement. *Journal of Endovascular Therapy* 2006; 13(1):62-71.
- (240) Konings MK, Bartels LW, Smits HFM, Bakker CJG. Heating around intravascular guidewires by resonating RF waves. *Journal of Magnetic Resonance Imaging* 2000; 12(1):79-85.
- (241) Eggebrecht H, Zenge M, Ladd ME, Erbel R, Quick HH. In vitro evaluation of current thoracic aortic stent-grafts for real-time MR-guided placement. *Journal of Endovascular Therapy* 2006; 13(1):62-71.
- (242) Health Canada. SUMMARY BASIS OF DECISION (SBD) VALIANT® THORACIC STENT GRAFT with XCELERANT® DELIVERY SYSTEM. Medtronic Inc. [Application Number 122390. Licence Number 77678]. 4-3-2009.
Ref Type: Generic
- (243) Naoum JJ, Ismail N, Peden EK. The current status of endovascular repair of abdominal aortic aneurysms (EVAR). *Methodist DeBakey Cardiovasc J* 2011; 7(3):11-14.
- (244) Broker HS, Foteh KI, Murphy EH, Davis CM, Clagett GP, Modrall JG et al. Device-specific aneurysm sac morphology after endovascular aneurysm repair: evaluation of contemporary graft materials. *J Vasc Surg* 2008; 47(4):702-706.
- (245) Chuter TAM. Durability of Endovascular Infrarenal Aneurysm Repair: When Does Late Failure Occur and Why? *Seminars in Vascular Surgery* 2009; 22(2):102-110.
- (246) van Herwaarden JA, Muhs BE, Vincken KL, van PJ, Teutelink A, Bartels LW et al. Aortic compliance following EVAR and the influence of different endografts: determination using dynamic MRA. *J Endovasc Ther* 2006; 13(3):406-414.
- (247) Zhong H, Matsui O, Xu K, Ogi T, Sanada J, Okamoto Y et al. Gene transduction into aortic wall using plasmid-loaded cationized gelatin hydrogel-coated polyester stent graft. *J Vasc Surg* 2009; 50(6):1433-1443.
- (248) Kannan RY, Salacinski HJ, Odlyha M, Butler PE, Seifalian AM. The degradative resistance of polyhedral oligomeric silsesquioxane nanocore integrated polyurethanes: an in vitro study. *Biomaterials* 2006; 27(9):1971-1979.

- (249) Kannan RY, Salacinski HJ, De Groot J, Clatworthy I, Bozec L, Horton M et al. The antithrombogenic potential of a polyhedral oligomeric silsesquioxane (POSS) nanocomposite. *Biomacromolecules* 2006; 7(1):215-223.
- (250) Ghanbari H, Kidane AG, Burriesci G, Ramesh B, Darbyshire A, Seifalian AM. The anti-calcification potential of a silsesquioxane nanocomposite polymer under in vitro conditions: potential material for synthetic leaflet heart valve. *Acta Biomater* 2010; 6(11):4249-4260.
- (251) Kidane AG, Burriesci G, Edirisinghe M, Ghanbari H, Bonhoeffer P, Seifalian AM. A novel nanocomposite polymer for development of synthetic heart valve leaflets. *Acta Biomater* 2009; 5(7):2409-2417.
- (252) Molitor P, Barron V, Young T. Surface treatment of titanium for adhesive bonding to polymer composites: a review. *International Journal of Adhesion and Adhesives* 2001; 21(2):129-136.
- (253) Michiardi A, Aparicio C, Planell JA, Gil FJ. New oxidation treatment of NiTi shape memory alloys to obtain Ni-free surfaces and to improve biocompatibility. *Journal of Biomedical Materials Research Part B-Applied Biomaterials* 2006; 77B(2):249-256.
- (254) Bakhshi R, Darbyshire A, Evans JE, You Z, Lu J, Seifalian AM. Polymeric coating of surface modified nitinol stent with POSS-nanocomposite polymer. *Colloids Surf B Biointerfaces* 2011; 86(1):93-105.
- (255) Bakhshi R, Darbyshire A, Evans JE, You Z, Lu J, Seifalian AM. Polymeric coating of surface modified nitinol stent with POSS-nanocomposite polymer. *Colloids Surf B Biointerfaces* 2011; 86(1):93-105.
- (256) Chong CK, How TV, Harris PL. Flow visualization in a model of a bifurcated stent-graft. *J Endovasc Ther* 2005; 12(4):435-445.
- (257) Chong CK, How TV, Black RA, Shortland AP, Harris PL. Development of a simulator for endovascular repair of abdominal aortic aneurysms. *Ann Biomed Eng* 1998; 26(5):798-802.
- (258) Gawenda M, Knez P, Winter S, Jaschke G, Wassmer G, Schmitz-Rixen T et al. Endotension is influenced by wall compliance in a latex aneurysm model. *Eur J Vasc Endovasc Surg* 2004; 27(1):45-50.

- (259) Corbett TJ, Callanan A, Morris LG, Doyle BJ, Grace PA, Kavanagh EG et al. A Review of the In Vivo and In Vitro Biomechanical Behavior and Performance of Postoperative Abdominal Aortic Aneurysms and Implanted Stent-Grafts. *Journal of Endovascular Therapy* 2008; 15(4):468-484.
- (260) Walker RD, Smith RE, Sherriff SB, Wood RF. Latex vessels with customized compliance for use in arterial flow models. *Physiol Meas* 1999; 20(3):277-286.
- (261) Doyle BJ, Morris LG, Callanan A, Kelly P, Vorp DA, McGloughlin TM. 3D reconstruction and manufacture of real abdominal aortic aneurysms: from CT scan to silicone model. *J Biomech Eng* 2008; 130(3):034501.
- (262) Williams PL, Warwick R, Dyson M, Bannister LH. *Gray's Anatomy*. New York: Churchill Livingstone; 1989.
- (263) Corbett TJ, Doyle BJ, Callanan A, Walsh MT, McGloughlin TM. Engineering silicone rubbers for in vitro studies: creating AAA models and ILT analogues with physiological properties. *J Biomech Eng* 2010; 132(1):011008.
- (264) Vorp DA, Mandarino WA, Webster MW, Gorcsan J, III. Potential influence of intraluminal thrombus on abdominal aortic aneurysm as assessed by a new non-invasive method. *Cardiovasc Surg* 1996; 4(6):732-739.
- (265) Chuter TA. Durability of endovascular infrarenal aneurysm repair: when does late failure occur and why? *Semin Vasc Surg* 2009; 22(2):102-110.
- (266) Harris PL, Vallabhaneni SR, Desgranges P, Bacquemin JP, van Marrewijk C, Laheij RJF. Incidence and risk factors of late rupture, conversion, and death after endovascular repair of infrarenal aortic aneurysms: The EUROSTAR experience. *Journal of Vascular Surgery* 2000; 32(4):739-749.
- (267) Kolbel T, Dias N, Resch T, Holst J, Sonesson B, Malina M. In situ bending of thoracic stent grafts: clinical application of a novel technique to improve conformance to the aortic arch. *J Vasc Surg* 2009; 49(6):1613-1616.
- (268) Mestres G, Maeso J, Fernandez V, Matas M. Symptomatic collapse of a thoracic aorta endoprosthesis. *J Vasc Surg* 2006; 43(6):1270-1273.
- (269) Muhs BE, Balm R, White GH, Verhagen HJ. Anatomic factors associated with acute endograft collapse after Gore TAG treatment of thoracic aortic dissection or traumatic rupture. *J Vasc Surg* 2007; 45(4):655-661.

- (270) Neschis DG, Moaine S, Gutta R, Charles K, Scalea TM, Flinn WR et al. Twenty consecutive cases of endograft repair of traumatic aortic disruption: lessons learned. *J Vasc Surg* 2007; 45(3):487-492.
- (271) Steinbauer MG, Stehr A, Pfister K, Herold T, Zorger N, Topel I et al. Endovascular repair of proximal endograft collapse after treatment for thoracic aortic disease. *J Vasc Surg* 2006; 43(3):609-612.
- (272) Kolbel T, Dias N, Resch T, Holst J, Sonesson B, Malina M. In situ bending of thoracic stent grafts: clinical application of a novel technique to improve conformance to the aortic arch. *J Vasc Surg* 2009; 49(6):1613-1616.
- (273) Manning BJ, Ivancev K, Harris PL. In situ fenestration in the aortic arch. *J Vasc Surg* 2010; 52(2):491-494.
- (274) Wang X, Li X. Fluid-structure interaction based study on the physiological factors affecting the behaviors of stented and non-stented thoracic aortic aneurysms. *J Biomech* 2011; 44(12):2177-2184.
- (276) Walsh EG, Holton AD, Brott BC, Venugopalan R, Anayiotos AS. Magnetic resonance phase velocity mapping through NiTi stents in a flow phantom model. *J Magn Reson Imaging* 2005; 21(1):59-65.
- (277) Kuehne T, Saeed M, Moore P, Gleason K, Reddy G, Teitel D et al. Influence of blood-pool contrast media on MR imaging and flow measurements in the presence of pulmonary arterial stents in swine. *Radiology* 2002; 223(2):439-445.